UNIVERSITÉ DE STRASBOURG

ÉCOLE DOCTORALE DE PHYSIQUE ET CHIMIE-PHYSIQUE

IPCMS, UMR 7504

THÈSE présentée par :

Vincent DAVESNE

soutenue le : **19 novembre 2013**

pour obtenir le grade de : **Docteur de l'université de Strasbourg et du Karlsruhe Institute of Technology**

Discipline/ Spécialité : Physique et Chimie Physique

ORGANIC SPINTRONICS : AN INVESTIGATION ON SPIN-CROSSOVER COMPLEXES FROM ISOLATED MOLECULES TO THE DEVICE

THÈSE dirigée par :

BEAUREPAIRE Éric	Dr., IPCMS Université de Strasbourg
WULFHEKEL Wulf	Prof. Dr., Karlsruhe Institute of Technology

RAPPORTEURS :

EVERS Ferdinand	Prof. (Apl.) Dr., Karlsruhe Institute of Technology
MOLNÁR Gábor	Dr., Laboratoire de chimie de coordination de Toulouse

---

AUTRES MEMBRES DU JURY :

ALOUANI Mebarek	Prof. Dr., IPCMS Université de Strasbourg
HUSEMANN Ulrich	Prof. Dr., Karlsruhe Institute of Technology

SUMMARY

Extrapolation of Moore's law dictate that the size of electronic components should enter soon in the nanometer range, what will require new technological solutions. Among them, organic spintronics is viewed as a cheap, printable, flexible solution that furthermore allows the use of the spin of the electron, in addition to the propagation of its charge. Spin-crossover (SCO) molecules such as $Fe(phen)_2(NCS)_2$ (Fe-phen) and $Fe\{[3,5\text{-dimethylpyrazolyl}]_3BH\}_2$ (Fe-pyrz) are particularly promising from this point of view. Indeed, they consist in metallo-organic complexes that can undergo a spin transition between a S=0, low spin (LS) state and a S=2, high spin (HS) state under various external stimuli such as temperature, pressure or light.

We have deposited Fe-phen and Fe-pyrz by thermal evaporation in order to study single molecules, thin films and thick films on silicon and transition metal surfaces (Cu(100) and Co(100)). We have then investigated the properties of such systems with a wide range of analysis techniques, such as scanning tunneling and atomic force microscopy (STM and AFM), magnetic susceptibility, X-ray diffraction and X-ray absorption spectroscopy.

We have confirmed that the latter technique is not neutral: below 60K, the x-ray illumination excites the LS molecule in a metastable HS state. We have compared this effect, named soft x-ray induced excited spin state trapping (SOXIESST) to the light induced excited spin state trapping (LIESST), and found that it was similar excepted that it was non-resonant. The amplitude of the SOXIESST depends on the intensity and structure of the illuminating beam. We have used a simple model to analyze the experimental data, and we conclude that the HS → LS relaxation rate exhibits a plateau between 10 and 40K, and a thermally activated part above 40K. The metal-ligand charge transfer states seem to be primordial in the efficiency of the effect; the cooperative behavior (namely, the interaction between SCO molecules) is suggested to also play a role.

Thin films results confirms that both spin states coexist on both transition metal surfaces. We observe that when the thickness decreases a) the cooperativity of the thermal spin transition is reduced and b) the thermal spin transition temperature is modified, reduced for Fe-pyrz on silicon, but on the contrary increased for Fe-phen. In the case of ultra-thin films of Fe-phen we quantify the first propriety using a phenomenological model of the spin transition with a cooperativity term. We observe at the interface a domain where the molecules are “pinned”, which means that their spin state (either HS or LS) cannot be switched by electrical field, current, SOXIESST effect or

LIESST effect. In this domain, at least on transition metal surface with similar lattice parameters, the HS proportion seems to depend exclusively on the coverage, and not on the nature of the substrate or the molecule. Above 2 monolayers (ML), the direct influence of the substrate decreases and we observe a transition domain where a part of the sample is now sensitive to thermal and x-ray induced spin transitions, even if the cooperativity is reduced. Above 4ML, the sample exhibits a “thin film” domain, where the thermodynamic parameters deduced from the model reach “thin film” values, at approximately 44% (Cu) 49% (Co) of bulk ΔH and 29% (Cu) 41% (Co) of bulk ΔS. The subsequent layers do not behave as the bulk: they still exhibit a significant pinned part. The sharpness of the transition however increases when the thickness increases. When this thin film reaches a sufficient thickness, the behavior of the subsequent layers should get back to bulk behavior, but the transition from thin to thick films could not be observed in this study. A simple model was found to be unsuitable to explain the evolution of the HS fraction with thickness of the ultra-thin film samples: Fe-phen layers on transition metal surfaces present a non-trivial spin transition. Surprisingly, Fe-phen molecules do not seem magnetically coupled to the Co layer: this could reflect the contamination of the Co surface by what we believe to be phen groups.

Single Fe-phen molecules on Cu(100) have been observed at 4K using a STM. They can be either in the LS or the HS state and any attempt to switch the spin state by applying a tip voltage failed. We can however retrieve the spin transition by introducing a passivating CuN layer. Isolated Fe-phen molecules on Cu(100)//CuN can then be electrically switched reproducibly between the HS and LS states, leading to a single-molecule device whose state can be deterministically selected.

Preliminary electrical measurement results of vertical devices Au/Fe-phen film/Au exhibit two main features: a drop in the resistivity at 23K that depends on the temperature sweep direction and the magnetic field applied, and a “diode” effect at a temperature compatible with the spin transition, that consists in a peak in electrical resistivity of 2 or 3 orders of magnitude when measuring negative voltage compared to a positive voltage of identical magnitude. The temperature at which this peak occurs depends on the applied magnetic field, the voltage, and the temperature sweeping direction. The peak height decreases when the temperature of the peak reaches the spin transition of the bulk. We consequently believe that the electrical properties of the junction impact the spin transition temperature of Fe-phen, and that the “diode” peak is a consequence of the disorder induced by nucleation of one of the spin phase in the other at the spin transition.

These results form the first steps towards the construction and understanding of a technological SCO electrical device.

RÉSUMÉ

Alors que la taille des composants électroniques atteint la limite des méthodes conventionelles, de nouvelles solutions technologiques sont envisagées. Parmi elles, la spintronique organique est considérée comme une alternative peu coûteuse, imprimable et flexible qui additionellement permet d'utiliser le spin de l'électron, en sus de sa propagation. Les molécules à transition de spin (SCO) telles que la $Fe(phen)_2(NCS)_2$ (Fe-phen) et la $Fe\{[3,5\text{-dimethylpyrazolyl}]_3BH\}_2$ (Fe-pyrz) sont particulièrement prometteuses de ce point de vue. En effet, ce sont des complexes metallo-organiques qui présentent une transition entre un état bas spin (LS) avec S=0 et un état haut spin (HS) avec S=2 lorsque qu'un stimuli extérieur lui est appliqué, comme la température, la pression ou une illumination.

Nous avons déposé des molécules isolées, des couches minces et des couches épaisses de Fe-phen et Fe-pyrz sur des substrats de silicium amorphe et de monocristaux de deux métaux de transition, Cu(100) et Co(100). Nous avons alors étudié les propriétés de ces systèmes à l'aide d'un large spectre de techniques d'analyse, telles que la microscopie à effet tunnel (STM) et à force atomique (AFM), la susceptibilité magnétique, la diffraction des rayons X et la spectroscopie d'absorption des rayons X (XAS).

Nous avons pu confirmer que ce dernier effet n'était pas neutre: en-dessous de 60K, l'illumination par rayons X excite une molécule LS dans un état HS métastable. Nous avons comparé cet effet, appelé le piégage d'état de spin excité induit par rayon X (SOXIESST), avec le piégage d'état de spin excité induit par la lumière (LIESST), et conclu que les deux étaient similaires, mis à part que le SOXIESST est non-résonant. L'amplitude du SOXIESST dépend de l'intensité et de la structure du faisceau incident. Nous avons employé un modèle simple pour analyser les données expérimentales, et conclu que le taux de relaxation HS → LS présente un plateau entre 10 et 40K, et une partie thermiquement activée au-delà de 40K. Les états de transfert de charge métal-ligand semblent primordiaux pour l'efficacité de l'effet; nous suggérons que la coopérativité joue également un rôle lors de l'effet.

Les résultats sur les couches minces confirment que les deux états de spin coexistent sur les surfaces métalliques. Nous observons que lorsque l'épaisseur diminue, a) la coopérativité de la transition de spin thermique est réduite et b) la température de la transition de spin thermique est modifiée, réduite pour la Fe-pyrz sur silicium, mais au contraire augmentée pour la Fe-phen. Dans

le cas des couches ultra-minces de Fe-phen sur des substrats de métaux de transition, nous quantifions la première propriété à l'aide d'un modèle phénoménologique incluant un terme de coopérativité. Nous observons à l'interface un domaine où les molécules sont “épinglées”, c'est-à-dire que leur état de spin (HS ou LS) ne peut être changé par un champ électrique, un courant, l'effet SOXIESST ou l'effet LIESST. Dans ce domaine, au moins sur les métaux de transition avec des paramètres crystallographiques similaires, la proportion de HS semble ne dépendre que de la couverture en molécules, mais pas de la nature du substrat ou de la molécule SCO. Au-delà de 2 monocouches (ML), l'influence directe du substrat faiblit et nous observons un domaine de transition où une partie de l'échantillon est sensible à la température et aux rayons X, même si la coopérativité est réduite. Au-delà de 4ML, l'échantillon présente un domaine “couche mince”, où les paramètres thermodynamiques déduits du modèle atteignent des valeurs “couche mince”, à approximativement 44% (Cu) 49% (Co) du ΔH massif et 29% (Cu) 41% (Co) du ΔS massif. Les couches subséquentent ne se comportent pas comme dans le massif: elles présentent toujours une partie “épinglée” importante. La transition de spin est toutefois plus abrupte lorsque l'épaisseur augmente. Lorsque la couche mince atteint une épaisseur suffisante, les propriétés de l'échantillons devraient se rapprocher du massif, mais la transition entre couches minces et épaisses n'a pu être observée dans cette étude. Un modèle simple d'évolution de la proportion de HS en fonction de l'épaisseur n'a pas été suffisant pour expliquer le comportement de l'échantillon: le comportement en spin des couches de Fe-phen sur des surfaces de métaux de transition est non-trivial. Surprenament, les molécules de Fe-phen ne semblent pas couplées au substrat: cela pourrait refléter la contamination de l'interface par ce que nous pensons être des groupes phen.

Nous avons observé des molécules isolées de Fe-phen sur une surface de Cu(100) à 4K par STM. Elles sont soit dans l'état LS soit HS, et nos tentatives pour les faire transiter en appliquant un voltage sur la pointe ont échoué. Nous pouvons toutefois récupérer la transition de spin en introduisant une couche passivante de CuN. Les molécules isolées de Fe-phen sur Cu(100)//CuN peuvent alors être reproductiblement switchées électriquement entre l'état HS et l'état LS, constituant un dispositif monomoléculaire dont l'état peut être sélectionné déterministiquement.

Les résultats préliminaires de mesures électriques sur des dispositifs verticaux Au/film Fe-phen/Au présentent deux caractéristiques principales: une chute de résistivité à 23K qui dépend de la direction d'évolution de la température ainsi que du champ magnétique appliqué, et un effet

“diode” à une température compatible avec la transition de spin, qui consiste en un pic de résistivité de 2 à 3 ordres de grandeur lorsque qu'on mesure un voltage négatif comparé à un voltage positive de même amplitude. La température de ce pic dépend de la direction d'évolution de la température, du champ magnétique appliqué, et du voltage. L'intensité relative du pic decroît lorsque la température du pic atteint la température de transition thermique du bulk. En conséquence, nous pensons que ce pic est dû à une augmentation du désordre à la transition de spin induite par le courant.

Ces résultats forment les premiers pas vers la construction et la compréhension d'un dispositif technologique à transition de spin induite par stimuli électrique.

Special Thanks...

...To Elodie, who went through a lot while I was going through the rest,

...To my supervisors Eric Beaurepaire and Wulf Wulfhekel, who were the best supervisors I could hope for, I consider myself very lucky to have been under their supervision during those 3 years,

...To my fellow PhD brethen of the IPCMS, especially Manuel Gruber, Filip Sleicher, Saber Gueddida and Dimitra Xenoti for the DMONS and Zo Raolison, Marc Lenertz, Matteo Balestrieri, Aurélie Walter, Delphine Toulemon, Olivier Gerber for the DCMI and also Anis Amokrane who made the time in Strasbourg so enjoyable,

…To the whole team at the KIT, especially Toshio Miyamachi, Timofey Balashov, Tobias Märkl, Michael Schackert, Moritz Peter but a heartly thanks to everyone, who have been as awesome as they were friendly, and certainly a great group to work and party with,

… To the DEIMOS team, notably Philippe Ohresser, Fadi Chouekani and Edwige Otero who had to deal with our silly scientific questions and chamber contaminations,

…To the coworkers at the IPCMS, Samy Boukari, Fabrice Sheurer, Loïc Joly, Martin Bowen, Victor Da Costa, Pierre Panissod, Jacek Arabski, Guy Schmerber, Pierre Rabu, Guillaume Rogez, for directions, discussions, technical help and cake,

...More specifically for STM work Manuel Gruber and Toshio "Magic" Miyamachi, for Optical measurements and reflectometry Guy Schmerber, for the making the capricious equipement of the hybrid work Jacek Arabski and Christophe Kieber, for SQUID Alain Derory, for SEM Jacques Faerber, for the Fe-phen synthesis and answers to dumb questions Guillaume Rogez, and for the multiplexor Pierre Panissod,

...To my friends and family from Strasbourg, Karlsruhe and elsewhere, who were always there to share a bit of science even if they did not understand, because neither did I,

…And finally to the CDFA and the French-German University who made this co-tutorship possible.

"Je sers la science et c'est ma joie" -Disciple

"I'm doing science and I'm still alive" -GlaDOS

Contents

ABREVIATIONS

AFM	Atomic Force Microscopy
DFT	Density Functional Theory
Fe-phen	$Fe(phen)_2(NCS)_2$
Fe-pyrz	$Fe\{[3,5\text{-dimethylpyrazolyl}]_3BH\}_2$
HAXIESST	Hard X-ray Induced Excited Spin State Trapping
HOPG	Highly Oriented Pyrolytic Graphite
HS	High Spin
LS	Low Spin
LIESST	Light Induced Excited Spin State Trapping
NIESST	Nuclear Induced Excited Spin State Trapping
NMR	Nuclear Magnetic Resonance
MLCT	Metal-Ligand Charge Transfer
ML	Monolayer
SAM	Self-Assembled Monolayer
SCO	Spin-crossover
SEM	Scanning Electron Microscopy
SOXIESST	Soft X-ray Induced Excited Spin State Trapping
STM	Scanning Tunneling Microscopy (I/V)
STS	Scanning Tunneling Spectroscopy (dI/dV)
UHV	Ultra-High Vacuum
XAS	X-ray Absorption Spectroscopy
XMCD	X-ray Magnetic Circular Dichroism

GENERAL INTRODUCTION

The field of electronics is faced today with multiple technical and scientific challenges, as the ultimate device dimension achievable by conventional technology might be reached soon. A wide range of alternative strategies are currently being investigated. Among them, organic electronics is considered as a cheap, printable, flexible solution[1]. Spintronics is considered as an innovative solution, allowing for a technological leap towards devices that will rely on the spin of the electron and not only its mere propagation[2]. Organic spintronics[3–5], a quite young field, is combining both approaches.

Spin-crossover (SCO) molecules represent a special domain, particularly promising in this field. SCO molecules are metallo-organic complexes where the metal center exhibit a transition of its spin state between a low spin (LS) and a high spin (HS) state under various external stimuli such as temperature, pressure or light. Discovered by Cambi *et al.* in 1931[6], such molecules have been the object of a continuous interest since then. The most popular SCO molecules are based on Fe(II)[7], and exhibit a spin transition between a S=0, LS state and a S=2, HS state. An essential characteristic of SCO molecules is their cooperative behavior, that controls the shape of the transition. This transition can be smooth or abrupt, complete or not, with or without hysteresis, all depending on the inter-molecular interactions. The recent trend towards the synthesis of low-dimensional SCO materials has motivated the community to investigate more into details this cooperative behavior, and this is where this thesis contributes.

This work aims at providing insights on isolated molecules, thin films, and thick films of two SCO molecules $(Fe(phen)_2(NCS)_2$[8], named Fe-phen, a prototypical compound, and $Fe\{[3,5\text{-dimethylpyrazolyl}]_3BH\}_2$[9], named Fe-pyrz, a less well-known compound, obtained by thermal evaporation on surfaces and studied by scanning tunneling microscopy (STM), X-ray absorption spectroscopy (XAS) and a wide range of analysis techniques. Our final objective was then to use the insights acquired on low-dimensional systems of SCO molecules to build a device for practical applications.

The first chapter is an introduction to the effect of Spin-crossover, from the basics in chemistry and thermodynamics to the technological results. The second chapter describes the molecules and surfaces used, and the third the experimental details. Chapter IV discusses the results of our study

on isolated molecules and thin films of Fe-phen by STM, and of our study on thick films of Fe-phen and Fe-pyrz. Chapter V then describes our results on the study of powder samples and then thin films of Fe-phen by XAS. Finally, chapter VI exhibit our preliminary results on multilayer vertical devices. A general conclusion ends the manuscript, calling back our principal findings.

Note: in this work, “chapter” refers to the main header (I, II, III...), “part” to the second header (I.1, I.2, I.3...) and “point” to the third header (I.1.i, I.1.ii, I.1.iii...).

Spin-crossover

a review of the scientific and technical insights on the phenomenon

This introduction to the field of spin-crossover (SCO) molecules aims at giving the reader the tools for a clear understanding of the results and relevance of this thesis. Starting from the basics of transition metal chemistry to the practical applications of SCO devices, this chapter is intended as a review of the state-of-the-art in the field of single-metal center SCO molecules. Dinuclear[10–12], trinuclear[13], polynuclear[14], networked[15] and polymeric[16–18] SCO systems exist, but form a different category of materials that will not be discussed in this review.

I.1 What is the spin-crossover?

I.1.i Metal complexes and ligand field theory

The chemistry of transition metal complexes is driven by the valence d-orbitals of the transition metal cations. In the free atom, all d orbitals are degenerate : in the Cartesian representation, these are the d_{z^2}, d_{xy}, d_{yz}, d_{xz} and $d_{x^2-y^2}$ (see Fig. I.1) and they have the same energy.

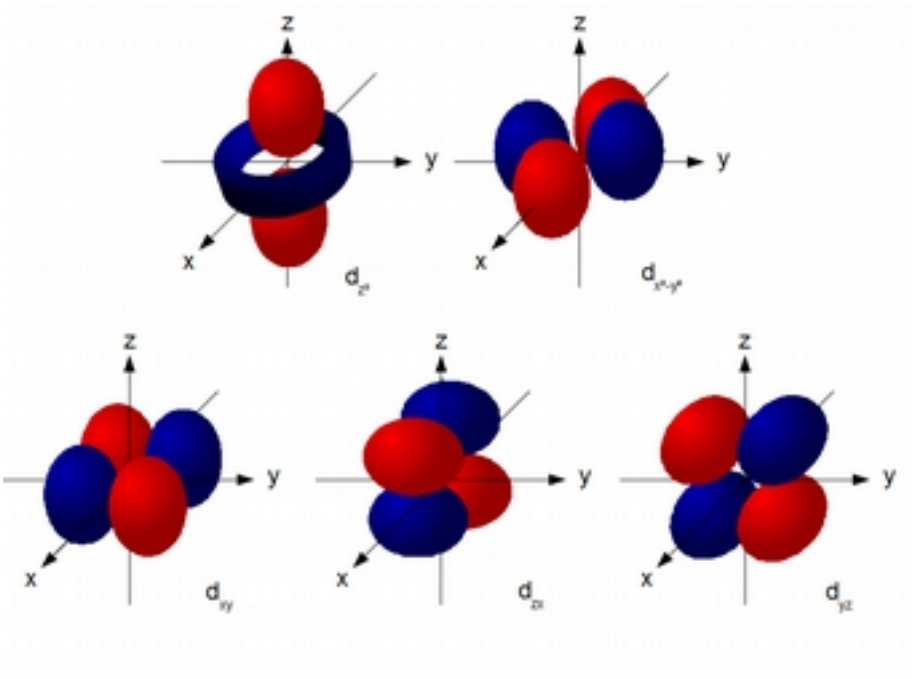

Fig. I.1 : Shape of d orbitals of a single transition metal atom, considering the nucleus as a point charge at the origin of axes. Red identifies parts where the orbital wavefunction is positive, blue where it is negative.

When ligands are added, the atomic d orbitals interact with the s and p orbitals (typically) of the ligands relevant to the symmetry at hand, and they form molecular orbitals as described by the ligand field theory (LFT). The coordination number of the resulting metal complex and the ligand structural arrangement depend on various parameters, the most important being the number of electrons in the metal ion d orbitals, the presence of double-bonds and the relative sizes of the ligands and the metal ion: early and big transition metals, smaller ligands and few double bonds favor high coordination numbers. The symmetry of the complex can range from the rare linear and trigonal planar geometries for respectively two and three-fold coordination, to tri-capped trigonal prismatic for nine-fold coordination or even icosahedral geometries for some lanthanide and actinide complexes. The most commons are listed with a set of examples in Fig. I.2, as well as an example of a set of molecular orbitals in tetrahedral geometry.

(a)

Coordin--ation Number	Geometry	Examples
2	Linear	$Cu(NH3)_2^+$[19], $Hg(CH3)_2$
3	Trigonal planar	$Pt(PPh_3)_3$[20], $[HgI_3]^-$
4	Tetrahedral	$Ni(CO)_4$[21,22]
	Square planar	$Ni(CN)_4^{2-}$[22]
5	Trigonal bipyramidal	$[Mn_2(tren)_2(NCO)_2]^{2+}$[23]
	Square pyramidal	Hemoglobin
6	Octahedral	Most transition metal complexes
	Trigonal prismatic	Solid MoS_2[24]
7	Pentagonal bipyramidal	ReF_7
	Capped octahedral	$W(CO)_4BR_3$
	Capped trigonal prism	$Mo(NCR)_7^{2+}$
8	Square antiprismatic	IF_8^-
9	Tri-capped trigonal prismatic	ReH_9^{2-}

(b)

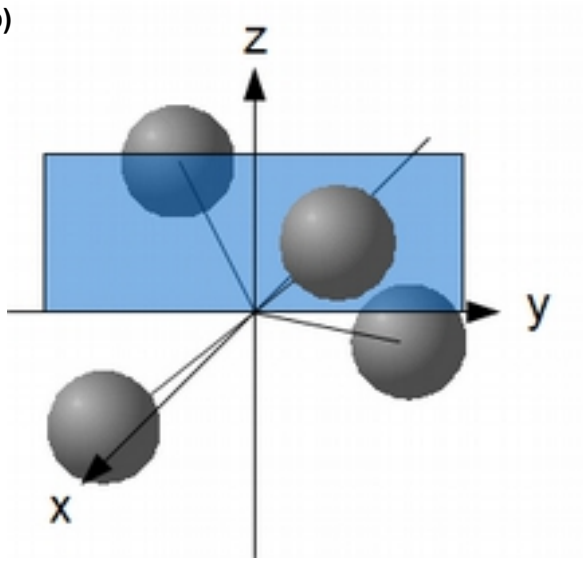

(c)

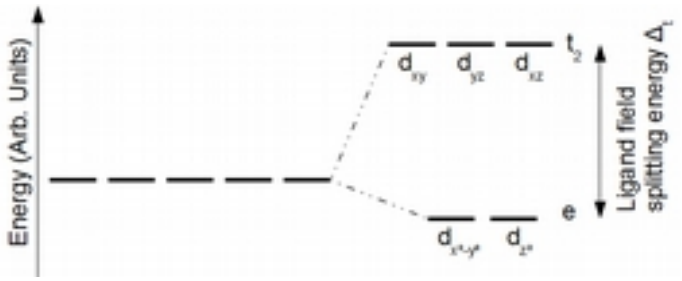

Fig. I.2: (a) Table of common geometries associated with the coordination number of the complex, with examples. (b) shows in gray the position of the ligands in tetrahedral geometry, influencing the relative energies of the d orbitals: the d_{xy}, d_{yz} and d_{xz} have an anti-bonding interaction, while d_{x2-y2} and d_{z2} have a non-bonding interaction. The degeneracy is lifted following the diagram (c). t_2 and e are the notation of the irreducible representation of the geometry of the resulting orbitals according to group theory.

Of course, one has to keep in mind that these represent limiting geometries: if all the ligands are different, then asymmetrical steric repulsion and electrostatic interaction will distort the structure. The Jahn-Teller effect[25,26] occurring in orbital nonlinear spatially degenerate molecules (most often of octahedral geometries) can also modify the structure, as in their case reducing the symmetry of the complex lifts a degeneracy in the electrons orbitals, reducing the energy of the complex. More geometries can be found in the book by Y. Jean[27].

I.1.ii Spin state, spin-crossover and the particular case of Fe(II) complexes

Usually, the metal d electrons will follow Hund's rule and fill up the orbitals starting from the lowest energy atomic orbitals, with one electron per orbital, and all spin parallel. For some transition metals, the competition between the pairing energy of the different electrons and the ligand field splitting will result in complexes of a different spin state for the same geometry: if the ligand field splitting is large enough, the energy lost by reducing the electron-electron repulsion and the quantum mechanical exchange energy will be less important than the energy increase when filling a higher-energy orbital[28]. Although this is known but very rare and controversial for tetrahedral complexes[27–29], as the low ligand field splitting favors high spin tetrahedral complexes, the most common geometry where this happens is the octahedral. The electronic configuration of transition metals in octahedral geometry is summarized in Fig. I.3, as well as a diagram of the filling of the molecular orbitals for a d^6 complex, such as Fe(II)-based complexes, for low spin (maximum electrons paired) and high spin (electrons obeying Hund's rule, maximum multiplicity) states.

d^n	Ion	Unpaired electrons		configuration	
		LS	HS	LS	HS
d^1	Ti^{3+}	1		t_{2g}^1	
d^2	V^{3+}	2		t_{2g}^2	
d^3	Cr^{3+},V^{2+}	3		t_{2g}^3	
d^4	Cr^{2+}, Mn^{3+}	2	4	t_{2g}^4	$t_{2g}^3 e_g^1$
d^5	Mn^{2+}, Fe^{3+}	1	5	t_{2g}^5	$t_{2g}^3 e_g^2$
d^6	Fe^{2+}, Co^{3+}	0	4	t_{2g}^6	$t_{2g4} e_g^2$
d^7	Co^{2+}	1	3	$t_{2g}^6 e_g^1$	$t_{2g}^5 e_g^2$
d^8	Ni^{2+}	2		$t_{2g}^6 e_g^2$	
d^9	Cu^{2+}	1		$t_{2g}^6 e_g^3$	
d^{10}	Cu^+, Zn^{2+}	0		$t_{2g}^6 e_g^4$	

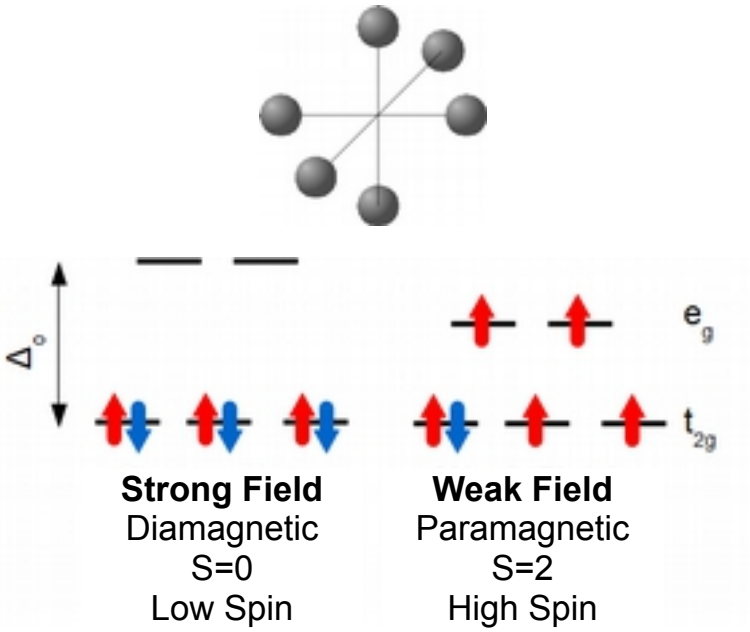

Fig. I.3: Electronic configuration of transition metals in octahedral geometry, for low spin (LS, also noted $^1A_1$ configuration) and high-spin (HS, also noted $^5T_2$ configuration) states, and the energy diagram of a d^6 transition metal ion in octahedral geometry (position of the ligands noted above in gray), for both spin states. Only the d^4 to d^7 electronic configurations can have LS-HS interconversion.

The value of the ligand field, the crystal field splitting energy, is often noted as 10Dq in the literature. The ligand field depends on several parameters: ranked from lower ligand fields (favoring high-spin, HS) to higher ligand field (favoring low-spin, LS), the ligands are I^- < Br^-< S^{2-} < SCN^- < Cl^- < NO_3^- < N_3^- < F^- < OH^- < $C_2O_4^{2-}$ < H_2O < NCS^- < MeCN< pyridin < NH_3 < ethylenediamine < 2,2'-bipyridine < 1,10-phenantroline (phen) < NO_2^- < PPh_3 < CN^- < CO and the metal ions Mn^{2+} <Ni^{2+}

< Co^{2+} < Fe^{2+} < V^{2+} < Fe^{3+} < Co^{3+} < Mn^{4+} < Mo^{3+} < Rh^{3+} < Ru^{3+} < Pd^{4+} < Ir^{3+} < Pt^{4+}.[27,30]

But with the same given set of metal and ligands, some of the complexes can undergo a spin-state change when some external stimuli (such as a change in temperature) is applied: this phenomenon is called *spin-crossover* (SCO). Indeed, the ligand field also depends on an essential parameter: the metal ion-ligand structure. The further from the ion the ligands are, the smaller the ligand field is. Therefore, for the SCO complexes, changing this length may switch the spin state. This alteration in the metal-ligand bond lengths and bond angles is considered universal, and therefore observing this alteration by crystallographic means is considered an easy way to determine the spin state of the complex.[31–36] One should note, however, that often the orbital degeneracies are lifted by Jahn-Teller distortions[37], but this does not contradict the explanation for the phenomenon.

SCO was first observed in Fe(III) dithiocarbamate complexes by Cambi *et al.* [6]in 1931, but since the Fe(II)-based complexes, reported by Baker and Bobonich in 1964[8], are better known, we therefore focus from now on those complexes. They exhibit a SCO between a low-spin, S=0 state, and a high-spin, S=2, state. About 90% of the complexes investigated exhibit a N_6 coordination sphere[38]. The latest developments in the field of mononuclear SCO complexes are further described in the review by Weber[39].

I.1.iii Thermodynamics at work

The spin state of the system is determined by the free energy G = H -TS, with H the enthalpy, T the temperature and S the entropy term. At constant pressure, the difference of free energy between HS and LS is given by $\Delta G = G_{HS} - G_{LS} = \Delta H - T\Delta S$ for an ensemble of N_a molecules. The thermodynamically stable phase is the one with the lowest free energy.

To start with, let us consider the enthalpy term, ΔH. The main contribution is from ΔH_{en}, which represents the zero-point energy difference between the minima of potential energy for LS and HS states due to the variation in bond length and therefore, in ligand field[7,40].

$$\Delta H = H_{enHS} - H_{enLS} \tag{I.1}$$

Note that the potential well of the LS state is more narrow than the one of the HS state because the allowed metal-ligand bond oscillations frequencies are higher in the LS state than in the HS state[41]. These quantities are represented in Fig. I.4(a).

The entropy term, ΔS, is mostly constituted of two contributions[42]: the electronic contribution ΔS_{el}

and the vibrational contribution ΔS_{vib}. The electronic contribution is linked to the ratio of degeneracies between both states, and is written as:

$$\Delta S_{el} = N_a \times k_B \times \ln[\frac{\Omega_{HS}}{\Omega_{LS}}] \quad \text{(I.2)}$$

With Ω_{HS} and Ω_{LS} the degeneracies of HS and LS respectively. $\Omega_{HS}/\Omega_{LS} = 2S+1 = 5$ for Fe(II)[43], ΔS_{el} =13,38 $J.K^{-1}.mol^{-1} > 0$. The contribution of this factor accounts for a minor part of the entropy change[36,37,43–45]. As a note, the orbital degeneracies do not contribute to the entropy change, as they are lifted by Jahn-Teller distorsions[37].

The main contributions are from molecular and network stretching, bending and deformation vibrational modes of the molecule, ΔS_{vib}. Since vibrational disorder and the density of phonons is more important when the coordination sphere is extended (HS state) than when it is reduced (LS state), $\Delta S_{vib} = S_{vibHS} - S_{vibLS} > 0$.

We deduce that there must exist an equilibrium temperature $T_{transition} = \Delta H/\Delta S > 0$ where $\Delta G = 0$. Above this temperature the thermodynamically stable state is HS ($\Delta G < 0$), and below this temperature the thermodynamically stable state is LS ($\Delta G > 0$). At $T_{transition}$, the proportion of HS in the sample is therefore 50%. In the literature, this is also denoted as $T_{1/2}$.[46]

Let us now discuss the evolution with temperature of the proportion of HS molecules p_{HS} in the sample. If we consider N molecules, they can be either in HS with a ratio p_{HS} or LS with a ratio $(1-p_{HS})$. The free energy of the system can be expressed as :

$$G = p_{HS} G_{HS} + (1-p_{HS}) G_{LS} - TS_{mix} \quad \text{(I.3)}$$

With S_{mix} the entropy of mixing for an ideal solution of HS and LS state molecules, that has for expression :

$$S_{mix} = -R[p_{HS}\ln(p_{HS}) + (1-p_{HS})\ln(1-p_{HS})] \quad \text{(I.4)}$$

At the thermodynamic equilibrium, $\left|\frac{\delta G}{\delta p_{HS}}\right|_T = 0$, therefore we can deduce the proportion of HS according to the temperature:

$$p_{HS} = \frac{1}{1+\exp(\frac{\Delta H - T\Delta S}{RT})} \quad \text{(I.5)}$$

A graphical representation of this equation is presented in Fig. I.4, for $\Delta H = 8600$ J.mol^{-1} and $\Delta S =$ 48,78 J.mol^{-1}.K^{-1}, experimental values for $Fe(Phen)_2(NCS)_2$.[45]

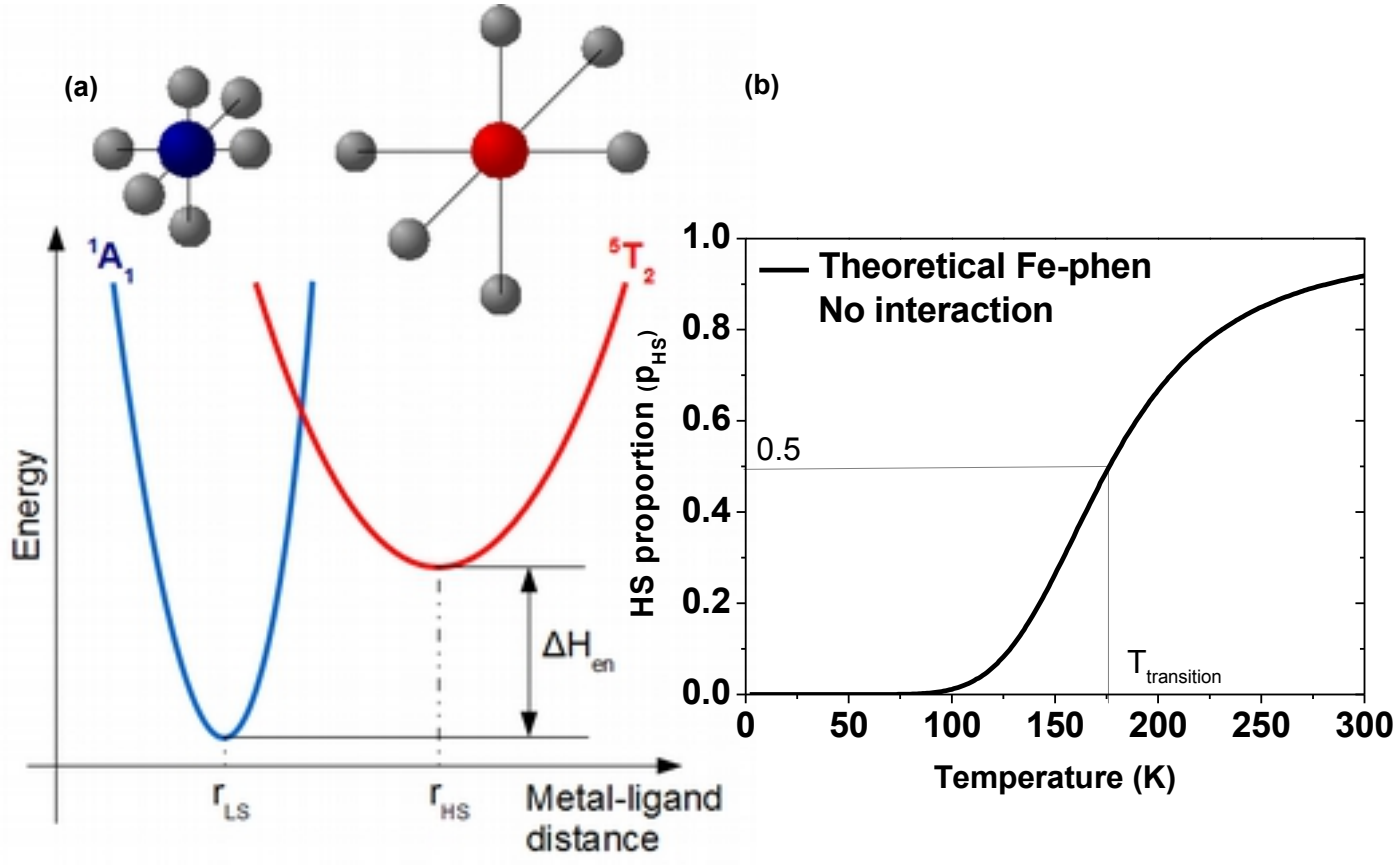

Fig. I.4 : (a) illustrates qualitatively the variation in enthalpy according to the metal-ligand bond length, and the consequent variation in the crystallographic cell, following the thermal spin transition illustrated in (b) by a plot of the equation I.5 for Fe-phen values. $P_{HS}(T)$ has a smooth shape, corresponding to a progressive spin transition over a large range of temperature.

But most experimental shapes for $p_{HS}(T)$ differ from this example. A smooth transition only occurs in weakly-cooperative systems, like diluted solutions or complexes with weak intermolecular interactions[7,44]. Actually, the intermolecular interactions will induce a cooperative behavior that expresses itself by an abrupt transition or even a hysteresis[7,47]. Even molecules that are chemically similar can exhibit totally different magnetic behaviors, as illustrated in Fig. I.5 with molecules from the $Fe(PM\text{-}L)_2(NCS)_2$ family that differ only on the aromatic-based L ligand: with L=TeA, the transition is smooth and incomplete; with L=AzA, the transition is still smooth but complete; with L=BiA, the transition is abrupt and complete; with L=PEA, the transition presents a hysteresis and is considered complete. This extreme sensitivity on the ligands and inter-molecular interactions (as discussed in the next point) makes the prediction of the spin transition behavior of a SCO molecule a challenge.

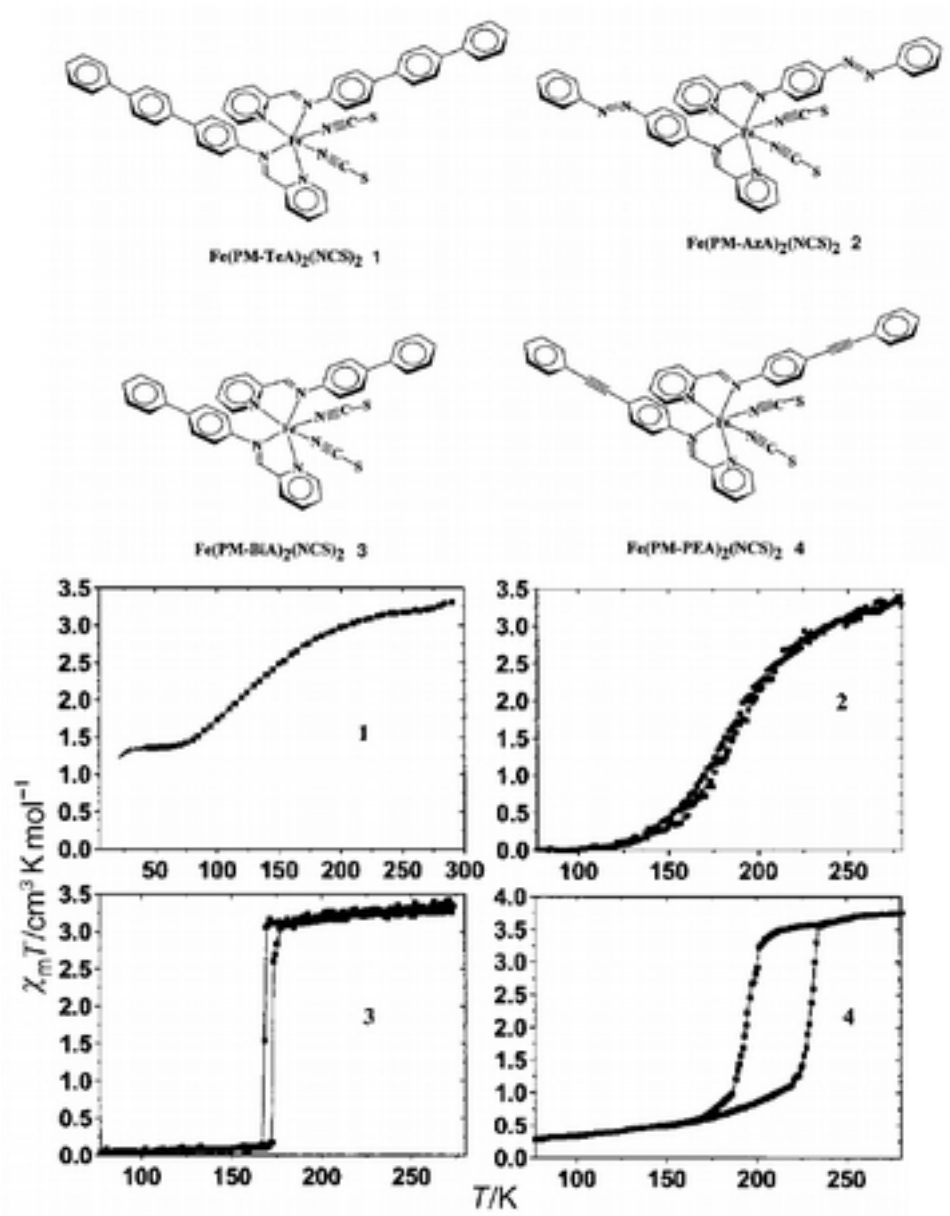

Fig. I.5: Chemical structure (top) and magnetic behavior measured by SQUID (bottom) of 4 SCO molecules of the $Fe(PM\text{-}L)_2(NCS)_2$ family. Despite their similar structures, each one exhibits a different magnetic behavior. Adapted from [47].

Several models exist, purely thermodynamic as above, Ising-like, Sorai, Vibronic or elastic[41,48]. We will use the original form of the thermodynamic model proposed by Slichter *et al.*[49] in 1972 to interpret the data presented with relatively few necessary parameters and for comparative purposes with the literature. A more general form based on the Kimmermann model was used with success by Rao *et al.* in their nuclear magnetic resonance (NMR) study of the Fe-phen spin transition[50], in which they found that this model describes well the results, better than a domain model like the model by Sorai *et al.*[45]. In this case, we can approximate the cooperative behavior of the molecules by adding a cooperative term, Γ, proportional to the product of the HS and LS

proportions in the sample, to the expression of the Gibbs energy[34,48]. Γ might be looked upon as the next term in a power series expansion of G in the variable p_{HS} satisfying the condition $(\delta G/\delta p_{HS})_{p,T}=0$. Γ is a phenomenological constant supposed to be temperature-independent in our case, and withstands making any assumptions on the origin of the cooperativity. That said, according to recent calculations by Kepenekian *et al.*[51,52], the main contribution to Γ comes from the electrostatic interactions in the crystal, especially in the case of hysteretic complexes. $\Gamma = \Delta Q(\delta V_{LS} - \delta V_{HS})$, with ΔQ the variation of charge held by the Fe(II) ion and $\delta V_{LS} - \delta V_{HS}$ the term relying on the fluctuation of polarization during the spin transition, a term highly dependent on crystalline stacking. The general form of the equation governing the HS proportion evolution according to the temperature is then given by:

$$T(p_{HS}) = \frac{\Delta H + \Gamma(1 - 2p_{HS})}{R\ln(\frac{1 - p_{HS}}{p_{HS}}) + \Delta S} \quad \text{(I.6)}$$

Depending on the relative values of ΔH, ΔS and Γ, the various shapes presented in Fig. I.5 can then be produced. Fig. I.6 exhibits examples based on the Fe-phen case already presented in Fig. I.4: Γ = 3000 J.mol^{-1} for the red curve, which fits quite well with experimental results presented in chapter II and is comparable with the slightly different cooperative parameter J_2 = 3850 J.mol^{-1} by Rao *et al.* [50]; Γ = 4000 J.mol^{-1} for the blue curve. The blue curve presents an “impossible” shape with a temperature range where two values of the HS proportions are obtained: in this zone, the molecules are bistable. This can be understood physically as the SCO sample exhibits a thermal hysteresis.

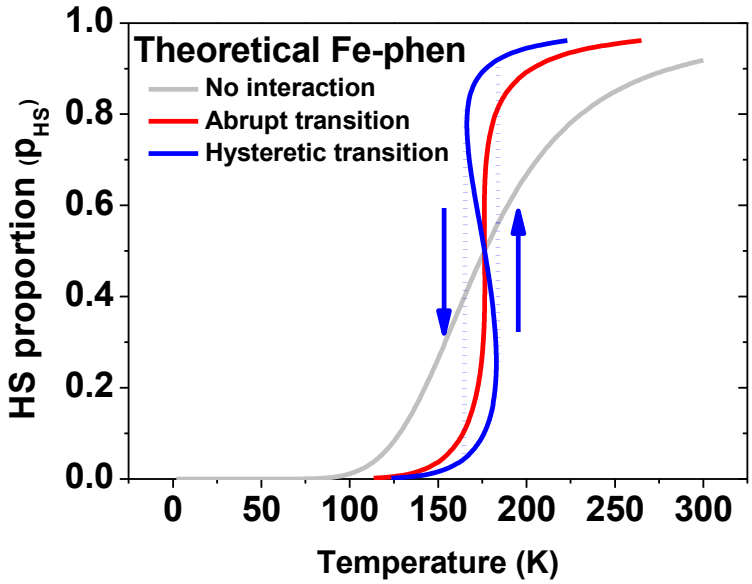

Fig. I.6: Plot of various calculated HS proportion evolution using equation I.6: (grey) Γ = 0 J.mol^{-1} ; (red) Γ = 3000 J.mol^{-1}; (blue) Γ = 4000 J.mol^{-1}. Dashed lines indicates the "real" thermal hysteresis that the blue curve describes, and arrows indicate the temperature sweep direction.

The spin-crossover process might involve more than two spin states, if the molecule of interest has several metal centers. The spin transition can therefore have several steps.[10,53,54]

I.1.iv On the origin of cooperativity

Cooperative behavior is one of the distinctive characteristics of spin transition in SCO materials. It relies on the interactions between SCO centers to produce a macroscopic effect. However, the medium used by this cooperativity, namely the nature of the interactions between SCO molecules, can change from one system to the other. The various theoretical models of spin transition also consider different origins[48], but they can be combined to improve the predictions when the need arises[48,55].

The spin transition itself can be considered either as a random event where the HS and LS molecules are dispersed regularly in the solid, like in the original model used by Slichter and Drickamer (inhomogeneous, process controlled by nucleation), or as a domain growth where the HS and LS molecules form domains, and the mean size of these domains provides insights on the cooperativity of the molecule, an approach pioneered by Sorai *et al.*[44,45] (homogeneous, process controlled by propagation). The different spin transitions triggers mentioned in part I.3 can favor one of those two types of transitions. For example, the light induced excited spin state trapping (LIESST) excitation effect is considered to be intrinsically inhomogeneous[56,57].

The "elastic" interaction arises from the volume change concomitant to the spin transition. The molecules are considered as spheres that interact with each other through the elastic medium, and is comparable to a phase transition, in a mean-field approach. This forms the basis of the Spiering model[58]. It can be compared to an internal "pressure" exerted by each molecule on its neighbors[59,60].

According to Kepenekian *et al.*, electrostatic interaction from polarization of the metal centers play a primary role in the hysteresis of the spin transition of Fe(II) SCO molecules[52]. This approach has the advantage that it makes cooperativity dependent on the Madelung field of the molecule, which facilitates the predictions.

"Weak" bonds were also a traditional focus of the community[53,61] in the context of cooperativity. They include notably π -π stacking, hydrogen bonds[62,63], sulfur bonds, Van-der-Waals interactions and metallophilic interactions[53]. Fe-phen in particular presents π -π interactions[32,64], and SCO molecules specifically designed to maximize π -π stacking were reported to exhibit thermal hysteresis up to 40K[65]. The cohesion of Fe-phen crystals is achieved by Van der Waals interactions[32,66], and Fe-phen also presents intermolecular S--C bonds[32].

A good tool to investigate the relative influence of these interactions on the thermodynamic parameters of the SCO molecules are density functional theory (DFT) and the various methods of ab-initio calculations[51,67–71]. Indeed, they allow the quantitative analysis of the importance of intra-molecular vibrations[43], as intra- and inter-molecular vibrations play a prominent role in the spin-crossover phenomenon[43]. As an example, in Fe-phen, ΔS, the main driving force behind the spin transition, is split into of a 30% electronic contribution[45,66,72], a 40% intra-molecular vibrations contribution[71], the rest believed to be phononic interactions contribution. Note that there is a disagreement in the litterature between the results of Bousseksou *et al.*[73] and Brehm *et al.* endorsed here, and those of Bučko *et al.*[66] that computed a 50% -at least- contribution of the vibrations. Although most of the models mentioned previously can be modified to include intra-molecular vibrations, such as the two-level Ising-like model by Bousseksou *et al.*[43], some are specifically designed with the purpose to address the coupling between phonons and the atoms of the SCO molecule, such as the Zimmermann model[74]. Those are named vibronic models[48].

Finally, since the cooperative behavior of SCO relies on inter-molecular interactions, it can be tuned by the addition of external molecules/solvents and/or metal dilution, by replacing the

central Fe with other metals[75]. It is widely known that dilution in solution severly restricts cooperativity[76], but a less severe effect can be reached by including solvent molecules in the crystalline lattice[77]. Another way is to dilute the SCO compound in a polymer matrix[78]. These methods allow the individual study and tuning of the various cooperative interactions mentioned previously.

For further studies in the field of SCO theoretical calculations, one can consult the reviews by Boča [48,55] and Enachescu[60].

I.2 Studying SCO behavior: experimental analysis techniques

Since the first study of a SCO molecule by Cambi *et al.*[6], the detection of the spin transition has been of central interest for the community. The techniques can be roughly divided in electronic techniques, which study the differences between the electronic properties of the spin states (Mössbauer, UV-Visible, XAS...); "volume" techniques, which rely on the variation of structural parameters such as the metal-ligand distance (X-ray diffraction) or the phase transition (heat capacity measurements); and magnetic techniques, which relate to the difference in magnetic properties of the different spin states (SQUID, MOKE...). Some of the most prominent techniques used in the field are presented in this point.

I.2.i Mössbauer spectroscopy

The recoilless nuclear resonance absorption of γ-radiation is a technique useful both for the identification of the spin state and the investigation of the environment of the Fe ion [38]. It relies on the absorption of γ-radiation by the molecule investigated, exciting a nuclear transition at an energy dependent on the oxidation number, the magnetic environment and the ligands. ^{57}Fe is a tool of choice for SCO studies by Mössbauer. An interesting application of the determination of the spin state of a SCO molecule by Mössbauer effect is the detection of moisture[79]. Fe-phen[80] and Fe-pyrz[81] have both been investigated with this technique.

I.2.ii Optical absorption and related techniques

The spin transition is often accompanied by a significant change in coloration, a fact that has been used for prospective technological applications[18] as discussed in the last part of this chapter. It is therefore possible to not only follow the spin transition by optical microscopy[82] and optical spectroscopy, but also to identify electronic states of the SCO molecules, as illustrated in Fig. I.7.

The identification of excited states has made this technique a precious tool to study effects such as the LIESST, discussed in the next point. Ultraviolet and visible light can be used for this purpose, as well as infrared Raman spectroscopy, for spin state identification but also to provide additional information on the vibrational modes[71,73].

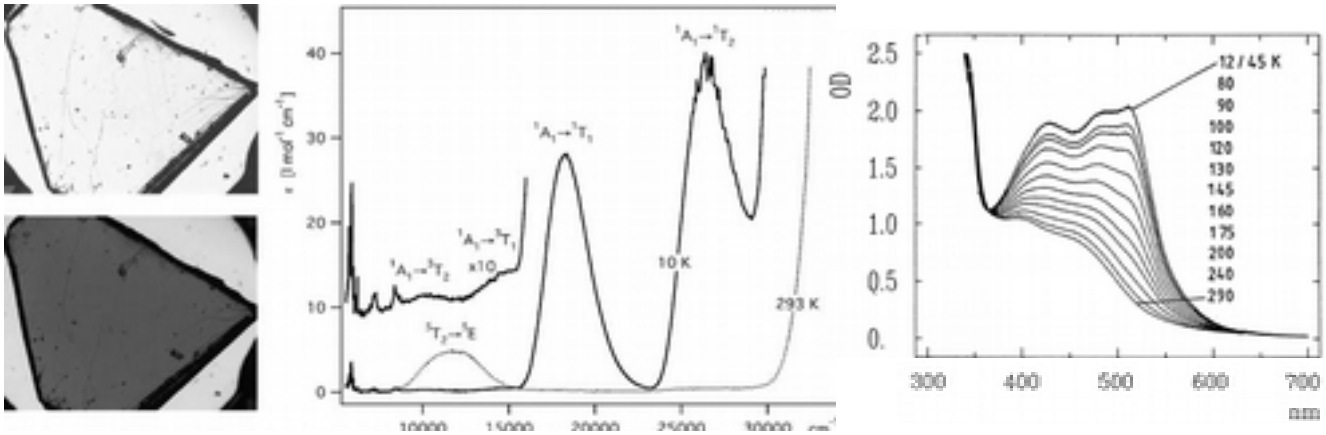

Fig. I.7: Pictures of a single crystal of $[Fe(ptz)_6](BF_4)_2$ at 293 K (top left) and at 10 K (bottom left), and the corresponding single crystal optical absorption spectra in the middle plot. On the right, absorption spectra of $[Fe(2\text{-mephen})_3]^{2+}$ embedded in a polymer matrix (PVA) as a function of temperature. Adapted from[83].

I.2.iii Magnetic susceptibility

Since the spin states of Fe(II) SCO complexes vary between a nearly diamagnetic S=0 state and a strongly paramagnetic S=2 state, it is natural that one of the favorite technique in the domain is the measurement of the magnetic susceptibility[38]. The Evans NMR method is generally applied for studies in liquid solution. For measurements on solid samples, the traditional balance methods (Faraday, Gouy) have been progressively replaced by superconducting quantum interference device (SQUID) magnetometers. The SQUID is based on superconducting loops containing Josephson junctions, and allows the measurement of extremely low magnetic fields. The temperature dependence of the susceptibility of a given sample can be measured, and the HS proportion can be extracted provided the respective susceptibilities of the pure HS and LS states are known. Since this is not always the case, the results given are usually the magnetic susceptibility multiplied by temperature versus the temperature, as illustrated in Fig. I.5. Furthermore, when the transition is complete, it is possible to obtain the parameter S with the equation $\chi=C/T$, with C the Curie constant. $C = \mu_B^2/(3k_BT)*Ng^2J(J+1)$, with μ_B the Bohr's magneton, k_B the Boltzmann constant, N the number of magnetic molecules, g the Landé factor and J the angular momentum quantum number.

I.2.iv X-ray diffraction

X-ray crystallography relies on the diffraction of an X-ray beam by lattice planes through elastic scattering to identify the position of atoms in a crystal. As discussed in the last point, the spin transition is also characterized by a drastic change in metal-ligand bond lengths and angles. For some molecules, it can even result in a crystallographic phase transition. Therefore, the X-ray diffraction technique can provide structural insights on the nature of the spin transition[84], and the relative orientation of the molecules in the crystal, which is of primordial interest for cooperativity studies[34,38]. Fig. I.8 presents the arrangement of the Fe-phen molecules in the crystal, a typical result obtained by X-ray diffraction. The π -π stacking is clearly visible.

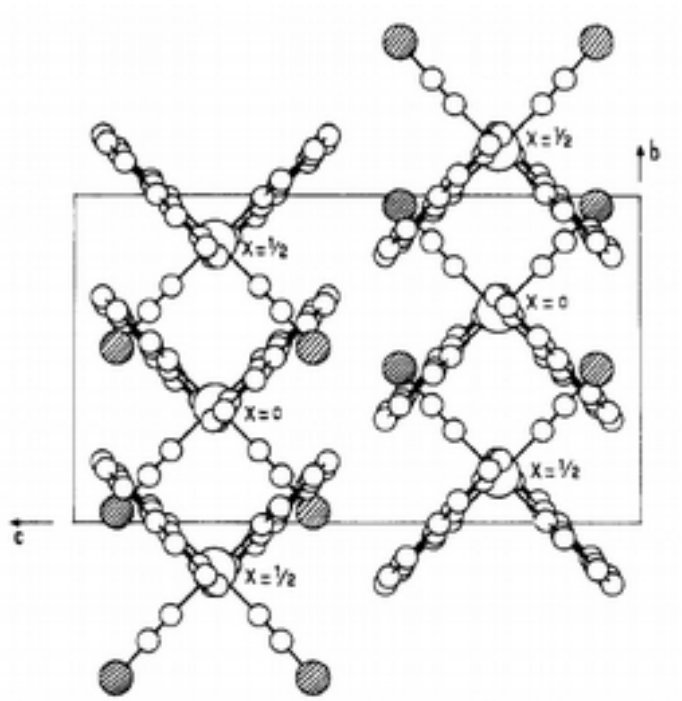

Fig. I.8: Projection of the molecular structure along the a axis for a $Fe(phen)_2(NCS)_2$ crystal. Reproduced from [32].

I.2.v X-ray absorption spectroscopy (XAS)

XAS is ideally suited to the investigation of SCO molecules[85], because it relies on the excitation of core electrons by X-rays, and therefore can provide information on both the electronic and local structure of a metal ion or a ligand. It can be divided into extended X-ray absorption fine structure (EXAFS)[31,86], that can provide relevant structural information when single-crystal X-ray diffraction is not available, including numbers, types, and distances to ligands and neighboring atoms from the absorbing element, and X-ray absorption near edge structure (XANES)[87,88], that yields insight mostly into electronic structure and symmetry of the metal site. A related technique is the wide-

angle X-ray scattering (WAXS), used to study short and medium range order, which makes it particularly useful for the study of SCO polymeric chains[17]. We describe more in details the application of this technique to our use in chapter III.

Other related X-ray techniques are the X-ray emission spectroscopy (XES) and resonant inelastic X-ray scattering (RIXS), which are powerful in elucidating the electronic structure, providing information on the electron energies, local geometry, spin and charge states[89].

I.3 Triggering the switch: a review

I.3.i Temperature

The main switching stimulus that was investigated historically and still the reference to this day, remains the thermal spin transition. The thermal switch occurs as long as the vibrational energy between the different spin states is of the order of magnitude of k_BT.[7]

As mentioned previously, the thermal spin transition curves can have very different shapes depending on the possible spin states and the cooperative behavior of the molecule.[38]

I.3.ii Pressure

Since the enthalpy H of a SCO molecule is expressed as H = E + pV, with E the energy, p the pressure and V the volume of the molecule, and since the volume of both spin states are different, the impact of the pressure on the spin transition was expected[53]. Granier *et al.* have shown on Fe-phen[90] and Hauser *et al.* on $[Fe(ptz)_6](BF_6)_2$[91] that the pressure will have only a small impact on the ligand field, which means that $p\Delta V_{HS\text{-}LS}$ will be the main factor in the effect. Increasing the pressure will generally increase the thermal spin-transition temperature, by favoring the low-volume form of the molecule, the LS state[54,91,92]. The influence of pressure can even impact the shape of the spin transition itself, as a unit cell contraction increases the number and the strength of intermolecular contacts[90], favoring cooperativity. However, some complexes like $[Fe(PM\text{-}PeA)_2(NCS)_2]$ form a new stable phase at high pressure, and this phase has a lower spin transition temperature, which yields an apparent decrease in the spin transition temperature when pressure is applied[93]. The effect can also depend on the hydrostatic or non-hydrostatic origin of the application of the pressure[54].

I.3.iii Electric and magnetic field

Electrostatic field control of the spin transition is still an open field. There is no doubt that electrostatic interactions plays a crucial role in the cooperative behavior of some SCO molecules[94], and therefore in the hysteresis, as seen for SCO molecules dispersed in polymeric matrices[95]. Results were obtained with linear junctions[96] and multi-metal complexes[97] but electrostatic field control of the spin state of bulk SCO samples still remains to be seen. Indeed, nanometric junctions or STM are necessary to produce large enough electric fields with reasonable voltages, which is one of the aims of this work.

On the other hand, magnetic field control of the spin transition was observed for bulk samples.[98] The application of a magnetic field favors the magnetic, HS fraction of the sample, shifting the transition temperature towards lower values. A significant drawback is that, similar to the pressure stimuli, intense fields have to be used to witness a sizable effect: a shift of only 2K is observed for a 5T field.[99,100]

I.3.iv Light

Light-induced excited spin state trapping (LIESST) is an effect of particular interest for us, in the light of our X-ray results described in a latter chapter. It was discovered in the case of solution by McGarvey and then in the solid state by Decurtins *et al.* in 1984[101]. It consists in the transition of a thermodynamic LS state to a metastable HS state by application of green light for Fe(II) (514nm for the $^1A_1 \rightarrow {}^1T_1$ transition, but other LIESST transitions are known[83]) at low temperature (usually below 60K). The metastable HS relaxes to the LS ground state, at a rate increasing with the temperature until no LIESST information can be written and detected in the system above the critical LIESST temperature, T_c(LIESST)[46] or T_{LIESST}. This, of course, depends on the methodology used, but a standard has been proposed by Létard *et al.*[46] to compare different systems. The Fe(II) complex holding the T_{LIESST} record at 132K is a $[Fe(L)(CN)_2].H_2O$ (L being a macrocyclic ligand) reported by Hayami *et al.*[102], therefore the practical considerations of the effect seems to be limited at the moment to spin transitions within the thermal hysteresis[103]. Since the initial studies, the LIESST effect was extensively investigated in several articles and reviews[53,83,104,105] noting among others phenomena that T_{LIESST} decreases when $T_{transition}$ increases and when the hapticity of the ligands decreases[41,46], the structural differences between the LIESST-induced metastable HS state and the thermal HS state[106], the dynamics and kinetic aspects of the process[57] until the full

phenomenon was described in all details[107]. It involves a cascade of excited states (by intersystem crossing[108]) illustrated in Fig. I.9, relaxing in a metastable HS state. The latest reviews on the subject favor the cascade ^{3}MLCT → ^{1}MLCT → $^5T_2$, which is suggested to be the main LIESST-inducing way[64,87,107,109]. Since the radiative transition HS → LS is forbidden, the metastable HS state can therefore exhibits very long lifetimes: for example, at 30K, 9 hours after illumination Fe-phen still exhibits a HS proportion of 94%[110].

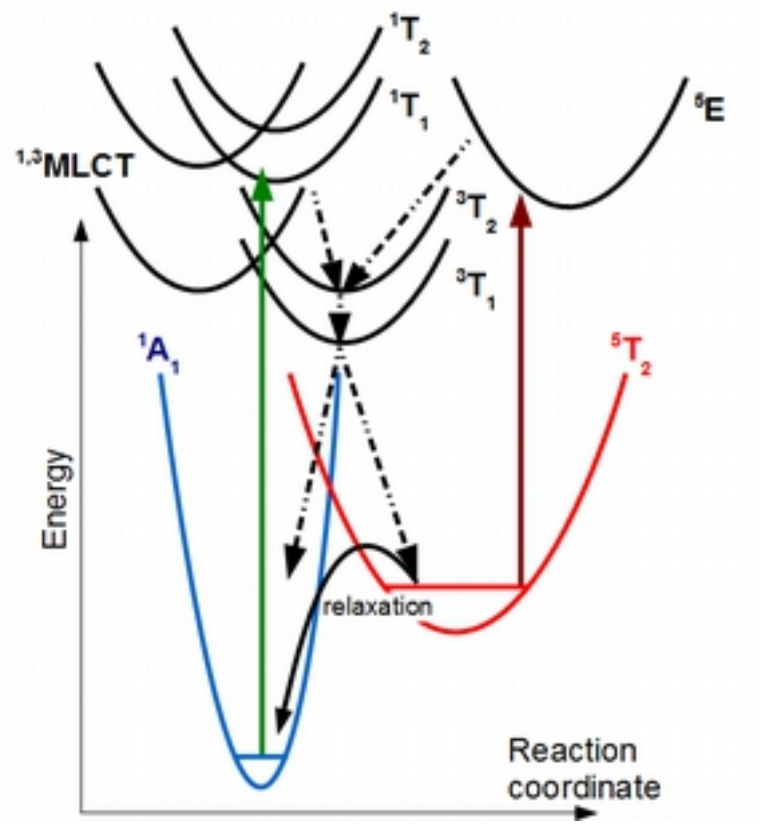

Fig. I.9: Typical energy diagram of the electronic states close to the LS and HS states. The ground $^1A_1$ LS state is excited by 514,5nm laser (green arrow) in a singlet ^1T_n state, that decays either directly back to $^1A_1$ or through a double intersystem crossing first to the triplet state ^3T_n, then to the metastable $^5T_2$ HS state or back to $^1A_1$. Also presented are the metal-ligand charge transfer (MLCT) states for the Fe(II) complexes containing ligands with π-systems[83,107]. The rev-LIESST proceeds similarly with an 820nm excitation (red arrow). Diagram inspired by several reviews on the subject[53,83,87,104,107].

The reverse phenomenon, rev-LIESST, is possible by the application of red light (820nm)[53]. In some particular cases, it is the LS state that can be the metastable state[111].

When the temperature is close to T_{LIESST}, the relaxation can be observed, as illustrated in Fig. I.10. The amplitude of the effect depends on the intensity of the light applied, and the excitation itself is a rather slow process at sufficiently low illumination values, with a maximum of metastable HS

reached in the range of 20 000 s.

The HS → LS relaxation can be understood as a non-adiabatic multiphonon process, where relaxation still occurs even at low temperature due to quantum tunneling. The phenomenological master equation for the LIESST process can then be, in a mean-field approach, expressed as[57]:

$$\frac{dp_{HS}(t)}{dt} = (1 - p_{HS})\, k_1(p_{HS}, I^{exc}) - p_{HS}\, k_2(p_{HS}, T) \qquad \text{(I.7)}$$

where p_{HS} is the relative population of the metastable HS state, $k_1(p_{HS}, I^{exc})$ is the light-induced transition rate, including a cooperative "response" factor depending on p_{HS}, a dependence, considered linear at first, on the intensity of the applied light, plus possibly a dependence on temperature usually neglected, and $k_2(p_{HS}, T)$ is the spontaneous relaxation rate of the excited state, including similarly a cooperative "response" factor depending on p_{HS}, and a dependence on temperature. k_2 itself can be decomposed, in the high temperature regime (>50K), as:

$$k_2(p_{HS}, T) = k(0, \infty)\, e^{\frac{-E_a}{k_\beta T}}\, e^{-\alpha\, p_{HS}} \quad , \qquad \text{(I.8)}$$

where $k(0,\infty)$ is the *apparent* spin-flip rate, E_a is the *apparent* activation energy and α the cooperative "response" factor, considered temperature independent by Enachescu *et al.*[57] in their temperature range (between 45 and 55K, as illustrated in Fig. I.10).

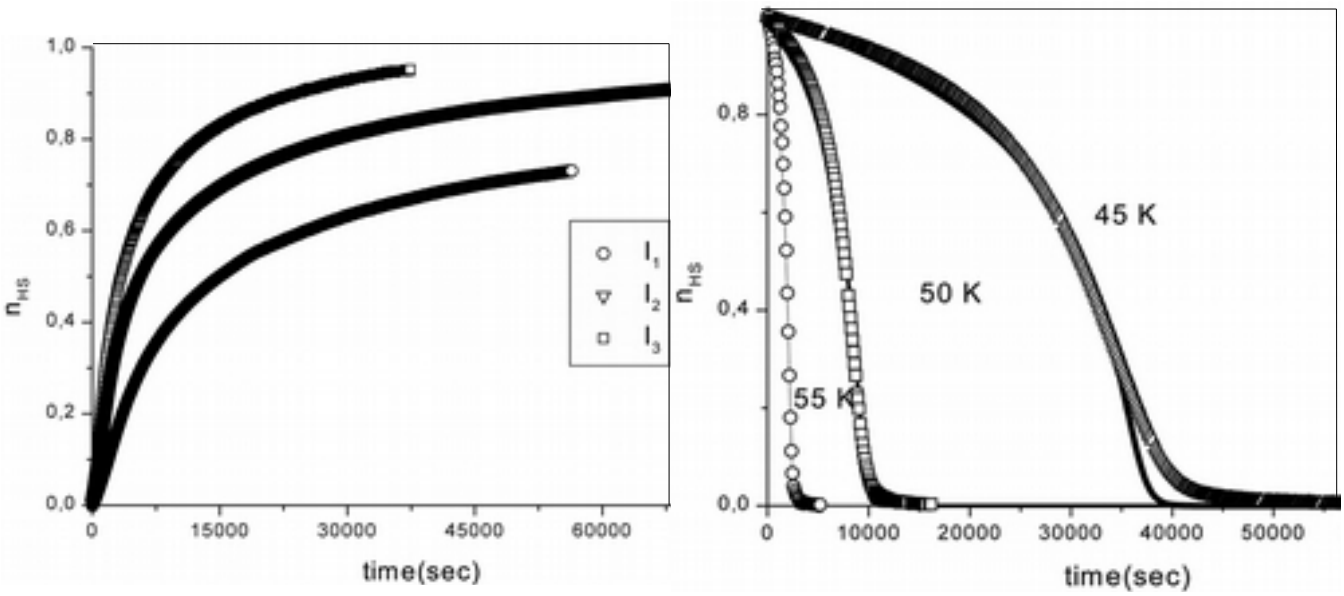

Fig. I.10: Intensity dependence of the LIESST effect depicted on the left panel ($I_1 > I_2 > I_3$), and relaxation of the metastable HS state on the right panel, data adapted from[57]. Lines correspond to fits using equations I.7 and I.8. The fit and the experimental results begin to diverge more strongly under 50K, as shown in the right plot.

"Apparent", because in fact at these temperatures the process corresponds to a thermally

activated tunneling from the HS to the LS state, as evidenced by Hauser *et al.*[83,108]. They proposed an elastic/vibrational model to account notably for the presence of relaxation at temperatures below 50K. In this framework, k_2 can be expressed as:

$$k_2(p_{HS},T)=\frac{2\pi}{\hbar^2\omega}\beta_{HL}^2 F_n(p_{HS},T) \quad , \tag{I.9}$$

where ħω corresponds to the vibrational quantum, β_{HL} is the electronic coupling matrix element, given by the second order spin-orbit coupling, in the case of Fe(II) complexes usually approx. 150 cm^{-1}, and $F_n(T)$ is the thermally averaged Franck-Condon factor, where n is reduced energy gap, a dimensionless measure of the vertical displacement of the potential wells relative to each other and $n=\Delta H^0_{en}/\hbar\omega + 2\Gamma(1-p_{HS})/\hbar\omega$ in the mean field approximation. At low temperature, k_2 becomes temperature-independent and can be expressed as:

$$k_2(p_{HS},T\rightarrow 0)=\frac{2\pi}{\hbar^2\omega}\beta_{HL}^2\frac{S^n e^{-S}}{n!} \quad , \tag{I.10}$$

where S is the Huang-Rhys factor, a dimensionless measure of the horizontal displacement of the potential wells relative to each other. At higher temperatures, the tunneling becomes thermally activated. However, the apparent activation energy is always smaller than the classical barrier. An illustration is given in Fig. I.11, and the model is more completely analyzed in the review paper by Hauser[83].

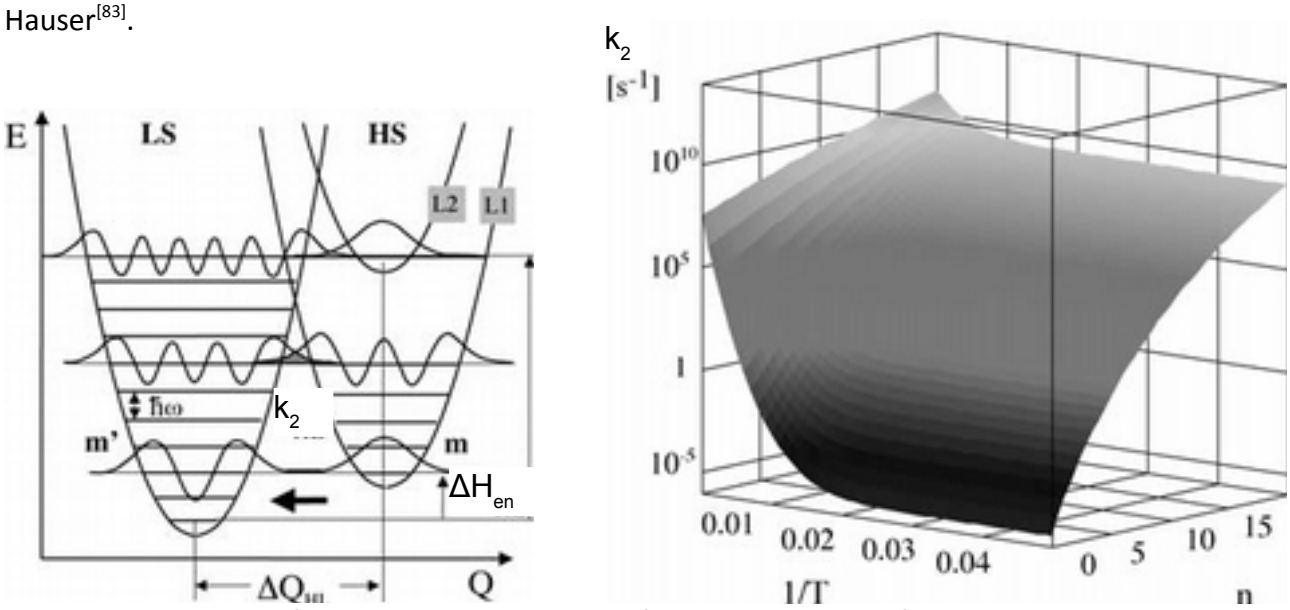

Fig. I.11: The left panel is a schematic view of the potential wells of the spin states along the totally symmetric normal coordinate. The zero-point energy difference, ΔH_{en} can be tuned by various external stimuli. The right panel is a plot of the calculated relaxation rate constant on a logarithmic scale according to the temperature and the reduced energy gap, n, with S=45, ħω=250 cm^{-1} and β_{HL}=150 cm^{-1}. Adaptated from[83].

Indeed, the LIESST effect is very sensitive to cooperative effects[59,104], which can generate thermal and optical hysteresis[95,112,113]. As a side remark, an "exotic" way to excite the sample is by radioactive irradiation[7,114], an effect labeled NIESST.

I.3.v X-rays

It was first observed by Collison *et al.*[115] that the application of soft X-ray irradiation leads to the trapping of the metastable HS state, an effect similar to LIESST. This effect, named by analogy SOXIESST, is believed to follow a process quite similar to the LIESST, with a cascade of excited states leading to the trapping of a HS state that would share the LIESST-induced metastable HS state properties. A severe drawback of this effect would be the breaking of the molecule under X-ray illumination, an effect called SOXPC, leading to the irreversible degradation of a part of the sample into a LS state compound[115]. Besides, a more recent study by Lee *et al.*[116] found no indication of the SOXIESST effect at 17K, even if the SOXIESST effect should appear at this temperature. Bernien *et al*.[117] has neither observed the effect, but their experiments were carried out at temperatures where the SOXIESST is not expected. Pillet *et al.*[64], that performed X-ray diffraction experiments on the LIESST-generated HS state using a MoKα source at 17 462 eV, have not observed the effect, possibly because it was masked by the LIESST. For all these reasons, despite the potential of the effect, the subject has not attracted a lot of interest so far. However hard X-rays (around 7000 eV) have also been shown to trigger the spin transition[118], promising an effect (the HAXIESST) with a higher penetration power.

While the use of X-rays (X-ray diffraction, EXAFS, XANES...) to study SCO molecules and processes has met a lot of success[31,34,77,85–87,107,116,119,120], the SOXIESST effect in itself has not received a lot of attention, and this is a strong motivation of the study as presented in chapter V.

I.3.vi Chemical stimuli

Different from the physical triggers reviewed until this point, the chemical stimuli can also be used to switch the spin state of SCO molecules.

Since the ligand field determines the spin state of the molecule, it is natural that the nature of the solvent in solutions of SCO molecules impacts the spin state, either directly[76,79] or by ligand exchange[76,95].

Usually, bond-breaking such as generated by SOXPC effect leads to irreversible spin-crossover. But

some recent examples of bridged compounds that exhibit a reversible bond-breaking -making SCO[121] exist.

Chemical stimuli are sometimes used in conjunction with physical methods, such as the strategy to alter the ligands by optical stimulus in order to obtain a similar effect as the LIESST but still present at higher temperatures, a promising effect called ligand-driven light induced spin change[53,122].

I.4 Why spin-crossover ?

I.4.i Nanoscale reach: how to obtain nano-sized SCO systems

The traditional methods of investigation usually involve SCO crystals or powders, a form that is incompatible with technological needs, for the construction of memory devices for example[123]. Furthermore, nanoscale SCO materials can exhibit new and interesting properties[120], as the results of this work will highlight.

- Nanoparticles, nanocrystals, and other nano-objects

To precisely control the size of SCO systems, the synthesis of nanoparticles and nanocrystals were carried out most commonly by the reverse-micelle technique[123]. It consists in the use of two water-in-oil or ethanol-in-oil microemulsions mixed to grow SCO nanocrystals of the desired size by varying the water/oil ratio and/or the concentration of the precursors[124]. The SCO molecules used for this purpose are mostly from the $[Fe(R\text{-}trz)_3]X_2$[125–127] and $[Fe(pz)][M(CN)_4]$[124] families, that are more networked molecules than really separate mononuclear SCO molecules. Nanocrystals still exhibit hysteresis[124,126] and LIESST[128], individual nanoparticles can be switched by light if their temperature is inside the thermal hysteresis loop[103], and surface treatments of the particles can modify the SCO behavior or provide additional functionalities[123]. The use of nanoparticles to electrically address SCO systems is seen as promising, using for example nanoparticles of core $[Fe(trz)_3](BF_4)_2$- surfactant shells[129] or directly nanocrystals of $[Fe(Htrz)_2(trz)](BF_4).H_2O$[130] to show the difference in conductivity between the two spin states and highlight the importance of the interfaces.

Among the “exotic” SCO nanoparticles system, one can cite the nanoball reported by Duriska et al.[131], a $Fe(II)(NCS)_2$-$Cu(I)(Tp^{4\text{-}py})(CH_3CN)$ association that exhibit thermally-induced, light-induced, and guest-induced (by complexation with an external, “guest” molecule) spin transition.

1-D nanowires or nanotubes of SCO systems have not been successfully produced[132] before 2012 (although enhanced shape anisotropy by confined growth[133] and patterning of nanocrystals[63,134] into 1-D-like systems were known), when the first example of the template assembly of a mononuclear SCO molecules into nanowires was reported by Martinho *et al.*[135]

A particular case of nanoscale SCO objects is represented by lateral junctions, illustrated in Fig. I.12. Single-molecule electron transport measurements can be performed using nanometer sized gaps of Au electrodes formed by electromigration of Au wires on the top of an oxidized Al gate, dipped in a solution of the SCO molecule functionalized by an anchor group. A difficult approach, investigated by Meded *et al.*[96]. After evaporation of the solvent, the transport properties of the system can be studied: the gate voltage can trigger the spin transition by charging the ligands. The group also observed a Kondo resonance.

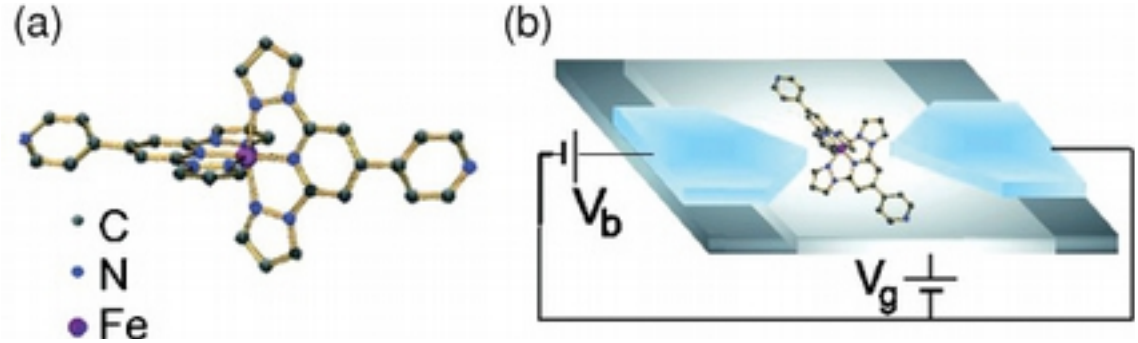

Fig. I.12: (a) The Fe(II)$(bpp)_2$ + pyridine anchor groups SCO molecule used for the (b) single molecule molecular junction setup. Reproduced from[96].

- Thin films and layer-built systems

Thin films are seen as a practical, technologically-friendly way to obtain nanoscale SCO systems. A wide range of techniques were experimented to obtain homogeneous thin films. Langmuir-Blodgett thin films are deposited from the surface of a liquid onto a solid by immersing (or emersing) the solid substrate into (or from) the liquid. It provides excellent thickness control and homogeneity, but the technique requires usually amphiphilic SCO complexes[136,137], and suffers from SCO layers stability issues[123]. Surface-assisted molecular self-assembly (self-assembled monolayer, SAM) is the formation of an organized molecular layer by adsorption on a surface. The thickness control and homogeneity are very good, and the layer stability is improved, but again few SCO molecules can undergo this process[138–140]. Drop casting[63,141,142] and spin coating[143] techniques allow for a wider variety of possible SCO molecules, but the solvent is usually a major drawback: it can be retained in the thin film, affecting transition properties, not all molecules are soluble and

finally the deposited layers lack order after the evaporation of the solvent[144]. Those experimental techniques also often use network/framework-type molecules, hindering the study of cooperativity of standard mononuclear SCO molecules.

Thermal evaporation, the method used in this thesis, is of course material-dependent. It can only be used with molecules that can resist decomposition under high vacuum, and some of our failed attempts proved that not all SCO molecules are suitable. As the first reviews on the subject highlight, a molecule suitable for thermal evaporation should be thermally stable, of low molecular weight, neutral, and with no solvent included in the lattice[145]. This severely restricts the range of possibilities, but it has several advantages: it avoids dilution of the molecules in a matrix or a solvent, it can be used in fully *in-situ* processes, it allows precise thickness control, down to isolated molecules, and it can be applied to patterning techniques[123]. The technique was only recently applied to SCO molecules, pioneered by our group with thick films of $Fe(phen)_2(NCS)_2$ in 2009[146]. LIESST behavior was found in vacuum-evaporated thin films of $Fe(H_2Bpz_2)_2(L)$[147,148] and an indication of the SOXIESST behavior was found recently on $Fe(H_2Bpz_2)_2$(2,2'-bipy)[148]. In the same family of molecules, $Fe(HB(pz)_3)_2$ thin films have been shown to be integrable into microelectrode devices, and their write-only memory capacities investigated[149]. Thanks to the possibility of depositing isolated molecules and ultra-thin films, the "pinning" effect of the surface on the spin state of the molecule was described in several articles[117,148,150–152], and the present work will describe this behavior more in details. This was confirmed by Bernien *et al*., who showed that using a weakly-interacting substrate like HOPG, the spin transition properties were preserved[153]. Similar results were found by Zhang *et al.*[150] on an copolymer surface PVDF-TrFe (however, the extant of the conclusions they reach is debatable). Electron-induced SCO of the second layer of a SCO molecule deposited on Au(111), where both spin states coexist[154], was shown to be possible[151]. It is representative of the novelty and difficulty of this technique, that these papers represent the *whole* corpus available about SCO molecules deposited on surfaces by thermal evaporation at the time of writing. Most of the field, in fact, has developed *during* the 3 years of this thesis. The X-ray absorption spectroscopy analysis technique is prominent among the analysis techniques employed in these studies[117,148,150,153].

To broaden the perspective, it was predicted that Fe-porphyrin, not a SCO molecule under normal conditions, could present a spin transition when thermally evaporated on constrained graphene[155,156].

I.4.ii Technological applications

With such a wide range of environment-sensitive properties and spintronic capabilities[1,2,18], it is not surprising that SCO molecules have attracted a significant interest from the community.

Thin films and nanoparticles can be patterned to suit the needs of device elaboration, in a complementary approach to those developed as described above[123]. It is interesting to note the diversity and the complementarity of the techniques used in this purpose: for example, the combined SAM/lithography technique of Molnár *et al.*[140] to produce nanoparticles of desired shape and size, or the combined drop-casting/stamp technique of Cavallini *et al.*[63] to produce 1-D-type structures. The use of this latter technique has further allowed them to reproduce CD-patterns with Fe-phen on silicon substrates[134] as shown on Fig. I.13.

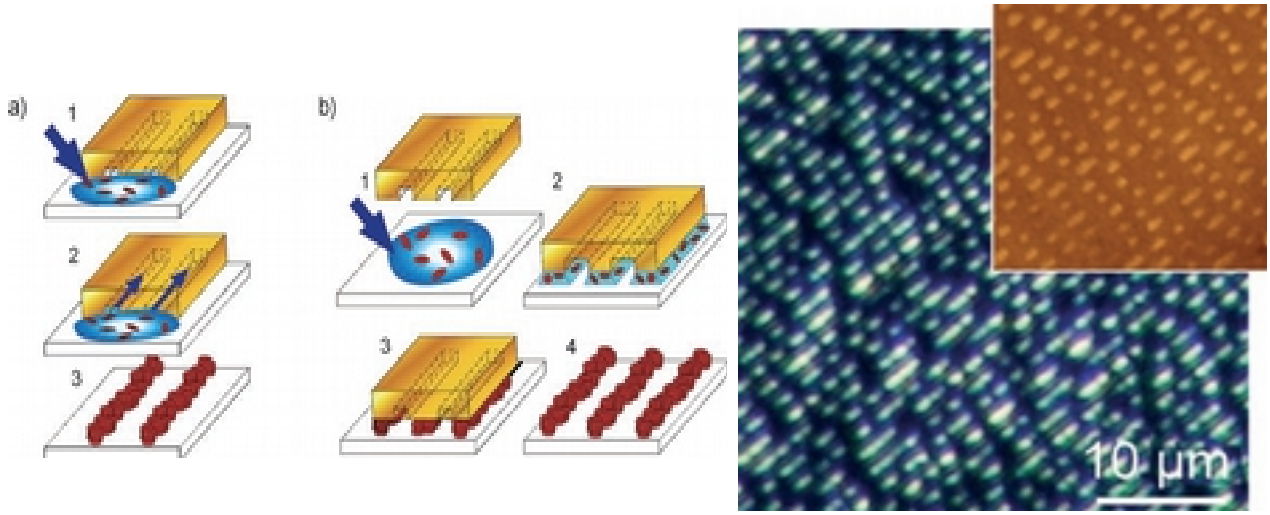

Fig. I.13: Schematic representations of (a) the micro-inject molding in capillaries process and (b) stamp-lithography controlled wetting process, and on the left a optical microscopy (insert AFM, vertical scale 0-80nm) picture of the pattern obtained by this latter process using a CD-pattern mold. Adapted from[134].

Some surprising developments have come from an unexpected exchange with biology, as Naik *et al.* have used a biomembrane to grow $[Fe(ptz)_6](BF_4)_2$ nanocrystals, using it as a natural stencil to transfer the patterns on Si wafers by conformational contact[157].

The practical applications range from moisture sensors[79] to digital displays[35], with an example of the latter illustrated in Fig. I.14. However, displays like the latter or presented by Kahn *et al.*[18] rely on thermal spin transitions and heating, a method not very suitable for practical displays. These real-world applications have just not yet reached industry, mostly because there are still scientific and technological barriers[120,158]. The parameter space where bistability can be reached is still too

small compared to industrial needs, and triggered effects such as LIESST happen at too low temperatures. It is unlikely that a "pure" SCO system will reach the requirements[158]. However, more "exotic" systems can be devised to make use of the high sensitivity to environment of SCO centers, for example in molecular sensing by guest-dependent SCO in a SCO framework[159].

Research applications, notably in the field of non-linear optics[158], are also considered.

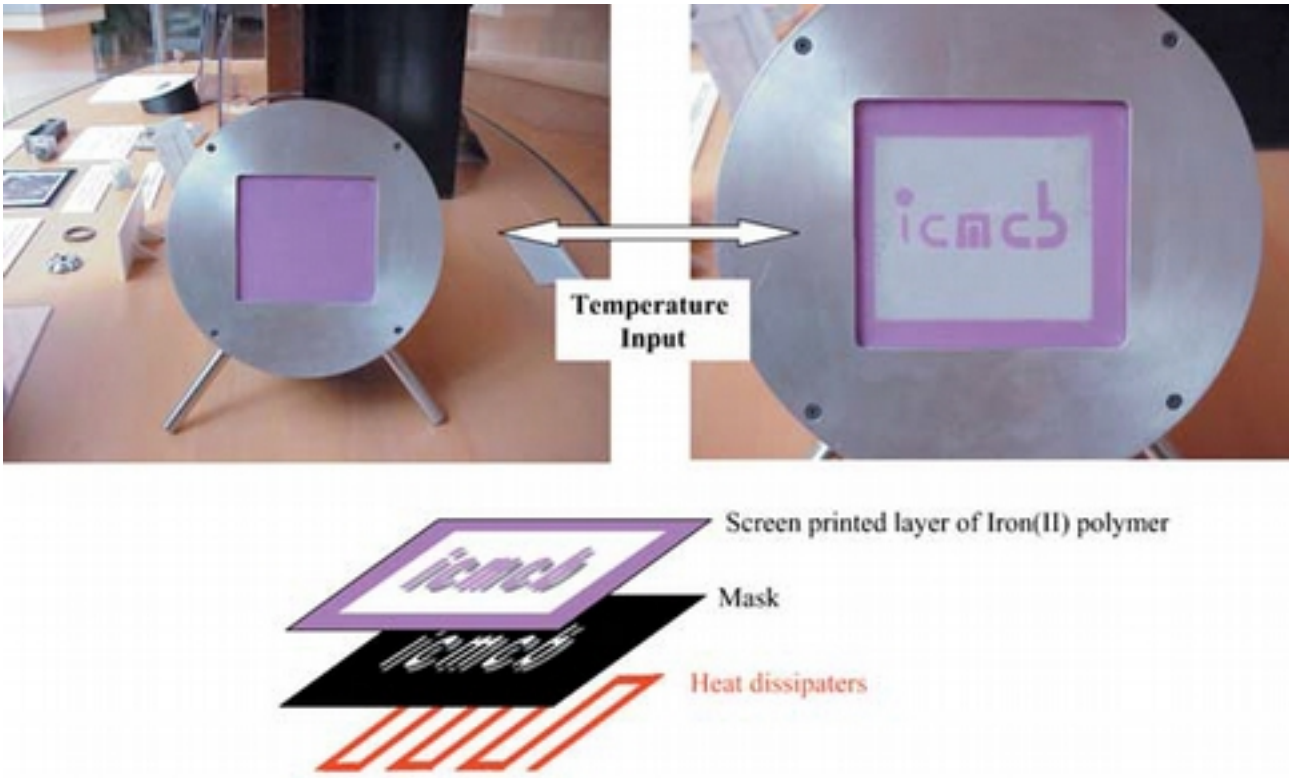

Fig. I.14: Picture of a temperature-driven lab display, copied from[158]. When turned on, the heat dissipaters increase the temperature of the mask, leading to a selective transition of the Fe(II) polymer from a purple LS state to a white HS state.

This work is therefore aimed at reducing the gap between the theoretical understanding of the phenomenon and the practical applications.

II Materials and Molecules

A fingerprint of the molecules investigated

This chapter is aimed at providing a background on the synthesis and the properties of the molecules used in this work, as well as on the surfaces employed. Fe-phen is a well-known, prototype compound, while Fe-pyrz has received less attention from the community. The surface state (roughness, impurities, orientation) is of course a determining factor for interface devices, and a fair bit of work was dedicated to obtain clean and smooth surfaces.

II.1 Molecules investigated: properties and synthesis

II.1.i Fe-phen

$Fe(1,10\text{-phenantroline})_2(NCS)_2$ (illustrated in Fig. II.1) is one the first SCO complex discovered. Reported by Baker *et al.*[8] in 1964, it was the object of a steady attention from the community ever since. It is the "historic" compound, with numerous studies and reviews paragraphs dedicated to it[38,84]. Fig. II.2 recalls the chemical and physical properties of the molecule.

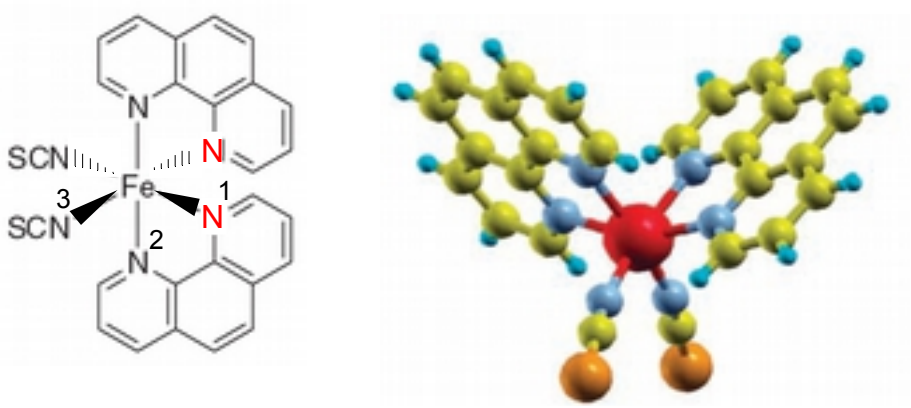

Fig. II.1: Representations of $Fe(phen)_2(NCS)_2$ molecule. As a note, the molecule is naturally present as a racemic mixture of the two chiral enantiomers. If 2 N from the 2 phen ligands are switched (as an example, the relevant N are highlighted in red on the left panel), then the resulting molecule while be different. This inversion in fact happens in the natural compound, it is therefore impossible to obtain an enantiomeric pure sample.

Formula	$FeC_{26}H_{16}N_6S_2$
Molar mass	532,2 $g.mol^{-1}$
Thermal spin transition temperature	$T_{1/2}$=176,3K[8]
Thermal hysteresis	1.8K, symmetric
Thermodynamic parameters	ΔH = 8600 $J.mol^{-1}$; ΔS = 48,78 $J.mol^{-1}.K^{-1}$ [45]

Fig. II.2: Chemical and physical properties of Fe-phen

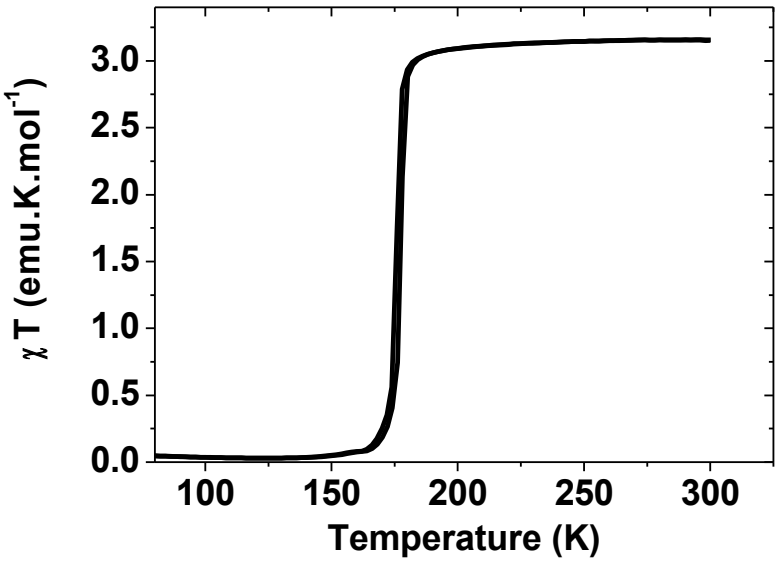

Fig. II.3: Magnetic susceptibility results for Fe-phen powder sample, acquired at 5000 Oe.

Effects sensitivity: LIESST[64]; Pressure[88,90]; SOXIESST[115]; HAXIESST[118]

Analysis techniques reported: DFT calculations for structure[36,66], thermodynamic parameters and vibrations[36,66,71,72]; Mössbauer[80]; Infrared[45,71]; UV-Visible; magnetic suceptibility[8]; X-ray Absorption Spectroscopy (experiment[85] and theory[119]); Raman[71,73]; NMR[50]; XPS[160]; X-ray diffraction[32]; Positron annihilation spectroscopy[38,161]; Muon spin rotation[162]

	LS[32] 130K	**HS (Thermal HS)[32] 293K**	**HS (LIESST HS)[110] 30K**
a (Å)	12,77	13,16	13,12
b (Å)	10,09	10,16	9,95
c (Å)	17,22	17,48	17,16
Volume (Å^3)	2219,0	2338,2	2240,1
Fe-N^1 (Å)	2,014	2,199	2,177
Fe-N^2 (Å)	2,005	2,213	2,184
Fe-N^3 (Å)	1,958	2,057	2,006

Fig. II.4: Crystallographic parameters and selected bond lengths for Fe-phen

All spin states have the same crystallographic system and space group, respectively orthorhombic and Pbcn D^{14}_{2h}, with four molecules per cell. The distorted octahedron of the HS state is particularly visible in the theoretical article by Reiher *et al.*[36]

The synthesis of this molecule impacts its spin transition properties, that is to say its shape and its completeness[32,35,80]. Two methods are commonly used: the “extraction” method, relying on the extraction of a phen group from $[Fe(phen)_3(NCS)_2].H2O$ (the one used in this study), and the

"diffusion" method, relying on the addition of a phen group to $Fe(NCS)_2$ in a methanol solution. Both methods leads to slightly different results due to the inclusion of solvents and impurities in the crystal lattice, but the extraction method yields the sharper and more complete transition of both.

Fe-phen was synthesized by G.Rogez at the IPCMS, following the standard extraction method established by Akabori *et al.*[163].

II.1.ii Fe-pyrz

$Fe\{[3,5\text{-dimethylpyrazolyl}]_3BH_2\}_2$ (illustrated in Fig. II.5) has received less attention in the spin-crossover field. The first tris(1-pyrazolyl)borate-based Fe(II) complex derivatives, including Fe-pyrz, was reported by Jesson *et al.* in 1967[9,164].This family of complexes is well-known in inorganic and coordination chemistry. Its spin-crossover properties were more thoroughly investigated in the following years, for example by Mössbauer spectroscopy in 1987 by Long et al.[81], giving insights in the field and temperature dependencies, but few studies were dedicated to the spin-crossover behavior of Fe-pyrz itself, although the family was the object of some reviews[165].

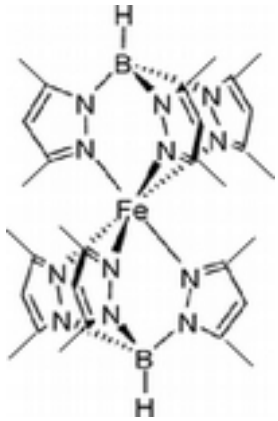

Fig. II.5: Schematic view of Fe-pyrz molecule. Unlike Fe-phen, this molecule is achiral.

Formula	$FeC_{30}H_{44}N_{12}B_2$
Molar mass	650,3 $g.mol^{-1}$
Thermal spin transition temperature	Cooling $T_{1/2}$=174K Heating $T_{1/2}$= 199K
Thermal hysteresis	26K at $T_{1/2}$, asymmetric (see Fig. II.7)
Thermodynamic parameters	Not reported

Fig. II.6: Chemical and physical properties of Fe-pyrz

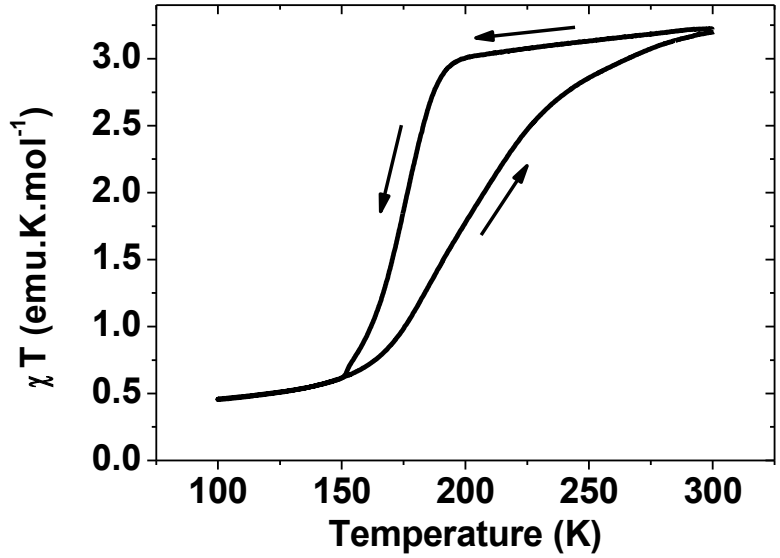

Fig. II.7: Magnetic susceptibility results for Fe-pyrz powder sample, acquired at 5000 Oe.

Effects sensitivity: Pressure[165]

Analysis techniques reported: Mössbauer[81]; X-ray diffraction[166]; magnetic susceptibility

	HS (Thermal HS)[166] 295K
a (Å)	8,82
b (Å)	10,22
c (Å)	10,79
α (deg)	116,4
β (deg)	85,2
γ (deg)	100,1
Volume (Å^3)	857,8
Fe-N^1 (Å)	2,19
Fe-N^2 (Å)	2,18
Fe-N^3 (Å)	2,15

Fig. II.8: Crystallographic parameters and selected bond lengths for Fe-pyrz

Fe-pyrz crystallize in a triclinic cell of the space group P-1, with one molecule per cell. Unfortunately, no LS X-ray diffraction is reported at the time of writing.

Fe-pyrz was synthesized by A.B. Gaspar from ICMOL using an improved method compared to that reported in the litterature[9]. The coumpound was synthetized under Ar atmosphere by adding dropwise 2 mmol of the salt K[HB(3,5-$(CH_3)_2$pz$)_3$] dissolved in methanol (15 mL) to a methanolic solution containing 1 mmol of $Fe(BF4)_2$•6H2O (5 mL). After complete addition of the K[HB(3,5-

$(CH_3)_2pz)_3]_2$ solution a white precipitate appears. The precipitate was washed with methanol and dried under vacuum, for a yield of 60%.

II.2 Surfaces

In order to build interface devices and systems, the quality of the surfaces where the SCO molecules are deposited must be carefully monitored.

II.2.i Native and thermal Si surfaces

After a serial of contaminated surfaces, we found out that our cleaning process needed to be improved. Therefore, we have treated Si(100)-native SiO_2 (called thereafter *native Si*) and Si(100)//500nm-thermal SiO_2 (called thereafter *thermal Si*) by a technique that protect them during the cutting process. The procedure followed is:

- Cover the substrate with protective laque.
- Cut the substrate with a cutting machine in the STnano class 100 clean room technology platform.

Then immerse the substrates in a serie of cleaning baths:

- Aceton, 5 min ultrasound.
- Aceton second bath, 5 min ultrasound.
- Ethanol, 5 min ultrasound.
- Isopropanol, 5 min ultrasound.

- Dry the substrates with N_2.
- 30 min oxygen plasma cleaning at 100W.

As a note, seven substrates were treated by batch. The result is presented in Fig. II.3.

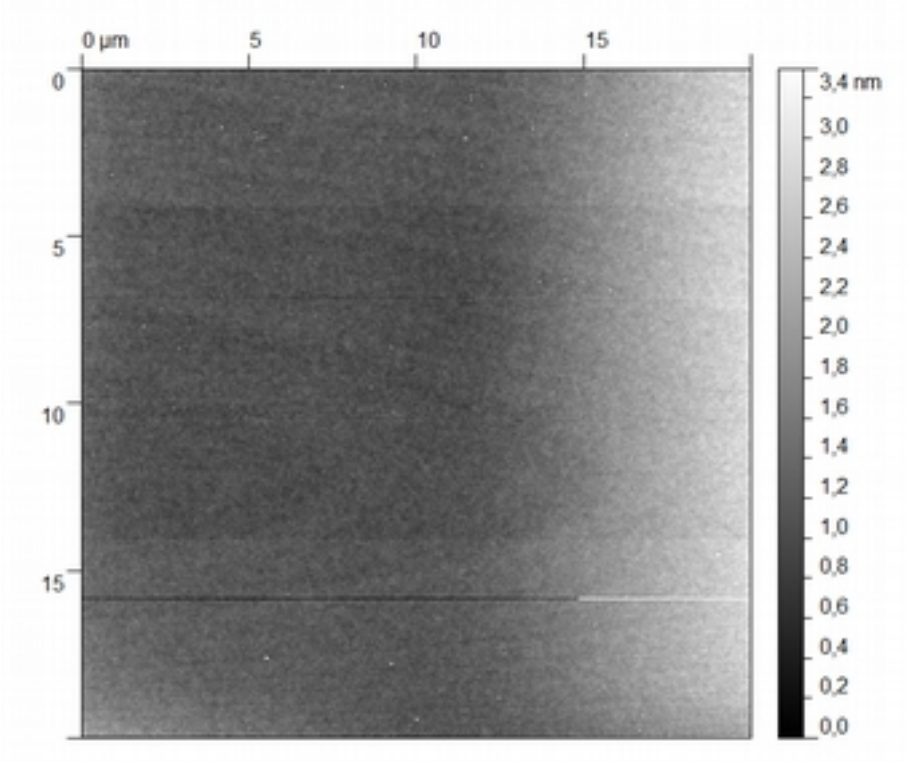

Fig. II.3: AFM picture of a Si/500nm SiO_2 surface treated with the process described above. Roughness RMS = 0,13nm, indicating a flat surface.

II.2.ii Monocrystal surfaces

The Cu(100) single crystals used in this work were cleaned in situ using a succession of light Ar^+ ion gun sputtering and sample annealing at 450°C. During XAS measurements, the quality of the cleaning was checked by Auger spectroscopy and during STM measurement directly by the STM. We obtained rather large terraces and a surface free of contamination, even after Fe-phen deposition (as observed in chapter IV). The Cu(100)//Co surface was made by thermal evaporation of Co on the previous Cu(100) surface, checked by Auger spectroscopy. We obtained approx. 12ML and 24ML of Co on Cu(100), but the subsequent Fe-phen deposition exhibited surface contamination by what we believe to be phen groups, as shown in chapter V.

III Methods and Machines

The experimental methods employed, practical considerations

This chapter is a description of the synthesis and measurement methods and machines, in order to provide relevant information for the following chapters. We also discuss the thermal evaporation technique used to produce the low-dimensional samples investigated in chapter IV, V and VI.

III.1 Thermal deposition

III.1.i The hybrid system and the Plassys setup

Thick films studied in IV and VI were deposited in two experimental setups. The hybrid system is a complete deposition system including a N_2-atmosphere glove box and separated chambers for metals and organics deposition, pictured in Fig. III.1. The sample plate holders in each chamber can be heated, and the sample plate holder in the metal deposition chamber can additionally be cooled down using a liquid N_2 system, allowing the deposition of the top electrode of our devices presented in chapter VI at substrates temperatures of -90°C. UHV is maintained by ion pump, turbomolecular pump, and before (but not during) deposition, titanium pump.

The Plassys setup, also pictured in Fig. III.1, is a simpler system, consisting in a single deposition chamber, and no substrate heating or cooling capabilities.

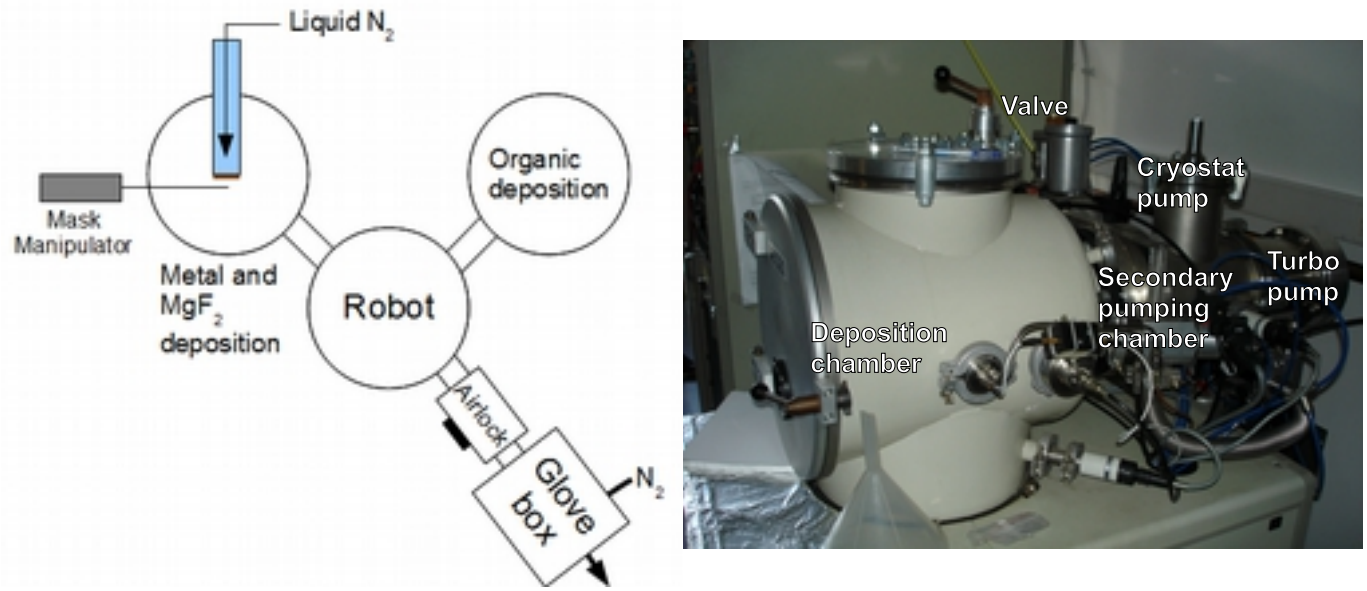

Fig. III.1: Left panel is a schematic view of the hybrid system. The samples enter/exit by the airlock. The right panel presents a picture of the Plassys setup. The samples enter/exit directly by the deposition chamber.

III.1.ii Thermal deposition

The films were deposited by thermal evaporation from evaporation cells, illustrated in Fig. III.2 for both systems. Hybrid cells are water-cooled, and have an elongated alumina crucible, which is heated by resistive wires coiled around the crucible. Base vacuum was 10^{-10} mbars in both chambers, and during deposition the pressure reached 10^{-8} in the metal deposition chamber and low 10^{-7} in the organic chamber. Plassys cells were tantalum boat crucibles, directly connected to the electrodes that heated the crucible. Base vacuum was 10^{-9} mbars and during deposition the

pressure reached high 10^{-7}mbars. Isolated molecules and thin films of Fe-phen, as presented in chapter IV, were deposited using an in-situ thermal evaporation cell of the STM system (180°C), which are similar to the hybrid cells except that they do not possess a water cooling. Thick films of Fe-pyrz, as presented in chapter IV, were deposited using the Plassys setup with a deposition temperature of 260 to 270°C. Deposition of the samples presented in chapter V was carried out using the STM or the hybrid cell, with a deposition temperature of 250°C.

Unfortunately, we have not been able to follow the Fe-phen deposition by a quartz microbalance, as it gave incoherent results, but the Fe-pyrz depositions were followed by quartz microbalance.

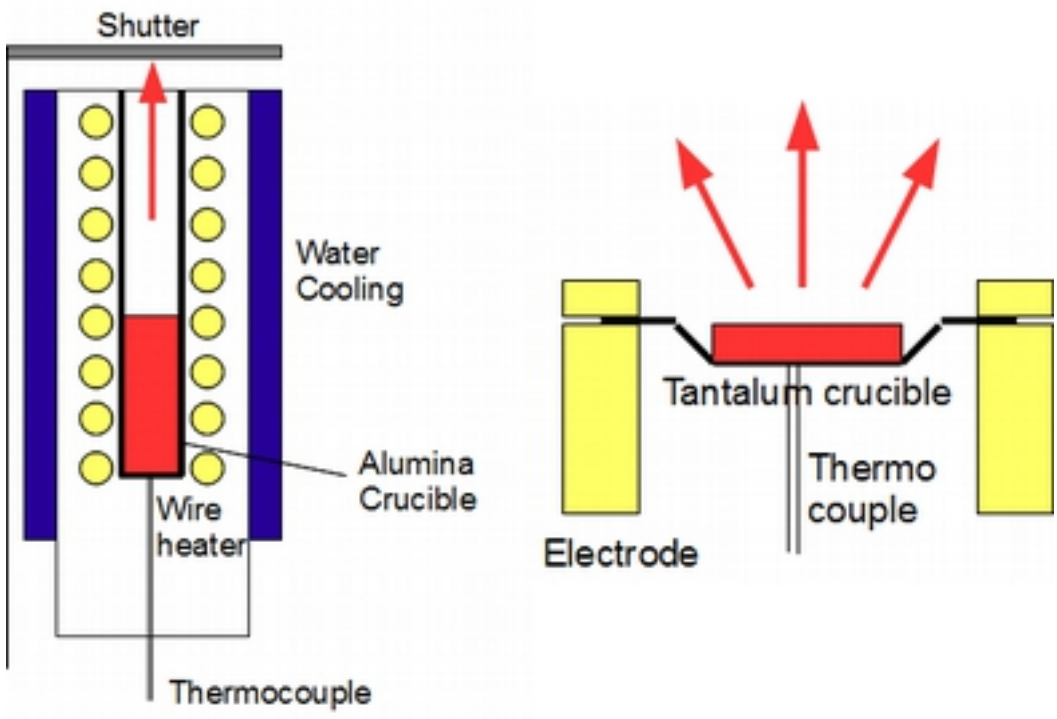

Fig. III.2: Schematic views of a hybride-type thermal deposition cell (left), also used for XAS experiments and a Plassys-type thermal deposition cell (right).

III.2 Thickness determination

A very important point for our study is the precise determination of the thickness of the thick film samples deposited. To achieve this goal, we have used mostly 2 techniques: X-ray reflectometry (also called X-ray reflectivity) and profilometry.

III.2.i X-ray reflectivity

X-ray reflectometry is a technique based on the observation of the intensity of the X-ray beam reflected by samples at grazing angles[167]. It is a non-contact technique for 2-200nm thicknesses with a precision of about 0,1-0,3 nm. A monochromatic X-ray beam of wavelength λ irradiates a

sample at a grazing angle θ, and the reflected intensity at the angle 2θ is recorded. The reflection at the interfaces will depend on the different electron density of the successive layers, which can be compared to the reflective index of classical optics. Above the critical angle of total reflection, the reflection from the different interfaces gives rise to interference fringes, from which can be extracted not only the thickness of the layer, but also other parameters like the roughness that have not been the focus of this work. This technique was used mostly to determine the thickness of Fe-phen samples in chapter VI. The Fe-pyrz samples were too rough to extract a thickness value.

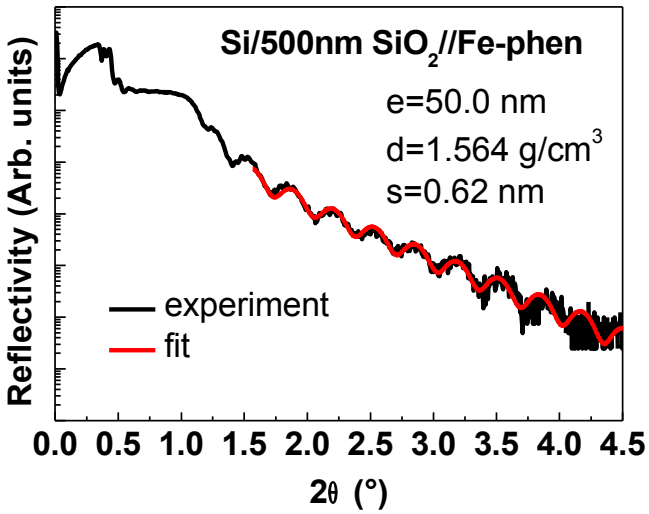

Fig. III.3: Plot of an X-ray reflectivity experiment (black), with a fit using the reflectometry equations (red). The fitted RMS exhibit the low roughness typical of Fe-phen thick films.

III.2.ii Profilometry

Profilometry is the simple use of a weighed diamond stylus brought into contact with the surface in order to draw profiles. Our measurements were done in the ST-Nano class 100 clean room using a Veeco Dektak 150 Surface Profiler, with a vertical resolution of 5nm. We have used notably this technique to measure the thickness of Fe-pyrz thick films.

III.3 Microscopy

III.3.i Atomic Force Microscopy

The atomic force microscopy (AFM) experiments were held at the IPCMS with a Digital Instruments Multimode SPM installed in 1997, in tapping mode. The experiments were held in the air and at ambient temperature. The tips were Nanosensors non-contact PPP-NCHR silicon tips.

III.3.ii Scanning Tunneling Microscopy

The scanning tunneling experiments (STM) were performed at the Karlsruhe Institut of Technology, using a custom-made liquid-helium-cooled 4K-STM[168], in ultra-high vacuum (under 2.0×10^{-10} mbar). The tips were prepared by chemical etching of a tungsten wire followed by flashing in ultra-high vacuum. The surfaces were cleaned by several cycles of Ar^+ sputtering and annealing, as described in II.2.ii. Fe-phen was then deposited on the surface by thermal evaporation at 180°C.

The scanning tunneling spectroscopy relies on the measurement of the tunneling current between a conductive tip and the probed surface. This tunneling current depends on the distance between the tip and the surface and the density of states of the surface, which means this technique can not only yield information on the shape of the sample, but also on its electronic properties.

III.4 X-ray photoelectron spectrocopy (XPS)

The principle of the XPS technique is the emission of electrons from atoms by absorption of photons. Photoelectron emission occurs when a photon transfers its energy to an electron, and since we know the energy of the photon and the spectrometer work function it is possible to obtain the electron binding energy by measuring the kinetic energies of the photoelectrons. The experiments were performed and analyzed by Yeuk Ting Law and Won Hui Doh of the team of Dr. Zafeiratos, at the LMSPC, with an Al Kα (1486.6 eV) source mounted on a Thermo VG scientific T190.

III.5 X-ray absorption spectroscopy

As already noted in the introduction, XAS is a powerful technique to investigate SCO, since it is element specific and measures the transitions from core electronic states of the metal to the excited electronic states (lowest unoccupied molecular orbitals, LUMO) and the continuum[169]. For Fe, the XANES used in this study relies on the excitation of a 2p electron to unfilled 3d orbitals, that gives rise to two absorption peaks: the L_3-edge for the 2p electron with J=3/2 and the L_2-edge for the 2p electron with J=1/2. The multiplet structure of those two peaks is typical of their chemical and electronic environment. Calculations in the last point of this part present the influence of Fe oxidation state and Fe geometry on Fe-L_3 and L_2 edge absorption spectra.

III.5.i Technical details and the DEIMOS beamline setup

The technique was carried out at the DEIMOS beamline of synchrotron SOLEIL[170]. XAS spectra were acquired in total electron yield mode, which means the photocurrent resulting from the ejection of photoelectrons from the sample is monitored[171].

Aside from the cryostat where the samples were illuminated, the beamline possess a full ultra-high vacuum environment for the in-situ deposition of the samples, plus analysis techniques such as STM and Auger spectroscopy. The powder samples were prepared by pressing the powder onto a tantalum plate that was adjusted onto a copper sample holder, which was then mounted in the cryostat for measurement. The thick samples were adjusted to the copper sample holders using tantalum wires, then transferred into the cryostat for measurement. The thin films were synthesized in-situ on Cu(100) and Cu(100)//Co substrates prepared as described in II.2.ii, and solded on tantalum plates adjusted to the copper sample holders, then transferred into the cryostat for measurement. The sample area was maintained in the dark unless noted.

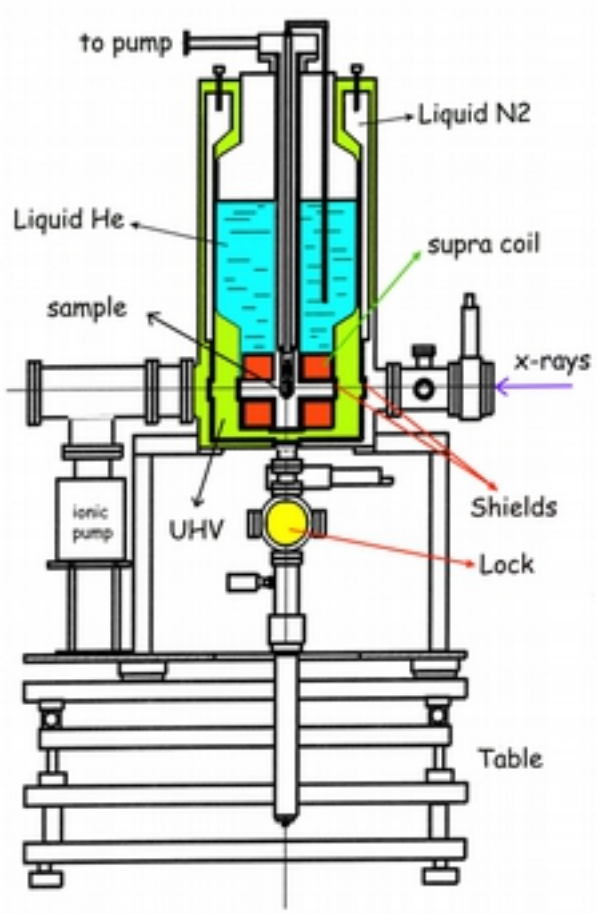

Fig. III.4: Schematic view of the experimental setup of a temperature-dependence magnetic field-dependence XAS beamline. The DEIMOS beamline include several preparations chambers under ultra-high vacuum after the lock. Adapted from the IPCMS website.

The beam structure and intensity were determined in chapter V to be of high relevance to the effects observed, notably the SOXIESST. We have acquired the results presented in chapter V of this thesis during 3 runs. The first run utilized an estimated photon density I_0=6.1×10^8 ph.s.mm^{-2} in single bunch filling mode: a single bunch of 20 mA is circulating in the synchrotron ring, illuminating the sample at a frequency of 0.847 MHz; for the second run I=6.4×10^9 ph.s.mm^{-2} ≈10I_0; and for the third run I=1.2×10^{10} ph.s.mm^{-2} ≈20I_0 both in hybrid filling mode: in this mode, 3/4 of the ring is filled with 312 bunchs of 1,36 mA, with the last quarter of one single 5mA bunch, illuminating the sample at a frequency of 352.2 MHz. The diaphragm openings were kept constant throughout the three series of measurements. The results presented in chapter IV used the same parameters as the third run.

III.5.ii The CTM4XAS program

CTM4XAS is a 2010 charge transfer multiplet program for the analysis of transition metal 2p and 3p core level excitations[172]. It is based on a semi-empirical approach that includes explicitly the

important interactions for the calculation of L edge spectra. This includes the core and valence spin–orbit couplings, the core-valence two-electron integrals (multiplet effects) and the core hole induced charge transfer effects. The CTM4XAS program uses as input the optical parameters Dq, Ds and Dt (with 10Dq the crystal field parameter) to characterize the desired geometries. Fig. III.5 illustrates the results obtained through calculations for (a) Fe^{2+} O_h symmetry with 10Dq = 1.1 and 2.2 eV and C_4 symmetry with the same 10Dq parameters and Dt = Ds = 0 (b) Fe^{3+} O_h symmetry with the same 10Dq parameters (c) Fe^{2+} C4 symmetry with the same 10 parameters and Dt = Ds = 1 eV.

The sensitivity to the electronic and geometric environment of the X-ray absorption of the Fe center is clearly visible.

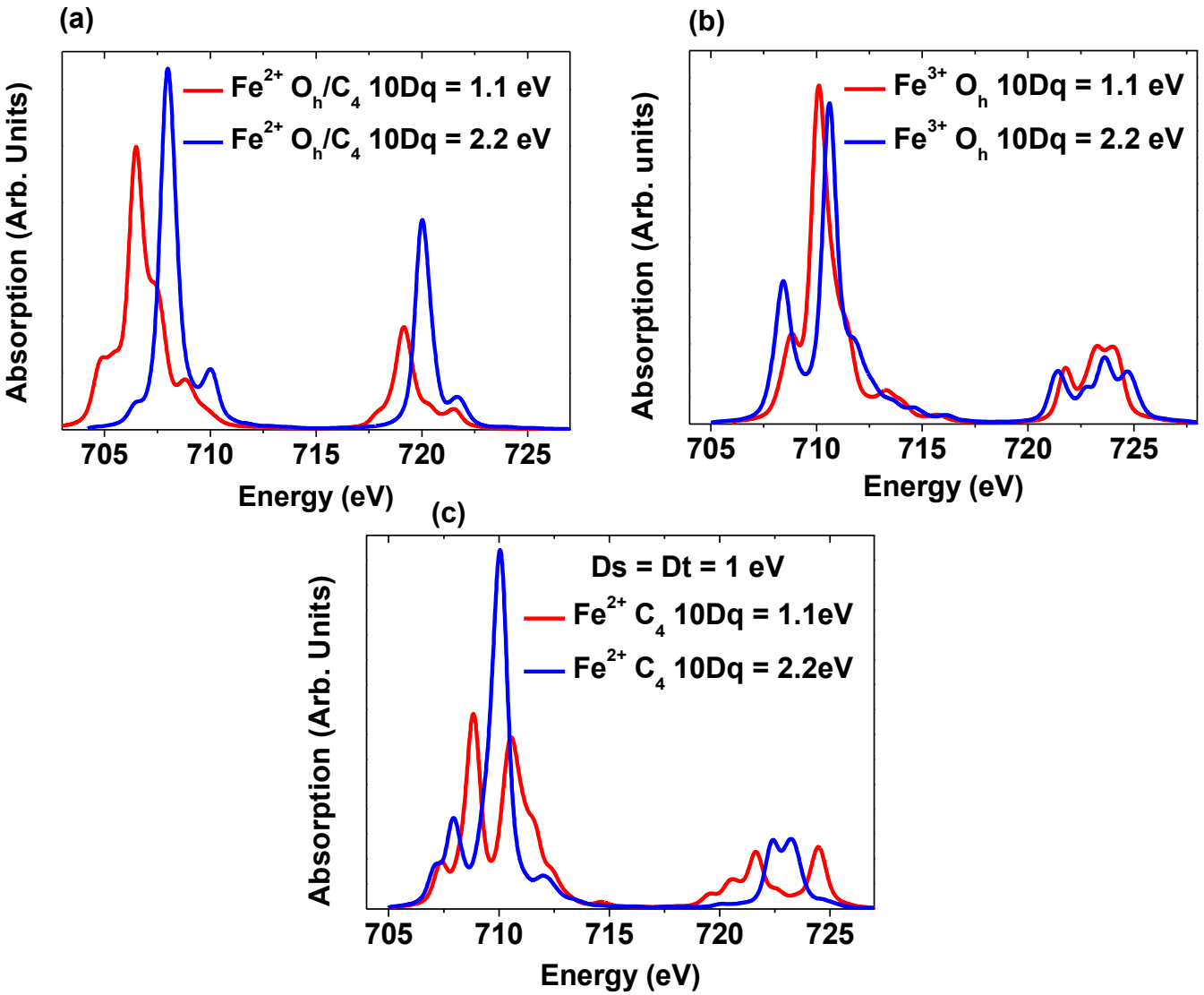

Fig. III.5: Calculated XAS spectra for (a) Fe^{2+} O_h symmetry with 10Dq = 1.1 and 2.2 eV and C_4 symmetry with the same 10Dq parameters and Dt = Ds = 0 (b) Fe^{3+} O_h symmetry with the same 10Dq parameters (c) Fe^{2+} C4 symmetry with the same 10 parameters and Dt = Ds = 1 eV, with no charge transfer for any of the calculations.

III.6 Optical absorption experiments

The optical absorption and transmission experiments were performed at the IPCMS on a Perkin-Elmer Lambda 950 in operation since 2007. It allows the measurement of the absorption and transmission of UV-Visible-Near Infrared light by thick films or powders with a wavelength resolution of 2 nm. For the thick films of Fe-pyrz deposited on quartz the absorbance and transmission were acquired, for the powder Fe-pyrz adjusted between two quartz plates the absorbance was acquired by measuring the reflectance with an integrating sphere.

III.7 Electrical testing of multilayers

The electrical conduction measurements were carried out on the so-called “Fert” bench, a setup specially designed for the measurement of devices under varying external conditions. A schematic view is presented in Fig. III.6. The device samples pads are connected with aluminum wires to the chips, and placed in the sample area, an area that was then primary pumped: the chapter VI elaborates on this subject. Temperature control was provided by a liquid He-cooled cold finger and an electric heating resistance, for a temperature range of 10 to 315K. Magnetic field control was provided by two coils on each side of the sample area, producing a field parallel to the bottom electrode direction, between -2 and 2T. The control and analysis capabilities were provided by a computer via a multiplexor, allowing the semi-automatic successive measurement of the electrical properties of several junctions.

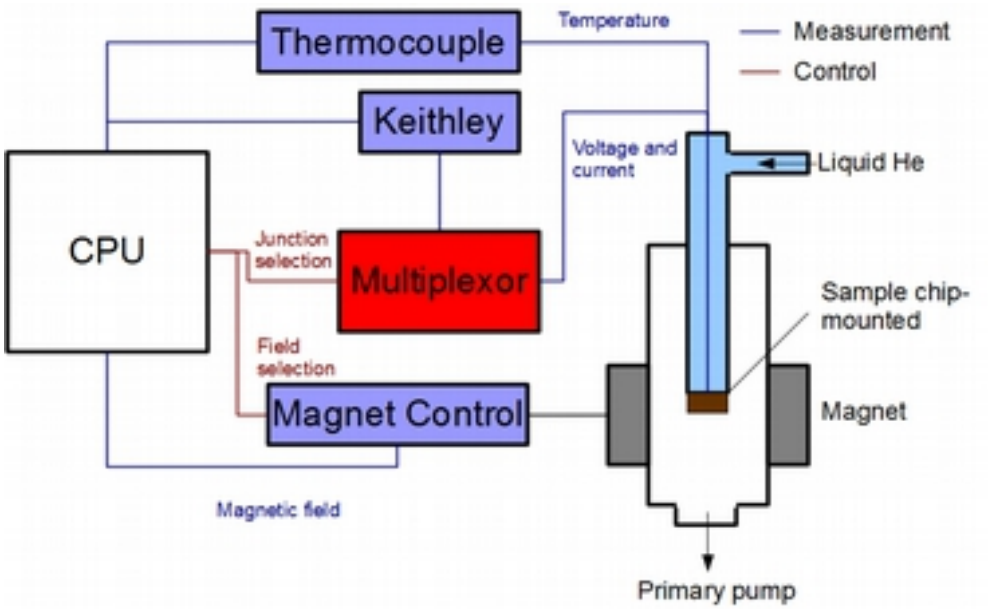

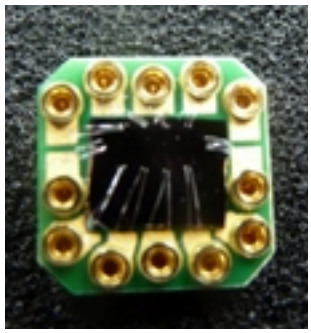

Fig. III.6 Schematic view of the Fert bench experimental setup. The wire connections from the sample are connected to the Keithley multimeter via the multiplexor junction selection. Several measurement modes are available: 2 points, 4 points, Van der Pauw. On the right is a picture of the chip-mounted sample, with 4 junctions per sample.

An improved version of this multiplexor, presented in Fig. III.7, was installed in an improved bench. This version made possible the full-automatic measurement of several junctions successively, and this for two samples instead of only one.

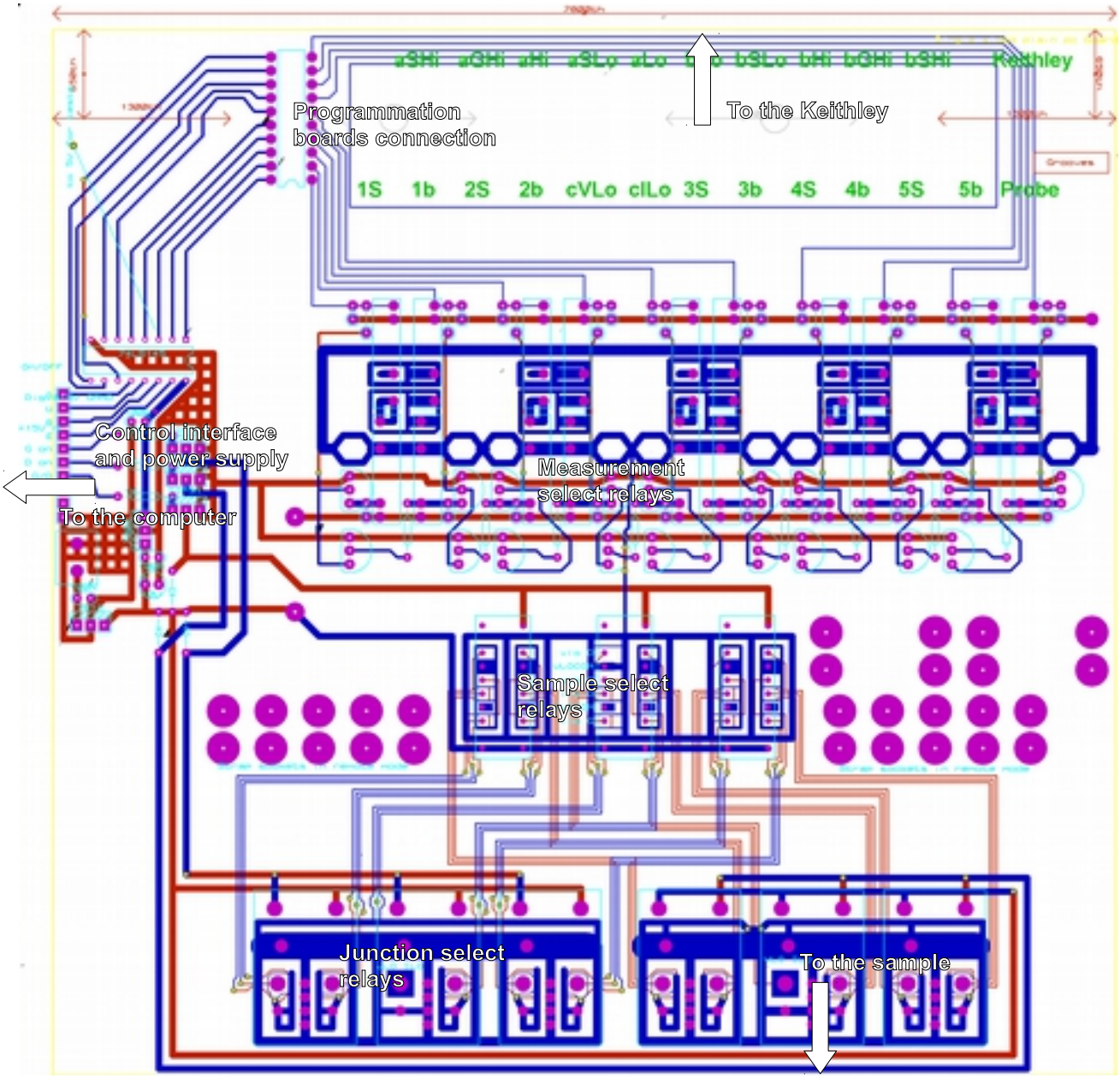

Fig. III.7: Cardboard design of the improved multiplexor. Note the grounding (thick blue) around the relays, to prevent induction and perturbations of the signal. The measurement type (2 points, 4 points, Van der Pauw) is set by programming boards at the top, that interface with the Keithley multimeter. The control interface with the computer then directs the different relays group to select the desired measurement type, on the desired junction and on the desired sample.

The resistance of the bottom electrodes was measured by simple 2 wires mode. The junctions electrical properties were measured by the 4 points method. It is a technique that get rids of the resistance of the contacts. Two points generate a current through the desired material. Two points between them measure the voltage. We then deduce the resistance of the material between the two closest points, as shown in Fig. III.8. The practical application of this technique to our devices is precised in chapter VI.

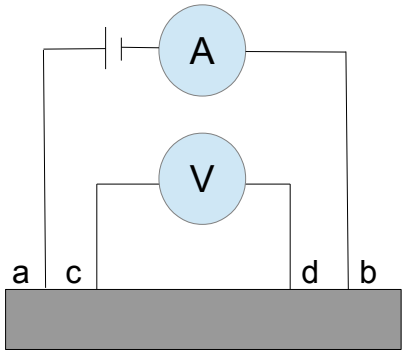

Fig. III.8: Schema of a 4 points measurement. Current is applied between (a) and (b), and voltage is measured between (c) and (d).

IV Insights on thick films and isolated SCO molecules

Results and discussion

Traditional electronics are reaching their limits, as the size of the magnets used to store memory bits begin to reach physical boundaries. Therefore, a solution would be to use individual SCO molecules to write information in the spin state. For this, we need to investigate the effect of low dimensionality on the transition mechanisms: does a thin film behaves like the bulk? Are the behaviors of thick films, thin films and isolated molecules identical? What is the impact of a surface on the transition? In this chapter, we will consider in a first phase the results of the study of isolated Fe-phen molecules and thin films by STM. We have succeeded in switching isolated SCO molecules deposited on surfaces, and the influence of the surface is essential. Unfortunately, we find that the STM technique is ill-suited to the study of films thicker than a few monolayers, therefore in a second phase, we will discuss the results of Fe-pyrz and Fe-phen by AFM, SQUID and IR-Visible absorption, and the limits of these techniques.

IV.1 A word on Fe-phen molecules on surfaces.

IV.1.i Single molecules on Cu(100) and Cu(100)//CuN surfaces

Fe-phen molecules have been sublimed at 180°C, and then adsorbed on Cu(100) and Cu(100)//CuN surfaces kept at ambient temperature. 4K STM pictures were then acquired, such as shown in Fig. IV.1 for Cu(100). We identify the two lobes as the "phen" groups of Fe-phen, and the molecule is adsorbed on the surface through the sulfur of the NCS groups. Two conformations can be observed: an "open" form, conformation I, and a "closed" form, conformation II. One can observe that even if the adsorbed molecules seem to follow 2 perpendicular crystallographic directions, both conformations can be observed on each axis. We suggest that the difference in conformations arise more from the local adsorption geometry of the sulfur bonding atom. We can identify the spin state of each molecule by scanning tunneling spectroscopy (STS): the conformation I presents a Kondo peak at the center of the two lobes, while the conformation II and the Cu substrate do not exhibit such a feature. The Kondo peak implies the presence of a magnetic "impurity" screened by the conduction electrons of the surface[173], therefore we can identify the conformation I as HS and the conformation II as LS. This feature has also been found in parallel by Gopakumar *et al.*[142] on a second-layer SCO molecule on Au(111), on single molecule magnets by Komeda *et al.*[174], and theorically and experimentally by Meded *et al.*[96] on charging the ligands of a single Fe(II) SCO molecule across a gated device, which supports our interpretation. As observed on Fig. IV.1, both spin states coexist on the Cu(100) surface. Further evidence for the coexistence of both spin states on the surface are the XAS results, developed in chapter V. The width of the Fano lineshape of a Kondo peak is proportional to the Kondo temperature[175], therefore a fit of the Kondo peak yields a Kondo temperature of 317K, which underscore how strong is the electronic hybridization between the Fe spin and the Cu substrate is. Despite applying high local electric fields (up to several GV m^{-1}), high tunneling voltages (±4 V) and high current densities (up to 1 µA per molecule) in the junction of the STM, we have not been able to switch the molecule. We suggest that this strong interaction is what prevents the spin state from switching. We define these molecules as "pinned": the Fe-phen molecules in a "pinned" state exhibit a spin state (either HS or LS) that cannot be switched, by electrical stimuli as presented in this part, and neither by thermal, light or X-ray stimuli, as presented in chapter V.

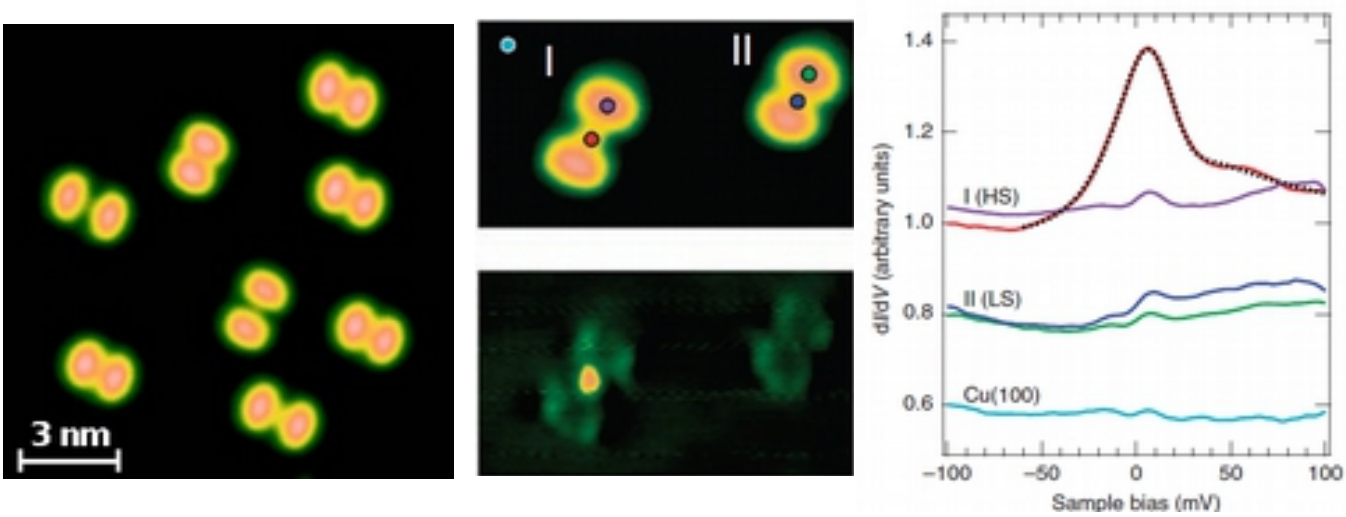

Fig. IV.1: Left panel exhibits a STM image of isolated Fe-phen molecules on the Cu(100) surface. We believe that the molecules sit phen-up, S-down on the surface, due to the strong affinity of S with the Cu surface. The two lobes correspond to the two phen groups. In the middle panel are compared the STM picture (top) and the dI/dV picture taken at +10mV (bottom) of the two conformations, proving that the Kondo resonance is positioned at the center of the conformation I molecule. The right panel is a scanning tunneling spectroscopy (STS) plot of the center and lobe positions for both configurations, and the Cu(100) substrate: the colored lines correspond to the place with the colored dot on the top middle panel. The black dotted line denotes a Fano lineshape fit for the Kondo resonance.

It appears then necessary to reduce the substrate-molecule interaction to allow for tip induced transition. To this end, we inserted a monoatomic CuN layer to reduce the hybridization[176]. We still witness a coexistence of two conformations, α and β, as illustrated by Figure IV.2. But their shape differs, this time, by the presence or the absence of a "bump" in the center of the molecule. By using the previous method, we can identify each of these conformations to a spin state by looking for the Kondo resonance. We observe its typical peak at 0 bias on the dI/dV plot of the α conformation, but not for the β conformation or the substrate. The Kondo temperature is significantly lower, about 105K, which is a sign of reduced interaction. Contrary to Fe-phen on bare Cu(100), Fe-phen on Cu(100)//CuN can be electrically switched reproducibly between the HS and LS states, leading to a single-molecule device whose state can be deterministically selected. If we position the STM tip over the center of the highly-conductive, α conformation (identified as HS), and increase the bias voltage above +1,2 V, the molecule will switch to a low-conductivite, β conformation (identified as LS). In turn, we can switch back to HS by applying a voltage below -0,8 V. This cycle is illustrated in Fig. IV.2. Both states are stable, and the HS → LS (LS → HS) switch occurs exclusively when positive (negative) bias voltage is applied. The HS is more conducting than the LS since the Kondo effect provides an increased conductivity.

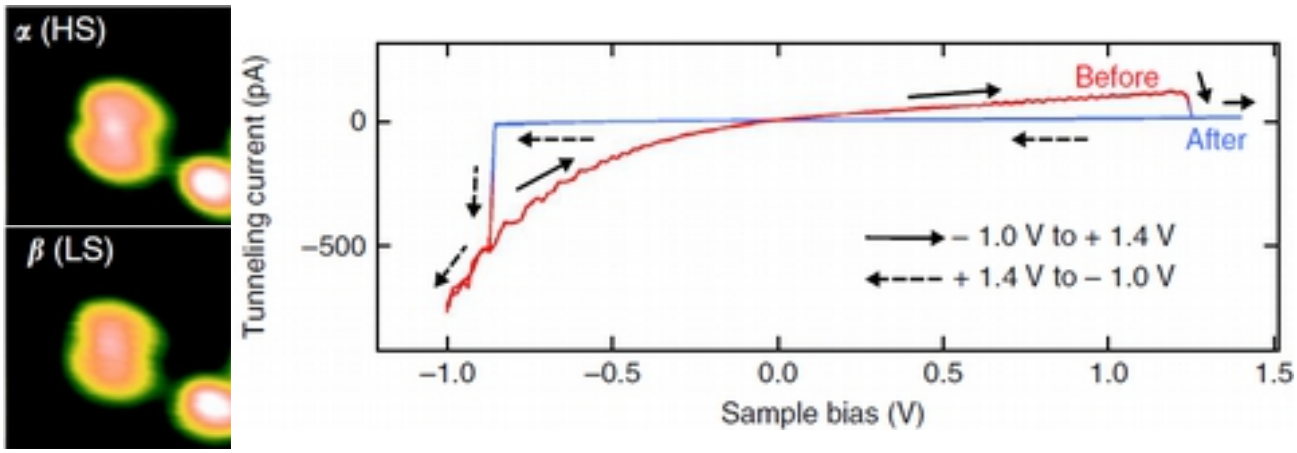

Fig. IV.2: The left panel presents the two conformations on the Cu(100)//CuN surface. The right panel is a plot of the tunneling current according to the sample bias recorded at the center of a molecule, exhibiting the hysteretic cycle.

IV.1.ii ~6 monolayers of Fe-phen: STM limits

During the process of finding a way to decouple the SCO molecule from the substrate, one of the methods experimented was to increase the thickness of the Fe-phen layer. Indeed, Fe-phen grows on the substrate in 2D layers, as illustrated in Fig. IV.3. Of course, this growth is not without defects, but another advantage from this method is that it is technologically easier to design a uniform switching layer with a regular addressing mechanism than to try to contact isolated molecules deposited irregularly on a surface. Therefore, we have investigated -relatively- thick samples to determine if the SCO behavior can be retrieved after a few layers. The thickness of the samples was estimated by evaluating the coverage of the previous sub-monolayers and some 2ML samples, that were used as a calibration, and extrapolating based on the deposition time.

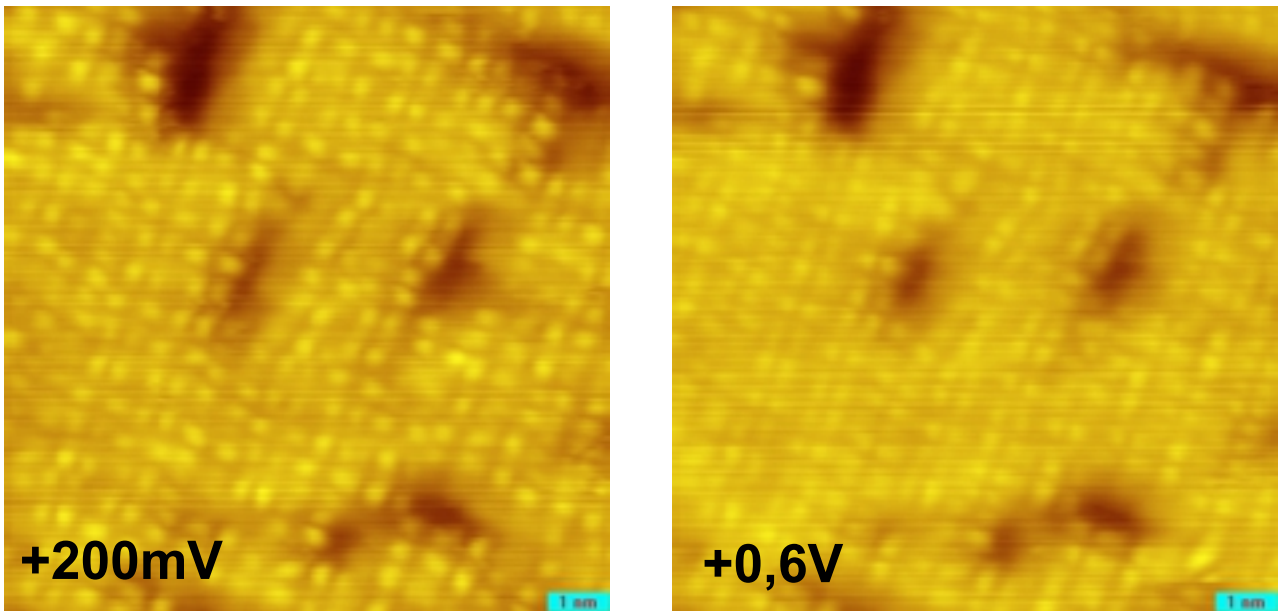

Fig. IV.3: STM pictures of a Cu(100)//~6ML Fe-phen sample at two bias voltages. The molecule seems to grow in quite well-ordered layers, despite some defects (holes). The pictures themselves were obtained with difficulty (due to low current), and are still quite blurry. The 2 conformations are hardly recognizable on a single picture.

As Fig. IV.3 exhibits, we can observe at first the similar 2 conformations on Cu(100)//6ML Fe-phen as on Cu(100). It is easier to observe the behavior of a group of molecules by selecting carefully an area to study, as shown in Fig. IV.4. With this closer look, we can observe that in fact only the "open" conformation exists on the topmost layer: the molecules are arranged in the order 1 horizontal (IV.4(A)), 2 vertical (IV.4(B)), and the proximity of the top lobes of the 2 vertical molecules gives the illusion of a "closed" conformation. Therefore, it seems that the topmost layer is nearly exclusively HS, which is a surprise since the 4K sample is well below the spin transition temperature. The HS → LS switch seems to occur earlier than on CuN, at +0,6 V (see IV.3(A), (C) and (D)), but this switch is not stable: the molecule A for example switches reversibly back to HS when the same area is scanned again at +200 mV. We did not manage to scan the surface using negative biases: in this mode, the tip attracts molecules from the surface and is damaged. Unfortunately, this was not the only issue that we were confronted with. We estimate the thickness based on deposition time and holes in layers beneath the top ones, but the determination of a precise thickness of the sample is one of the first difficulties with this technique. A second one is the identification of the two conformations: as can be observed, it is difficult to differentiate the two conformations on a single picture. It is necessary to have several to see which molecules changes their conformation. A third one is the identification of the spin state: since there are several layers of Fe-phen below the investigated top layer, it is impossible to use

the Kondo resonance to identify the spin state of a molecule. We identify "open" conformation to HS and "closed" conformation to LS, but this by analogy to the isolated molecules on the Cu(100) surface. Finally, we reach the limits of STM measurements: Fe-phen is not conductive enough to allow enough tunneling so far from the Cu(100) surface. If we still increase the thickness of the sample, it will become impossible to obtain a picture of the surface.

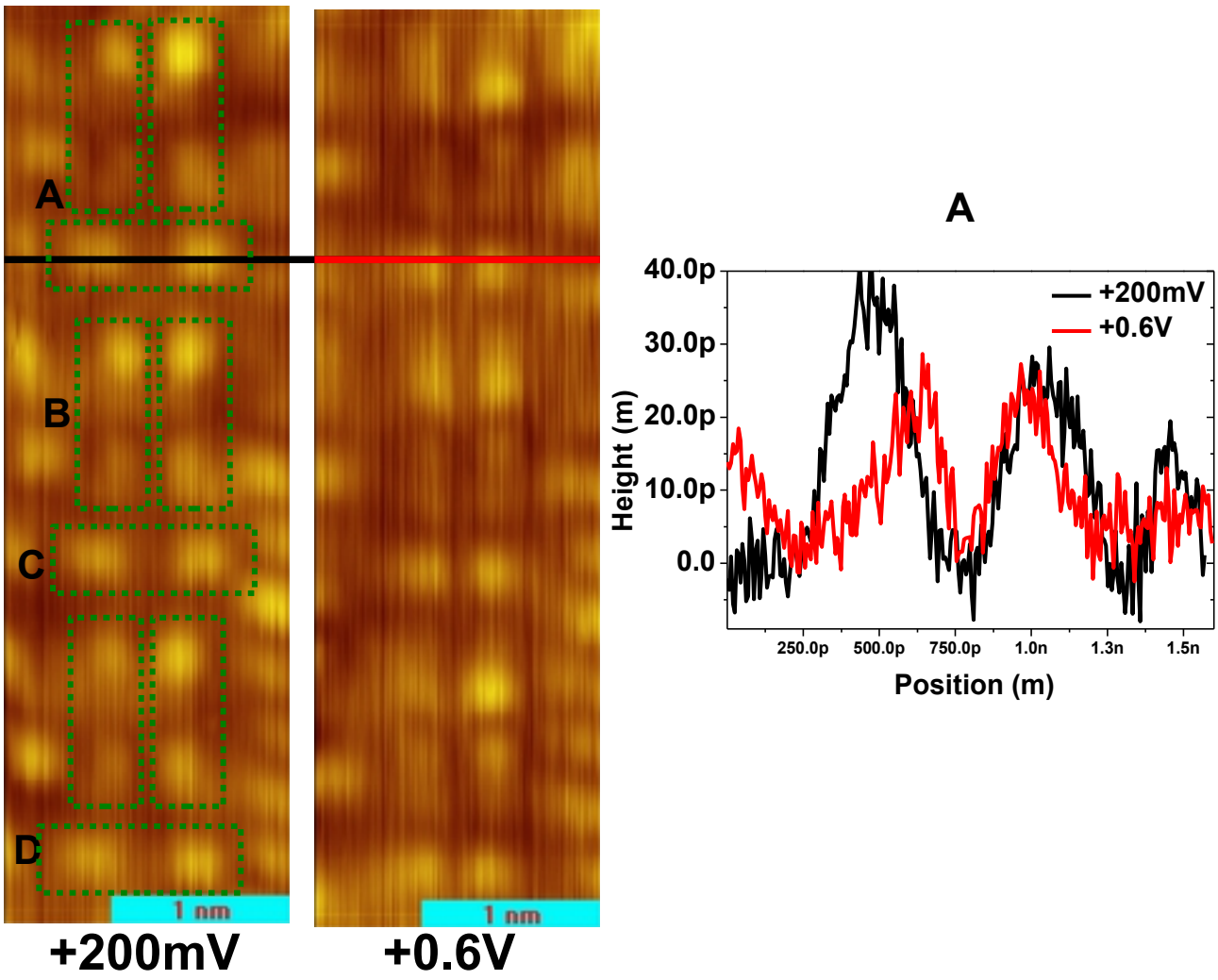

Fig. IV.4: On the left are presented STM pictures acquired on a selected area of the same sample as pictured in IV.3. The molecules are in HS state, and alternately vertical (A) and horizontal (B), which can be confusing. As expected, the molecules switch to LS when the bias voltage is increased (such as A, C and D). The right line plot exhibit such a switch, for molecule A: the molecule switch from an "open" to a "closed" configuration.

IV.1.iii Fe-phen thin films on transition metal surfaces: conclusion

Using STM measurements, we have established that the interaction with the surface plays a crucial role in the spin transition of SCO molecules, as was confirmed by several groups[148,153,177]. The Kondo effect has allowed us to identify the two spin states on the Cu(100) and the Cu(100)//CuN

surface. On the Cu(100), furthermore, a HS state molecule is in an “open” configuration and a LS state in a “closed” configuration, “open” and “closed” referring to the distance between lobes. If the influence of the substrate is too strong, as is the case with Fe-phen and Cu(100) surfaces, an electrically induced spin transition is prohibited, even if both spin states were shown to coexist on the surface. By adding a spacing layer such as CuN, it is possible to switch deterministically and reproducibly single molecules by applying a voltage pulse, between a HS, highly-conductive state and a LS, weakly-conductive state. The spin states are stable and do not switch back when the voltage cease to be applied. This behavior has later been confirmed by theoretical results from our colleagues Gueddida *et al.*[68]: they have observed that LS and HS Fe-phen molecules on the Cu(100) an CuN surfaces do not relax spontaneously from one state to the other, and that the total energy difference between both spin state exhibit a 50% reduction going from a Cu(100) to a CuN adsorption surface, thus facilitating the switch. This behavior is not observed when increasing the thickness of the layer instead of adding the spacing layer: the molecules are nearly exclusively HS on the topmost layers, and while the switch to LS can be observed, it is not stable. Furthermore, thicker layers are difficult to study by STM.

IV.2 Thick films: *ex-situ* studies

IV.2.i Fe-phen

The investigation of Fe-phen thin films by SQUID and XPS was done mostly during a previous study in our group[146], and we just recall here the main conclusions as a mean of comparison with Fe-pyrz, as well as a ground work for the last chapter of this thesis. It was shown possible to deposit homogeneous thermally evaporated films of Fe-phen that will retain their spin transition, as shown in Fig. IV.5. It was not noted in the original article, but the transition temperature seems higher in the thin film sample, at $T_{transition}$ = 186K, than in the powder sample $T_{transition}$ = 177K.

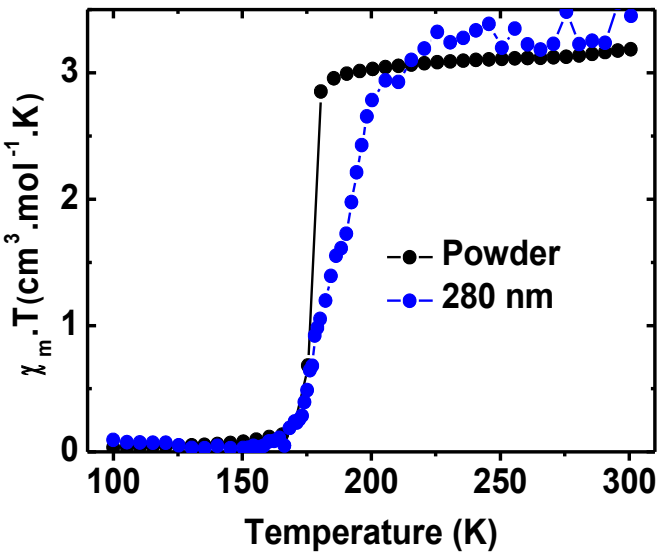

Fig. IV.5: SQUID acquired temperature dependence of the $\chi_M T$ of a powder and a thick simple sample on silicon substrate, adapted from [146].

IV.2.ii Fe-pyrz, powder and thick films: ensuring a successful deposition

Fe-phen is not the only molecule able to be deposited on surfaces, as multiple studies have shown[143,149,177]. We have thermally evaporated Fe-pyrz on Si(100)/SiO_2 surfaces, to see whether the thermal hysteresis will still be preserved in thin films. In particular, since this behavior is believed to be related to crystallographic phase changes[178], and since the synthesis technique is different from the literature, we wanted to check if this thermal hysteresis finds its origin in residual impurities (for ex. solvent), or if it is a property inherent to Fe-pyrz. We have deposited thick Fe-pyrz films on clean Si(100)/native SiO_2 (named thereafter *native Si*) and Si(100)/thermal 500nm SiO_2 (named thereafter *thermal Si*) surfaces, and tested them by various analysis techniques. Thicknesses were determined by X-ray reflectometry and profilometry.

The first results presented in Fig. IV.6 were acquired by X-ray photoelectron spectroscopy on a Si thermal//570-nm thick sample. As the samples were not prepared in situ, it is possible that the surfaces get contaminated by air during transport, despite precautions. And in fact, it happened: the XPS spectra exhibit a peak at O-1s energy, which is a sign of contamination by atmospheric species such as O_2 and H_2O. We rule out O from the SiO_2 because we did not observe a Si-2p peak. We tried to remove the topmost layers with a gentle Ar^+ sputtering, but despite previous successes with Fe-phen[146], this treatment appears destructive to Fe-pyrz layers. Indeed, after 20 min sputtering, the O content increases dramatically while N and C content decreases, which suggests

that oxides are formed under sputtering. However, if we neglect the O content during the analysis of the sample before sputtering, we observe that the experimental values of the composition are very close to the expected values.

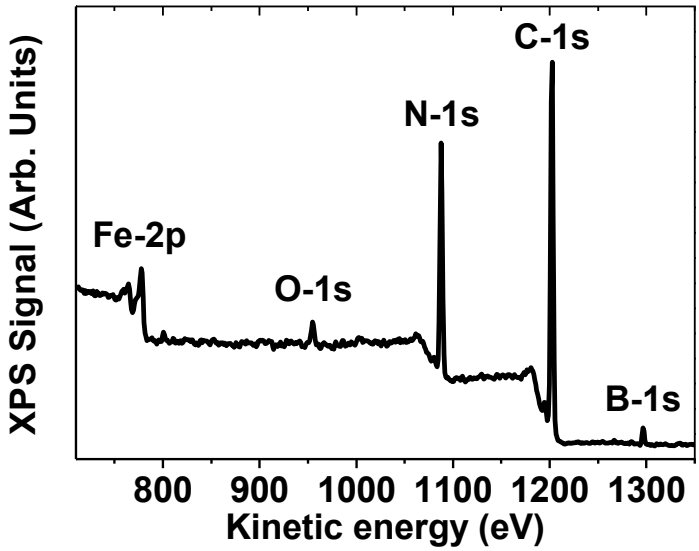

Atomic % of the sample		Fe-2p		O-1s		N-1s		C-1s		B-1s	
Theoretical		2,22		0		26,67		66,67		4,44	
Experimental		2,39	2,42	1,48	0	25,69	26,08	66,07	67,06	4,37	4,44
With O	W/o O										

Fig. IV.6: XPS element analysis of a 570-nm thick sample deposited on native Si. The plot correspond to the XPS spectrum before sputtering, and the table to a quantitative analysis based on the relative areas of the different peaks. If we do not consider the slight oxygen contamination (w/o O line), then it is clear that what we have deposited on the surface has the same composition as Fe-pyrz.

X-ray results, such as presented in Fig. IV.9, suggest that Fe-pyrz lays down on the surface rather amorphously, with an organization mostly along the main crystallographic axis (peak at 9.92°, slightly different from the powder main peak at 10.2°). Supplementary peaks only appears for samples above 570nm. Using the Scherrer equation[179], we have determined the size of the crystallites: the molecule seems to form nanometric structures on the surface.

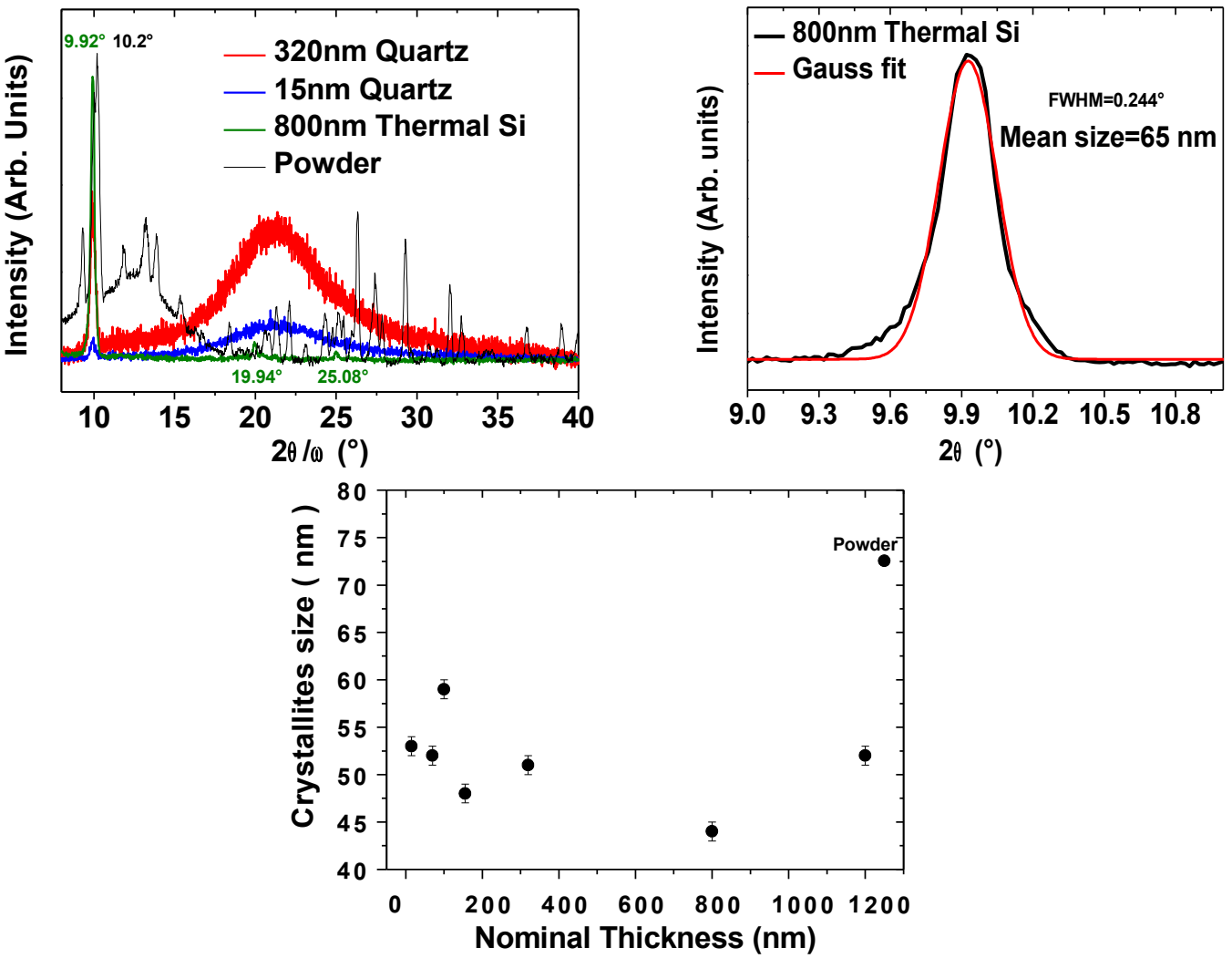

Fig. IV.9: Top left panel presents X-ray diffraction results for various thicknesses and substrates, including the powder reference. All spectra were acquired at ambient temperature. Top right panel is a zoomed in plot of the 800nm-thick sample on the thermal Si, with a gaussian fit of the main peak, used to determine the size of the crystallites using a standard Scherrer equation. $\lambda CuK_{\alpha 1}$=0.154056 nm. Bottom plot is a wider view of the crystallites size as a function of the thickness.

This is confirmed by AFM pictures of the surface as shown on Fig. IV.10. Contrary to Fe-phen[146], Fe-pyrz does not exhibit a homogeneous growth on the surface: its forms clusters and crystallites. At thicknesses below grain size, the grains are isolated. This is a behavior already observed for some SCO compounds: even if the structure of the molecules are very similar, they can lay down in the surface differently[177]. Therefore, it is difficult to really determine a thickness: the nominal thicknesses then indicate more a quantity of matter deposited on the surface than a number of successive layers. We have determined the nominal thicknesses of the thicker samples using profilometry and then extrapolated to the thinner samples. Under a nominal thickness of

approximately 30nm, the grains on the surface are then isolated. As we have not acquired results on transition metal monocrystals surfaces, the organization of the molecules can be different on these surfaces. We hope that with crystalline surfaces the layers would be more homogeneous, but similar results by Mahfoud *et al.*[149] on $Fe(HB(pz)_3)_2$ on Si/SiO_2 prompt us to be cautious. Further studies are expected to clarify this point.

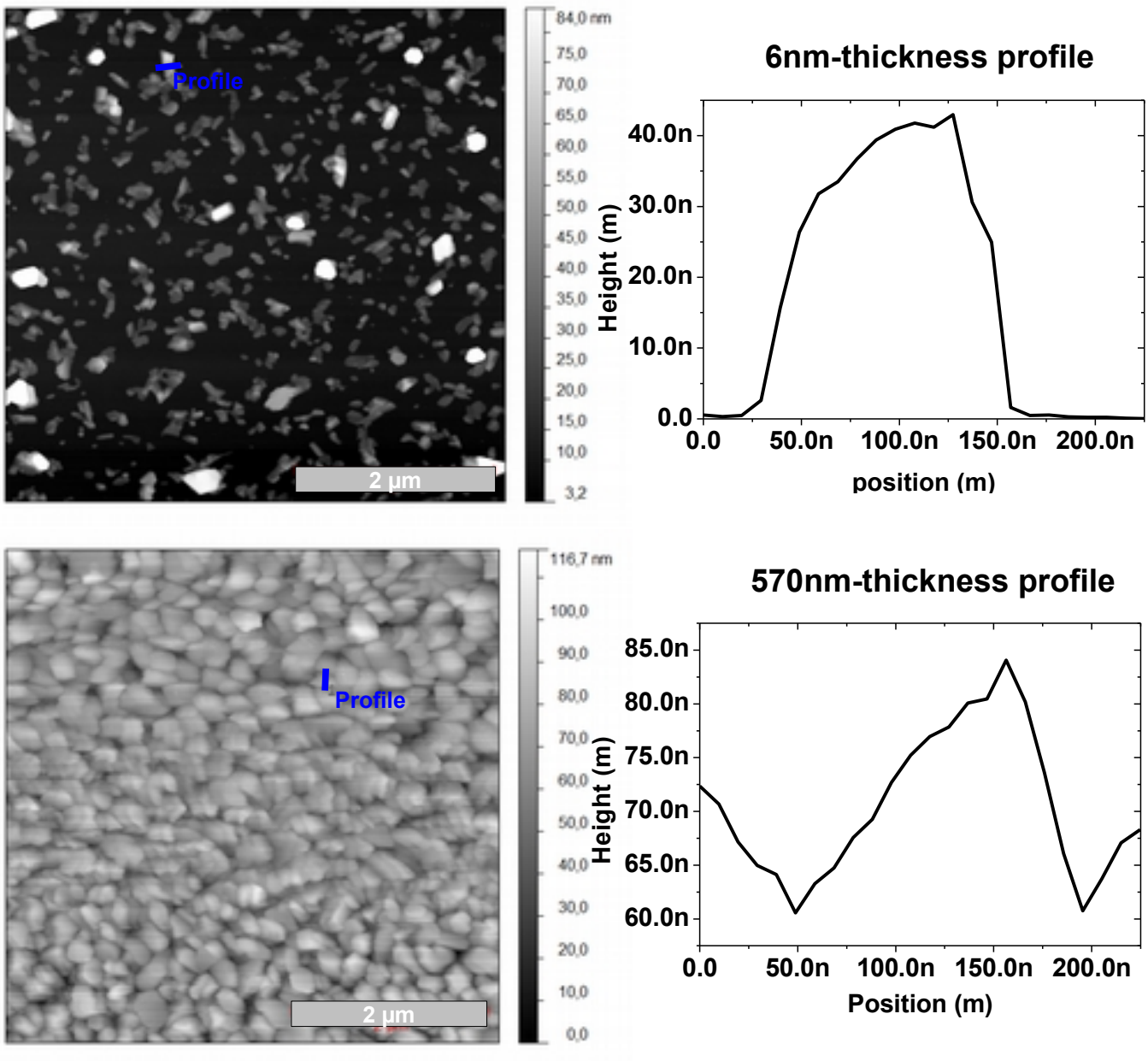

Fig. IV.10: AFM pictures and profiles acquired for 6nm estimated thickness (top) and 570nm estimated thickness (bottom) on thermal Si. The profiles correspond to the line profiles on the main pictures.

The layer morphology impacts optical absorption results on thick films grown on pure quartz substrates, as illustrated in Fig. IV.11. The transmission spectra reveal a low absorption in the

visible region, consistent with the white-pinkish color of the powder. The molecule absorbs much more in the UV region. We have calculated the direct optical gap using Tauc plots: the Tauc formula[180–183] establishes that $(\alpha h\nu)^{1/2}=B(h\nu-E_g)$ in the linear part of the Tauc plot, with $\alpha = \ln(1/T)/\text{thickness}$ the absorption coefficient, Eg the optical gap and B a parameter that gives a measure of the disorder in the crystal[182]. By plotting $(\alpha h\nu)^{1/2}$ as a function of hν and approximating the linear part, it is then possible to determine the direct optical gap of the sample. This method is widely used for semi-conductors[181,182] and organic thin films[184,185]. The thick films present a wider optical gap than the powder, and a drop in the optical gap when we reach discontinuous films is observed. We believe that the smaller gap of the powder (and the decrease in the width of the gap when the thickness increases above a critical value of 570nm) might be due to impurities introducing levels in the gap, impurities identified in the next paragraph.

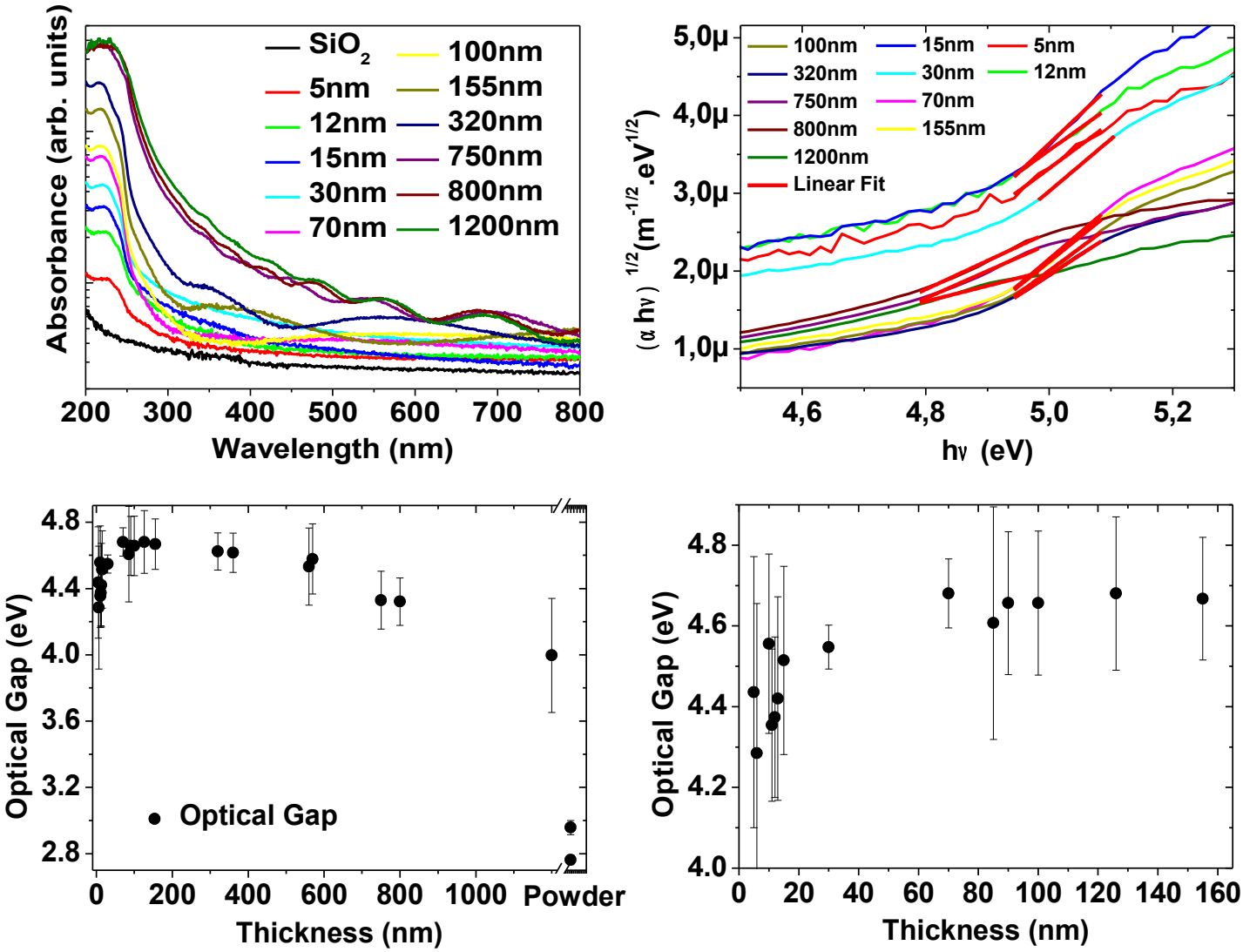

Fig. IV.11: Top left plot exhibit the absorption results for selected thicknesses and for the quartz substrate. The undulation after 300nm for the thicker samples is attributed to interferences. Top right plot is a Tauc's plot ($(\alpha\hbar\nu)^{1/2}$ dependence on the incident photon energy) for Fe-pyrz thick films of selected thicknesses, at room temperature. The colored curves correspond to experimental data, while the red lines are the linear fits, tangential to the curve, used to calculate the optical gap presented in the bottom left plot. The bottom right plot is a zoomed in fraction of the whole bottom left plot, focusing on the break at low thicknesses.

Further information on the layer can be obtained by X-ray absorption spectroscopy (XAS), with the total electron yield (TEY) acquisition mode. By comparing in Fig. IV.7 the reference spectra acquired with the powder sample and the thick film sample spectra at 100K and 300K, we can observe three points: a) the F contamination marked by a double peak at 691eV and 694eV (probably inherent to the synthesis technique using BF_4^-) disappears on the thick film sample; b) the spectra change from one type to the other, indicating a spin transition; c) a part of the thick film sample seems "HS-pinned" and do not switch. This is encouraging, as the spin transition seems preserved. In chapter

V, the role of XAS in investigating SCO complexes is more thoroughly expanded upon.

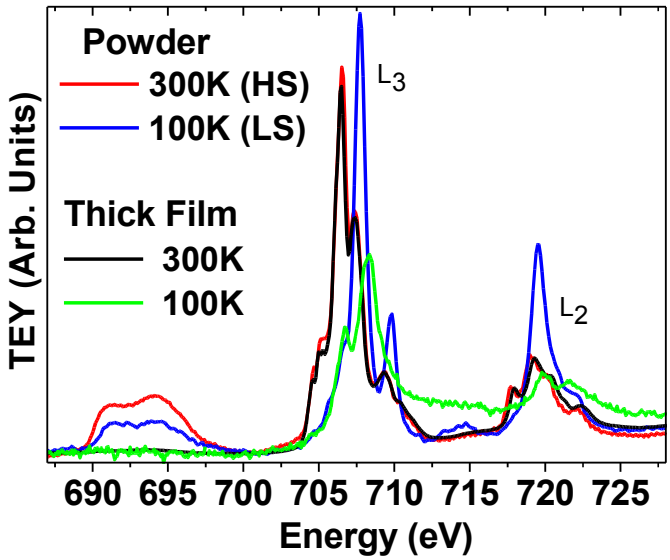

Fig. IV.7: XAS spectra of the Fe L-edges for the powder reference and the 570-nm thick film, normalized to the same integral, for temperatures above and below the spin transition temperature, at intensity $1{,}2\times10^{10}$ ph.s.mm^{-2} = $20I_0$. The ambient temperature spectra are clearly identical, while the low temperature thick film spectra visibly retain an estimated 24% HS-state (the determination of the HS proportion is described in part V.1). The edge jump (difference of intensity between 700 and 715 eV) for this last spectrum is noticeably higher than for the 300K-spectrum, for unclear reasons.

Of course, the most important question is: how do the samples switch? To answer this question, we turn towards SQUID measurements. As evidenced in Fig. IV.8, the hysteresis and its asymmetry are preserved, and it appears that the spin transition temperatures shift towards lower temperatures as the thickness decreases. Although this last effect was noted by Palamarciuc *et al.* [177] and observed but not pointed out by Naggert *et al.*[147], it could be also due to the alteration of the layer by air, as stated previously: more studies will be necessary to understand the full extension of this feature, as we have not yet been able to obtain an acceptable signal/noise ratio for thinner samples. Also, we have to report two difficulties inherent to such measurements that have a strong impact on our film results by SQUID: the evaluation of the quantity of molecules in the film, and the diamagnetic influence of the substrate. Despite careful measurement of the diamagnetic background of the native SiO_2 substrates after cleaning the substrate with acetone and ethanol from deposited molecules, it is indeed possible that the results are affected by this issue. We have dispersed the powder sample in an alcane glue (eicosane, $C_{20}H_{42}$), and the results exhibit a similar spin transition temperature shifted towards lower temperatures as in thick films.

This suggest a significant influence of the environment on the spin transition of Fe-pyrz.

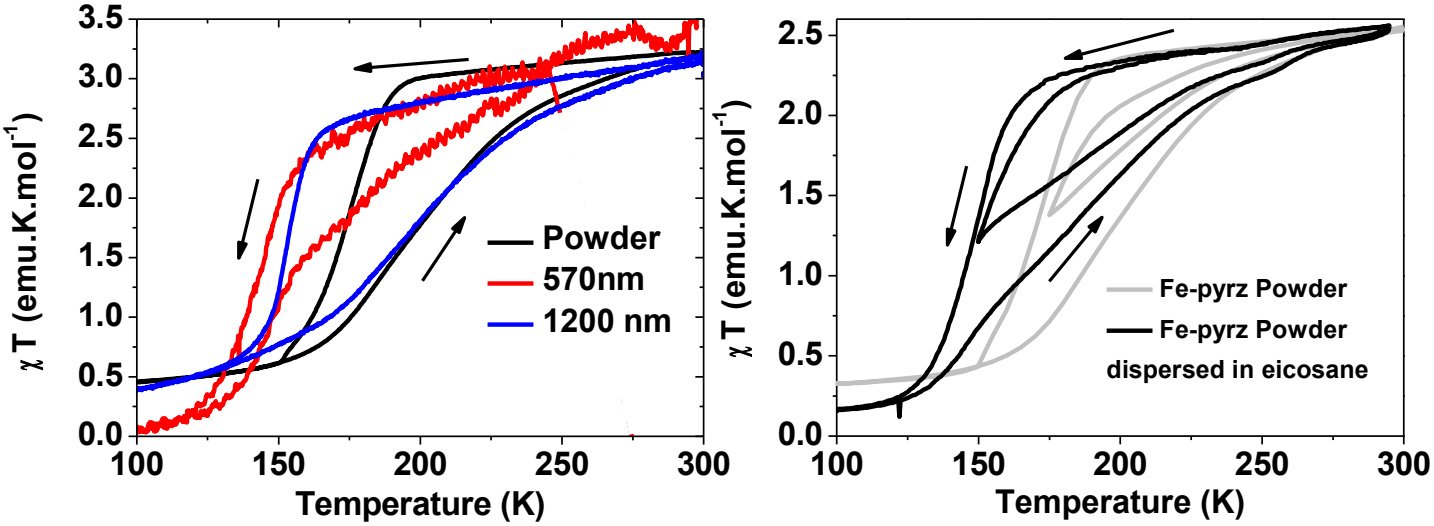

Fig. IV.8: The left plot presents SQUID magnetic susceptibility results for two thick films thicknesses (570nm and 1200nm on native Si) compared to the powder reference, with the arrows identifying the direction of the temperature sweep. The shift in spin transition temperature and the spin transition itself are clear. The right plot presents the results for the powder, in this specific example dispersed in eicosane (purely alcane) glue. One full transition cycle, and one 50%-100% HS cycle.

Finally, for powder samples, we have also interrupted the decrease in temperature at the mid-spin transition, and increased the temperature again, as presented in Fig. IV.8. Smaller cycles are necessary to fully confirm this, but this suggest that the asymmetry is not necessarily due to a crystallographic phase change. Indeed, if this was due to a crystallographic phase change, there would be a short range during the increase in temperature where the molecules that are LS in a HS-type crystallographic phase would transit back to HS with a similar high cooperativity, as suggested. However, we do not notice this. We rather suspect that the LS state is inherently less cooperative than the HS state.

IV.2.iii Fe-pyrz thick films: conclusion

We have successfully thermally deposited Fe-pyrz on Si/SiO_2 surfaces. The molecule retains not only its spin transition but also its wide thermal hysteresis, the first reported SCO molecule to do so. The spin transition seems to present a shift towards lower temperatures when the thickness is decreased, and also when the powder grains are physically constrained by glue. On the surface, the growth is 3 dimensional, and the molecule form crystallites, that are isolated from each other when the estimated mean thickness drops below 30nm. The optical gap increases at thick films thicknesses, a behavior we attribute to the presence of impurities in the powder and the thicker

samples, and the optical gap decreases at thin films thicknesses when the crystallites are not in contact any more. However, since the molecule grows heterogeneously on the surface, and do not form continuous films, it is difficult to assert the results for thin film “thicknesses”.

IV.3 Isolated molecules and thick films: conclusion

The STM results have proven the strong influence of a highly interacting surface on the spin transition of a SCO molecule adsorbed on the surface. We can identify the spin state of the isolated molecules by looking for the Kondo effect on the Fe site, and using this method we can infer that both spin states coexist at 4K on Cu(100) and Cu(100)//CuN surfaces. The molecules are “pinned” to the Cu(100) surface, namely that it was not possible the change the spin state of molecules (either LS or HS) through electrical means on Cu(100), but it is possible to deterministically and reproducibly switch isolated molecules by applying a voltage pulse, between a HS, highly-conductive state and a LS, weakly-conductive state on Cu(100)//CuN. This range of behaviors was later confirmed and expanded by theoretical results of isolated Fe-phen on Cu(100) and CuN[68], experimental STM results of two types of an isolated SCO molecule on a Cu(111) surface[177], experimental XAS results of a sub-monolayer of a strongly-interacting SCO molecule on a Au(111) surface[148] and experimental XAS results of a sub-monolayer of weakly-interacting SCO molecule on graphite[153]. Fe-pyrz does not grow as homogeneously as Fe-phen on thermal Si, and forms crystallites. Despite this, thick films of Fe-pyrz retain their spin transition and thermal hysteresis. We observe, however, a shift of the spin transition temperatures towards lower temperatures when the molecule is constrained by the environment, be it the surface of an eicosane glue. The optical gap was calculated, and the molecule absorbs light in the UV region.

The results, considered as whole, suggest that the environment and the shape of the sample of a SCO molecule will impact considerably its properties. But very small scale thin film samples (below 20nm thick) are difficult to investigate, and AFM offers limited insight in the spin transition itself. Therefore, X-ray absorption spectroscopy (XAS) can effectively cover a gap between isolated molecules and ultra-thin films investigated by STM on one side, and thick films investigated by SQUID and other “bulk” techniques like MOKE or optical absorption on the other side. More details follow in the next chapter.

V X-ray absorption spectroscopy of SCO molecules

Results and discussion

XAS is a tool of choice for the study of SCO molecules and magnetic molecules on surfaces[155]. Indeed, it is element-sensitive and allows the easy recognition of the spin state[85], while also providing information on the environment of the element investigated and on its electronic properties. It is highly sensitive, and therefore particularly adapted to the study of nanometric systems, but it can also be used on bulk samples, in opposition to other recent nanoscale-only analysis techniques like surface plasmons[186]. We have acquired the results described in this chapter during 3 experimental runs, with 3 different beam intensities noted I_0, $10I_0$ and $20I_0$ as described in part III.3. At first, we will focus on the precise use of this method, especially at temperatures below 60K, as the technique then presents an effect: the soft X-ray induced spin state trapping (SOXIESST). As described in chapter I, it consists in the formation of a metastable HS state when the molecule is excited by X-ray illumination. We will then investigate thin films of Fe-phen on Cu and Co surfaces using the experience of powder samples to uncover the spin transition properties of a SCO thin film.

V.1 Analysis of XAS spectra

V.1.i Determination of the HS proportion

The first step in studying SCO molecules by XAS, either in bulk or thin films, is finding how to identify the spin states, their electronic structures and their relative proportions. The most common way to do this is by using a combination of reference spectra taken when the powder sample is either pure HS state (280K) or pure LS state (100K) to fit the data for a mixed state, as is illustrated in Fig. V.1. The acquisition of reference spectra will be discussed in the next part. This technique is widely used[85,115–117,119,148,153] but of course it does not account for the eventual presence of a third spectrum type (like a transient state) or the evolution of the HS/LS proportion during a single measurement.

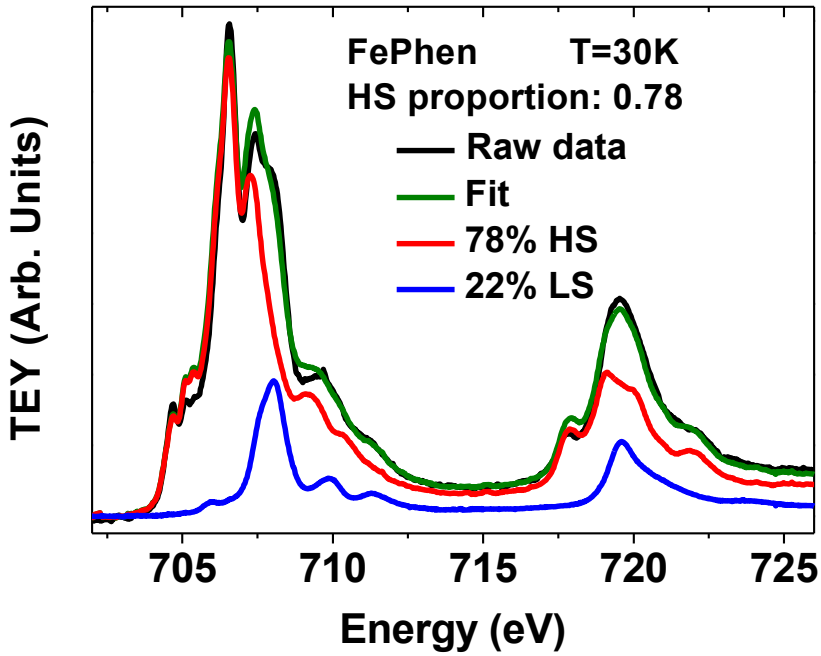

Fig. V.1: Raw powder Fe-phen XAS spectrum measured at T = 30K and I = $10I_0$ and fit to the raw XAS spectrum using a combination of the HS (red)/LS (blue) reference spectra (78% HS, 22% LS).

V.1.ii On the analysis of dynamic LS → HS transition by XAS

The reference spectra are each acquired at a temperature where the molecules are supposed to be in a pure spin state according to SQUID results. Both spectra were renormalized to the same integral, so that both spectra correspond to the same quantity of matter probed by the technique. This assumes that the integral of the signal for both pure spin states should be identical. It is possible to check this assumption by looking at the evolution of the integral over time during the

SOXIESST effect, when the sample gradually switches from the LS to the HS state. The plots in Fig. V.2 clearly confirm our assumption. The evolution of the integral value of the signal as a function of the HS proportion confirms that the integral of the signal is rather constant during the SOXIESST phenomenon between the low-HS (0.2 HS proportion in the Fig. V.2 example) and high-HS (0.8 HS proportion in the Fig. V.2 example) compositions of the sample, even if during the series this value can be higher. This can be explained by an evolution of the HS/LS proportion during an individual measurement, and this deviation stays limited.

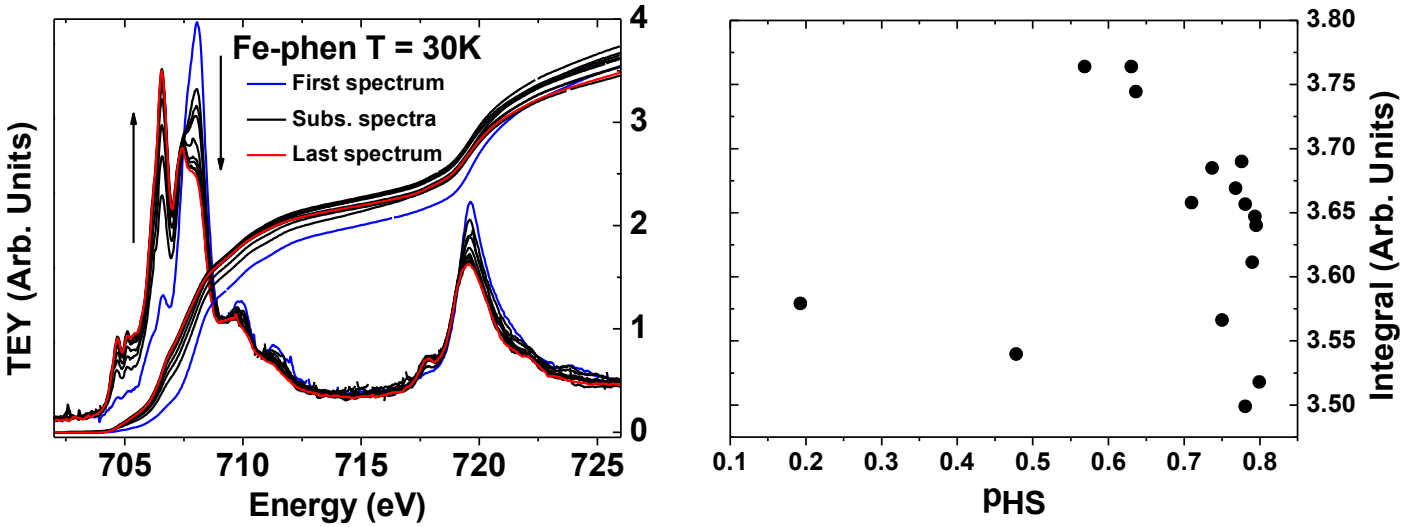

Fig. V.2: The left panel presents some of the successive XAS spectra for a Fe-phen powder sample at T = 30K and I = 10I_0, from the first (blue) to the last (red) of the series. Measurement time for each spectra was 1 minute. The amplitude of the HS main peak at 706,6eV is increasing while the amplitude of the LS main peak at 708.1eV is decreasing. Also presented is the mathematical integral of the data for the same series. Plotted in the right panel is the integral value taken at 726 eV as a function of the HS ratio extracted from the raw data.

V.2 Powder samples: the dynamics of the SOXIESST effect revealed

V.2.i Ground work: reference XAS and XMCD

As previously reported[115,116], we also observe the degradation of the Fe-phen molecule over time (the so-called soft X-ray photochemistry, SOXPC), which is manifested by the freezing of a LS state, probably through the removal of one of the ligand groups. But, at an estimated photon density of 6.4×10^{9} ph.s^{-1}.mm^{-2}, this process is sufficiently slow for Fe-phen: we estimate that the rate of this process is under 3% of the sample / hour under the X-ray beam. A similar behavior was observed for Fe-pyrz, with a rate of approximately 11% of the sample / hour at $6{,}1\times10^{8}$ ph.s^{-1}.mm^{-2}. As expected, at low illumination, both molecules suffer far less degradation. Therefore, we

recommend low XAS illumination parameters for the measurement of Fe(II) SCO compounds, as they still allow the easy recognition of the spin states while avoiding undesirable side-effects.

Referring to Fig. V.3, the Fe-$L_{2,3}$ edge spectra exhibit a clear temperature variation between two extremal spectra obtained at 280K or 300K, and 100K. These spectra were ascertained, in the literature[85,115,116,119], to belong to the Fe-phen pure HS and LS states, respectively. We can therefore use these spectra to determine the HS proportion, as explained in the previous point. The experimental results presented below are confirmed by theoretical results. We have performed calculations using the recent CTM4XAS program[172] to obtain spectra for theoretical HS and LS states. We have assumed a C_4 symmetry around the Fe atom, necessary for XMCD calculations, rather than the more traditional O_h symmetry, but the XAS results remain unchanged in one symmetry or the other as we kept Dt = Ds =0. As introduced in chapter I, the symmetry of Fe-phen is not ideal anyway, but distorted. We have then performed the calculations using a crystal field parameter 10Dq of 1.1eV for the HS, and 2.2eV for the LS, values close to the precedent calculations (respectively 1 and 2.2eV by Warner *et al.*[148], 0.9 and 2.2eV by Lee *et al.*[116] and 0.5 and 2.2eV by Briois *et al.*[119]). The theoretical spectra agree quite well with the experimental spectra, as presented in Fig. V.3, except for a 711eV band that is present in the Fe-phen experimental spectra, but not in the Fe-pyrz experimental spectra or the theoretical spectra. This band is a metal-ligand charge transfer band (MLCT), as evidenced by calculations including this effect[116]. The impact of this band on the SOXIESST effect is discussed in the last point of this part.

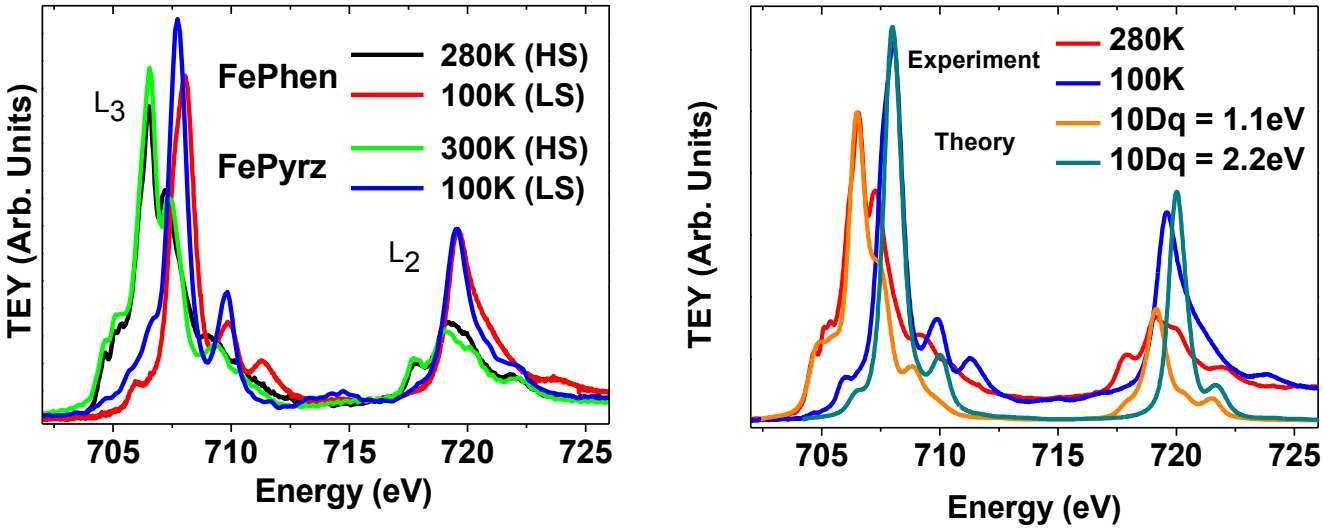

Fig. V.3: Plotted in the left panel are the XAS reference spectra for both molecules in both spin states, acquired on the powder at intensity I_0. Right panel presents XAS theoretical data obtained using the CTM4XAS program without inclusion of MLCT. 10Dq values are noted on the right plot, and Dt = Ds = 0.

It is also possible to confirm that the low-temperature HS state that is generated by SOXIESST is, in fact, a HS state, by doing XMCD at low temperature and calculating the spectrum of the HS-SOXIESST XAS, as presented in Fig. V.4. XMCD theoretical results are also in agreement with the experimental results: the main features of the XMCD experimental signal are reproduced by the theoretical HS XMCD signal, while the theoretical LS XMCD signal is nearly flat. The minor differences are attributed to the fact that the experiment measures also excited states, while our calculation is focused exclusively on ground states. Indeed, to be perfectly precise, we should carry out the calculations with different 10Dq values for the final, excited state than for the initial, ground state[119]. In Fig. V.4 is also presented the example of an XAS spectrum at T=30K, with the signal for 22% LS reference spectra substracted from the experimental data compared to 78% of the reference HS spectrum (measured at 300K). We conclude that the HS state obtained upon SOXIESST effect is almost equivalent to the high temperature HS state.

As a note, the HS-SOXIESST might be slightly different from HS-thermal, notably due to pressure from the LS matrix, following the example set by HS-LIESST.[106,110]

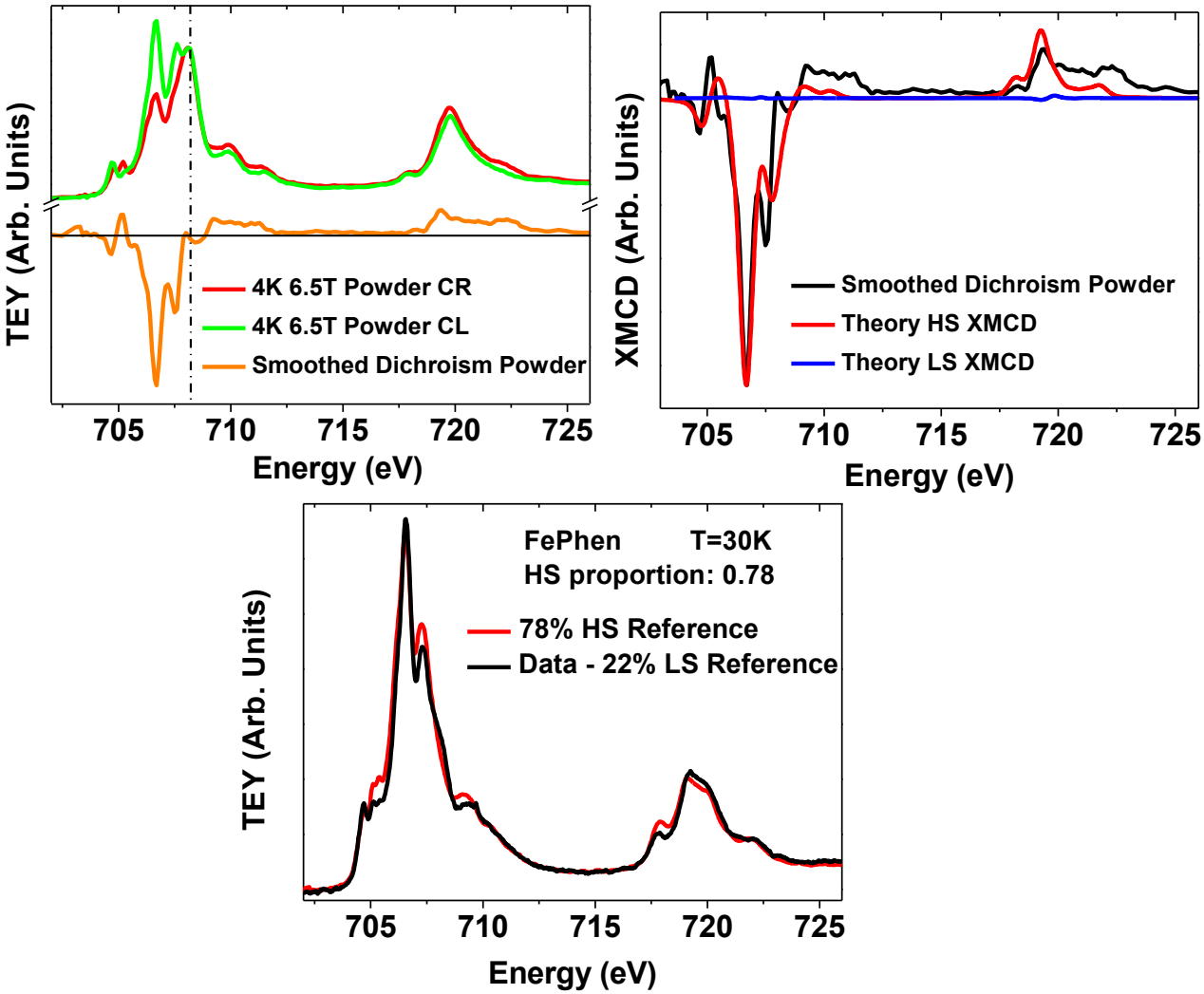

Fig. V.4: Calculated XMCD signals obtained by the CTM4XAS program on the top right panel (with M = 10 meV), compared with Fe-phen experimental results on the top left panel, that presents XMCD data obtained for a Fe-Phen powder sample at 4K and 6,5T. The dotted line is a visual aid for the LS main peak at 708.1eV, confirming that the LS part of the sample is non-magnetic and the HS is magnetic. The bottom plot is a comparison between 78% of the HS reference data and the experimental data acquired at 30K from which 22% of the LS reference data has been deleted.

V.2.ii SOXIESST statics and dynamics results

Since our experimental tool, namely XAS, can alter the HS proportion through the SOXIESST effect, particular care was taken in implementing the correct experimental methodology. Where noted, studies of the SOXIESST dynamics were obtained by acquiring a series of XAS spectra at a stabilized temperature, often only over the L_3 edge so as to gain in temporal resolution. The subsequent measurement of the HS proportion is then determined using the first XAS spectrum of this series, i.e. within one minute of sample illumination with X-rays. This inferred HS proportion is called the *virgin HS proportion*. The time stamp of each subsequent measurement corresponds to the

midpoint of the measurement. This allowed us to investigate the SOXIESST dynamics (see Fig. V.5).

We label the stabilized HS proportion due to SOXIESST the *SOXIESST HS proportion*, determined using the last XAS spectrum of the series. It is the HS proportion obtained at saturation. Subsequent measurements of the SOXIESST HS proportion were then achieved by first resetting the sample's HS proportion by heating the sample to 80-100K while blocking the X-ray beam, then stabilizing the subsequent temperature.

As another experimental protocol, we first measured a SOXIESST HS proportion at 4K, and then increased temperature to 60K while performing XAS measurements. The inferred value of this HS proportion is called the *SOXIESST without (w/o) reset HS proportion*. Unless noted, samples were not exposed to visible light before or during XAS measurements so as to avoid the LIESST effect.

When the additional impact of LIESST was investigated, visible light excitation was achieved using standard white light emitting diodes (LEDs). This is denoted as the *SOXIESST+ LIESST HS proportion*. We have also explored, starting from 4K and while maintaining X-ray and LED illumination, the temperature dependence of the HS proportion, which is then labeled the *SOXIESST w/o. reset + LIESST HS proportion*.

Typical examples of these denominations can be found in Fig. V.5.

For a given temperature, we have studied the temporal evolution of the HS proportion. Examples of this extensive study are shown in Fig. V.5. Comparing with previous results[57], despite the different photon flux, we observe that the process occurs in the same time frame as the LIESST. Indeed, both the SOXIESST and the LIESST reach saturation within hundreds to thousands of seconds. We also note that the SOXIESST-generated transition is not complete using an intensity of $10I_o$ since the LIESST effect, whether applied before or once the SOXIESST effect saturates, leads to a higher HS proportion (see right panel of Fig. V.5).

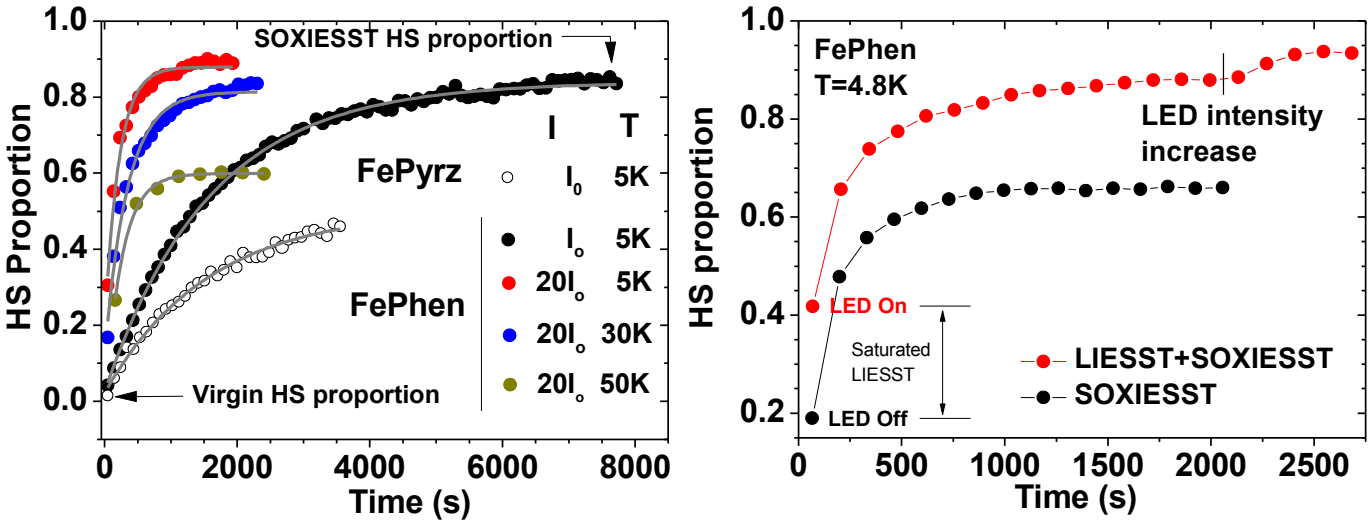

Fig. V.5: The left panel presents examples of the Fe-phen HS proportion dynamics that illustrate the impact of temperature and X-ray intensity. A Fe-pyrz dataset is also plotted for comparison. Lines represent fits using Equation IV.1. For each SOXIESST dynamics spectrum, the stabilized value of the HS proportion was used to plot the temperature dependence of the SOXIESST HS proportion shown in bottom middle. The right panel presents SCO dynamics promoted by SOXIESST alone and LIESST+SOXIESST for $10I_0$. The light-excited dataset was recorded by first illuminating the sample with light for 30 minutes to achieve a LIESST-saturated HS proportion, then recording the SOXIESST dynamics spectrum. At the mark, the LED intensity was increased to achieve a LIESST-induced increase in the HS proportion.

We plot in Fig. V.6 the temperature dependence of the HS proportion. Notably, we observe a hysteresis between the SOXIESST HS proportion (red) and either the SOXIESST HS w/o. reset proportion (green) or the SOXIESST w/o. reset + LIESST HS proportion (blue). This dependence of the HS proportion on the thermal history of the sample appears to be a kinetic effect since the LIESST HS (metastable) → LS relaxation speed is very slow at those temperatures: this is an effect very similar to the light-induced thermal hysteresis (LITH)[105] generated by visible light excitation, the soft X-ray induced thermal hysteresis. All measurement protocols yield the same SOXIESST HS proportion at T≈60K.

Contrary to previous studies[115] in which a complete transition was achieved, we observe only a partial HS transition. The HS fraction reached upon SOXIESST with $10I_0$ light intensity can be increased by applying visible-UV light excitation as illustrated in Figure V.6 by the red and green curves. However, we suppose that this is due to a weaker X-ray illumination in our experimental conditions (6.4×10^9 photons.s^{-1}.mm^2 for $10I_0$) in this first case, compared with 10^{11} in Collison et al.). This hypothesis is supported by our results at higher X-ray intensity $20I_0$, for which the conversion is nearly complete (see Fig. V.5 left panel).

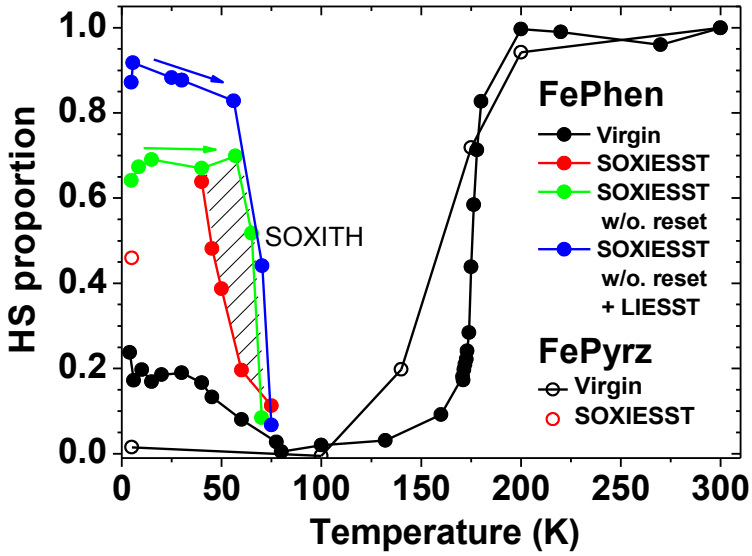

Fig. V.6: Temperature dependence of the Fe-phen HS proportion, obtained for $10I_0$, for the virgin HS proportion (black); for the SOXIESST HS proportion (red, lower temperature points follow the green curve); for the SOXIESST w/o reset HS proportion obtained while increasing the temperature from 4K under steady X-ray illumination (green); and for the SOXIESST w/o reset+LIESST HS proportion obtained while increasing the temperature from 4K under steady X-ray and white light illumination (blue). The hatched area correspond to the soft X-ray induced thermal hysteresis (SOXITH). A complementary subset of data, obtained using intensity I_0, is plotted for Fe-pyrz using open symbols.

V.2.iii Excited states and XAS

The previous study suggested that the SOXIESST and LIESST mechanisms should be similar[115]: a LS state transit to an excited state through intersystem crossing (ISC), then relaxes into either a LS or a metastable HS state. In turn, the HS state relaxes slowly to the LS state[101,108]. The SOXIESST process should therefore involve one or several excited state(s). Since these excited states should have a different electronic signature than the usual HS and LS states, it might be possible to identify them on fast spectra, by observing the residual of the fit. Fig. V.7 presents several residuals of successive XAS scans. From this data, we do not notice anomalous deviation from the noise present in the residual spectrum. It would also be difficult to identify a possible X-ray generated excited state, because the theory behind the SOXIESST process dictates that the LS → HS excitation occurs, even at temperatures above $T_{SOXIESST}$, but immediately relaxes.

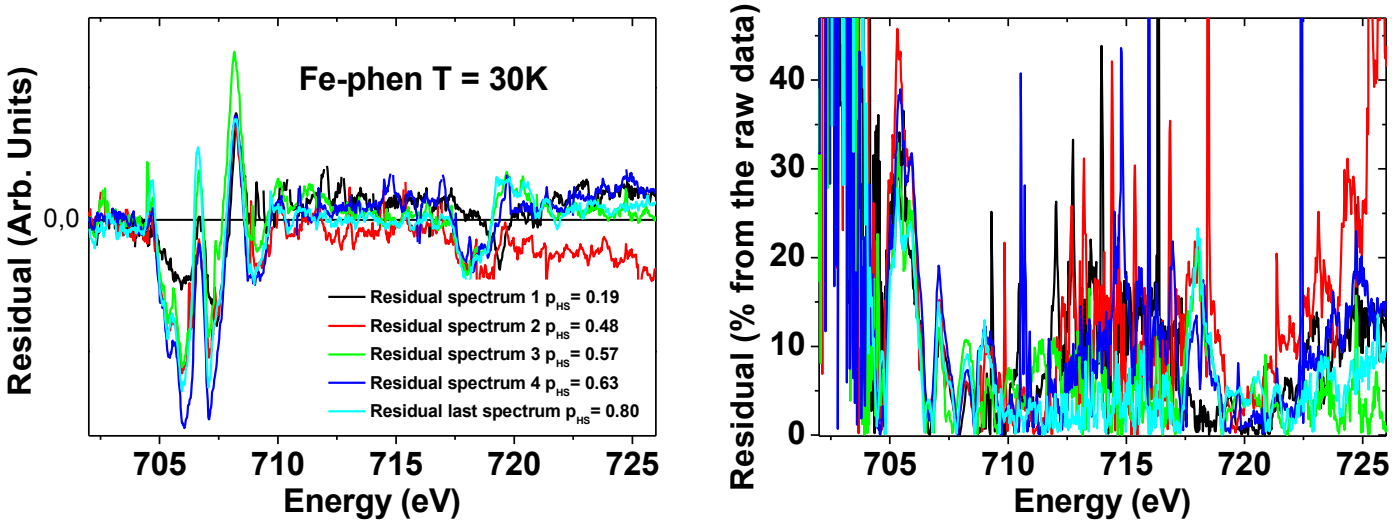

Fig. V.7: Left panel present several residual spectra between the raw data and the fit, notably used in Figure V.1. Right panel plot the same residuals, converted in percent of the raw data. While reproducible, it is difficult to attribute the deviations to a hypothetical third state rather than slightly inaccurate reference LS and HS spectra for example, especially since the deviations represent less than 1% at LS and HS main peak energies (708.1eV and 706.6eV respectively).

V.2.iv Fitting to a simple model

As a preliminary note, our experiments seem to indicate that the SOXIESST effect is not resonant. Indeed, we observe that the energy of the X-ray illumination and the HS proportion evolution are not correlated: the HS proportion dynamics are the same if we measure the subsequent spectra over L_3 and L_2 or only L_3. Evidence for this is exhibited in Fig. V.8: we have illuminated the sample with X-ray energies tuned before edge, at HS main peak and at LS main peak during 1200s, and then acquired a series of full-range XAS spectra. We wanted to observe if the SOXIESST effect was linked to one or the other absorption bands, but comparing with a series of full-range XAS spectra acquired over the same time window, we found that none of the specific exciting X-ray energies from the 3 tested produce more (or less) SOXIESST effect. The HS proportion obtained after illuminating the sample with an X-ray beam of a definite energy or with a wide range of energies is the same, whatever the range or the energy value. Therefore, we conclude that the SOXIESST effect is non-resonant, which is a significant difference from the LIESST effect. Taking into account the presence of the HAXIESST at higher excitation energies (hard X-ray regions, around 7000 eV), we suggest that either there is a continuum of excited states, or there is a common excitation process involving secondary electrons. Consequently, we suggest that the SOXIESST and the HAXIESST form two aspects of the same effect, the X-ray induced excited spin state trapping.

Besides, since the excitation is not selective we raise the question of the existence of a possible

reverse-SOXIESST phenomenon, similar to reverse-LIESST[7], and this reverse phenomenon is also anticipated for the neighboring effect HAXIESST[118]. In fact, since the excitation is not selective the reverse-SOXIESST is included in the general SOXIESST effect, as any X-ray excitation of the sample generate both LS → HS and HS → LS transitions.

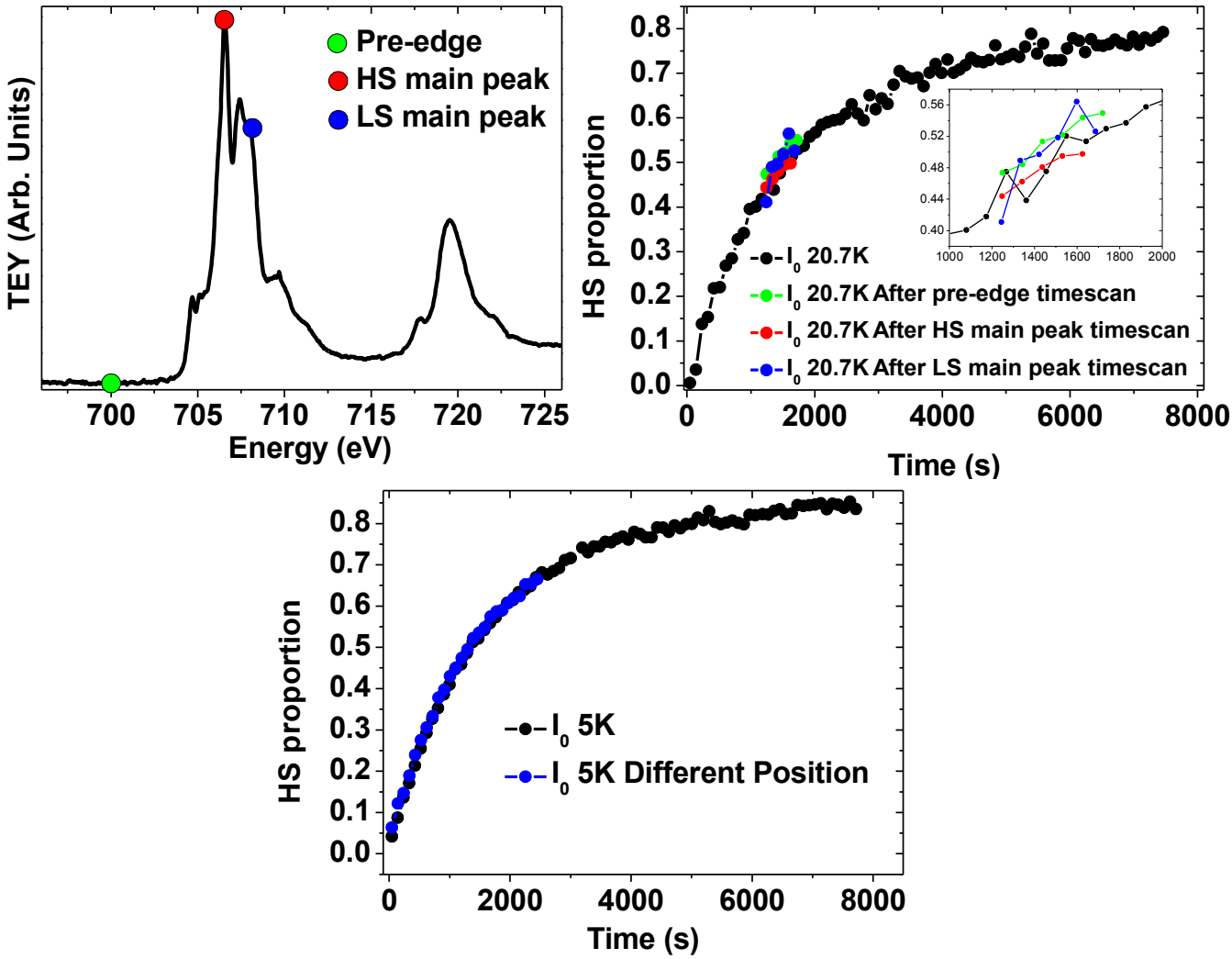

Fig. V.8: The top right panel exhibits SOXIESST dynamics acquired for a full series (black) and for several spectra acquired after illuminating the sample at a precise energy for 1200s (colored). The HS proportion obtained after this treatment is identical to the proportion obtained without the treatment, as shown in the insert. The precise energies at which the 1200s-illuminations (timescans) are held are illustrated on the top left XAS spectra, using the T = 30K example to highlight the energies with the same color code as on the right panel. Bottom panel exhibits two SOXIESST dynamics acquired at two different positions on the sample and the same temperature.

According to the literature[57], the LIESST excitation and relaxation dynamics are self-accelerated due to cooperative effects, which leads to non-linear dynamics as detailed in chapter I. In our case, we simplify the model compared to the first chapter, disregarding the excited state and the cooperative effect by just using the LS-to-HS conversion and the subsequent relaxation, with their

respective rate constants:

LS $\xrightarrow{k1}$ HS; HS $\xrightarrow{k2}$ LS

This leads to the following equation of evolution of the HS proportion:

$$p_{HS}(t) = \frac{-k_1}{k_1 + k_2} \times e^{-(k_1 + k_2) \times (t + t0)} + \frac{k_1}{k_1 + k_2} \quad , \tag{V.1}$$

which will give $1/(k_1+k_2)$ as the time constant and $k_1/(k_1+k_2)$ as the saturation (i.e $p_{HS}(t \rightarrow \infty)$).

We also confirm in Fig. V.8 that the effect is homogeneous across the sample: it is possible to acquire SOXIESST dynamics at different points of the sample with no difference.

Moreover, since we could not identify precisely the beginning of the excitation, we allow within the fitting procedure a time offset (t0) so as to grant some freedom to temporally position the initial point of the SOXIESST process and we position the timestamp for each spectra at the middle of the time window. The acquisition durations for one spectrum are varied, typically 60s.

At first, we ascertained that k_1 seems to be independent of the temperature above approximately 10K. This is in agreement with LIESST experiments, for which k_1 is considered to mostly depend on the intensity and the probability of conversion[57]. We thus fit the curves using a global k_1 for all the SOXIESST dynamics with the same X-ray intensity. For T>10K we find that k_1 for I_0 is $5{,}9\times10^{-4}$ s^{-1}; for $10I_0$ is $2{,}8\times10^{-3}$ s^{-1}; and for $20I_0$ is $3{,}0\times10^{-3}$ s^{-1}.

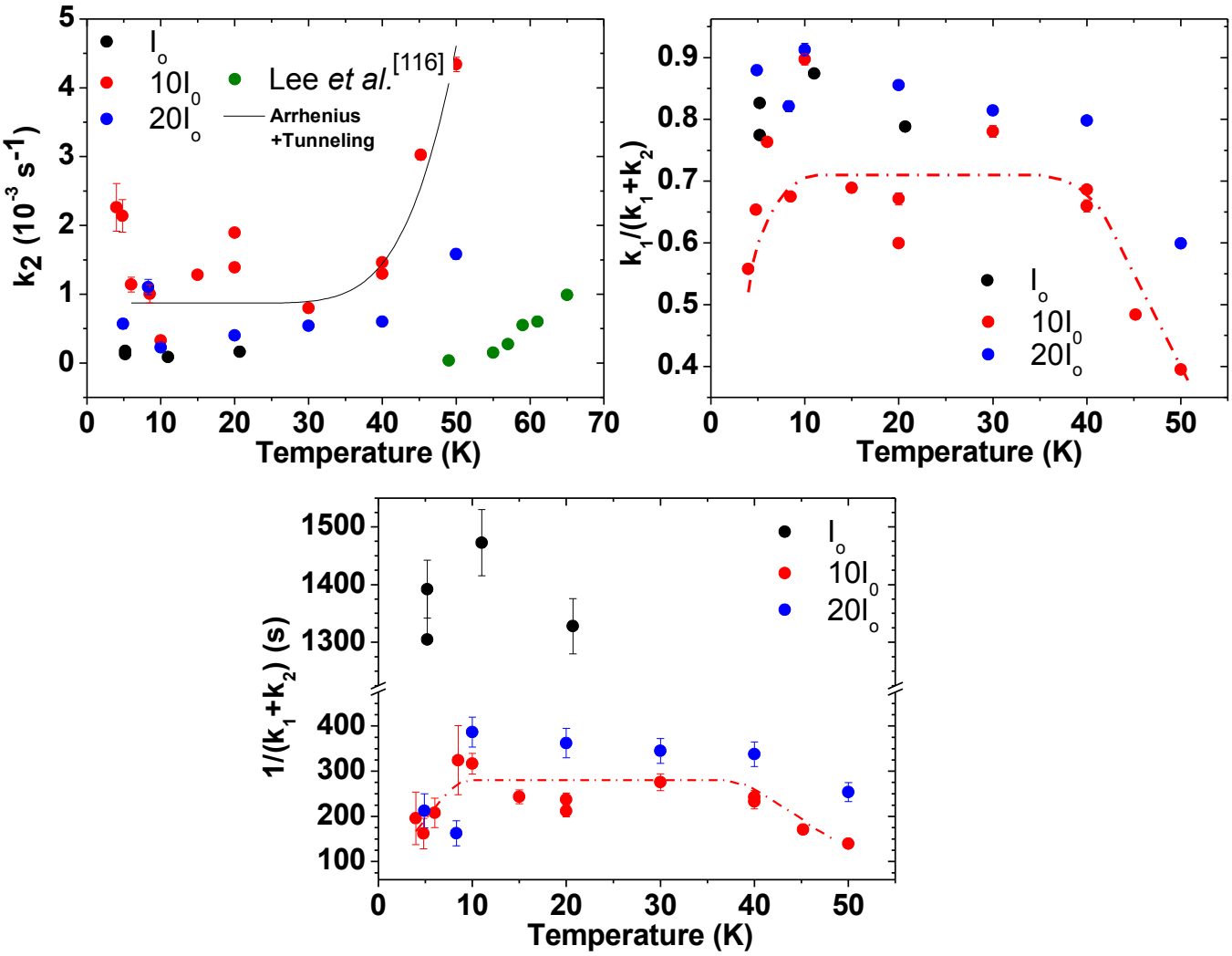

Fig. V.9. Temperature dependence of the fitted values of (top left) the HS → LS relaxation rate constant, with experimental values of Lee *et al.*[116] and a fit of the $10I_0$ data points based on Eq IV.2 (top right) the saturation, $k_1/(k_1+k_2)$, and (bottom) the time constant $1/(k_1+k_2)$, with dotted lines as visual aid for the eye, of the SOXIESST effect for Fe-phen powder, for each SOXIESST dynamics and each intensity.

The relaxation parameter k_2, which corresponds to the relaxation of the metastable HS state into the LS state, was already investigated in the case of the LIESST effect for several spin transition molecules[108]. Experimental values of k_2 resulting from LIESST determined by Lee *et al.*[116] are plotted in Fig. V.9 together with our results for comparison. The actual HS → LS relaxation, however, follows the equations for an ISC process[108], as described in chapter I, rather than the more common Arrhenius law. Above 30K[53], we should include in the law a cooperative term that depends on the HS proportion[83,105]: $k_2(T, P_{HS}) = k_2(T,0)\times\exp(-\alpha(T)\times P_{HS})$, α being proportional to the inverse of the temperature. This term is also present in the excitation. This could explain the dispersion in our results, since a slight HS proportion before illumination can induce drastic

changes in the k_2. However, our results make it impractical to try to obtain a reasonable value of α(T). Secondly, the ISC process presents a tunneling regime that makes it divergent from an Arrhenius model at low temperatures. In essence, some relaxation still occurs below 30K[53,83], as described in chapter I. To illustrate this discrepancy, we plot as a line in Fig. V.9 a fit of $10I_0$ corresponding to the following modified Arrhenius equation:

$$k2 = A \times e^{\left(\frac{-Ea}{k_B \times T}\right)} + \lim_{T \Rightarrow 0} k2(T) \qquad \text{(V. 2)}$$

Nevertheless, compared with the previous LIESST dynamics experiments, a qualitatively similar behavior is observed. Notably, we obtain a plateau from 4K to 40K[105], and above 40K, an exponential-like increase. We find E_a = 32 ± 17 meV, compared to 61 ± 9 meV for the LIESST-excited relaxation in the litterature[116]. Similarly, the relaxation rate is controlled mostly by the preexponential factor, as A = 6,4 for our results compared to 57 for Lee *et al*.[116]

For T<10K, we observe an apparent decreasing trend in the saturation (Fig. V.9 top right), as well as a decrease in the time constant (Fig. V.9 bottom). This behavior has already been noted for the LIESST effect using magnetic measurements for various SCO molecules[46,187], but it was attributed to various measurement artifacts. Some of the proposed factors, like the opacity of the sample preventing light penetration, zero-field splitting[46] and antiferromagnetic coupling in the case of dinuclear compounds, are however not expected with our XAS technique. Therefore, we suggest a new explanation for the behavior: this could reflect a decrease in the effective k_1, that we assumed temperature-independent in the analysis between T=10K and T=50K, possibly due to an increased molecular rigidity, which impairs the structural change associated with the spin transition. Essentially, low-temperatures "freeze" the given spin state and impair the switch. Oppositely, the molecules located at the grain boundaries or interfaces may remain more mobile, which results for T<10K in a "faster" transition and in a decrease in saturation. Our model does not account for this behavior, which would explain the anomalous increase in k_2 and decrease in the time constant at temperatures under 10K.

Our extensive dataset appears to show an inconsistent progression toward higher SOXIESST HS proportion with X-ray intensity: the saturation reached at 5K with the intensity $10I_0$ is inferior to the saturation reached with I_0, itself inferior to the saturation reached with $20I_0$ (respectively ~ 0.7,

0.8 and 0.9, compare top left and right panels of Fig. V.5, and consider the top right panel of Fig. V.9). At present, we surmise that this might reflect spin transition dynamics induced by the synchrotron source itself. Indeed, the I_o dataset was acquired in single bunch filling mode, while the other two datasets were acquired in hybrid mode. Since the single bunch filling occurs by bursts of 20 mA at 0,85 MHz, whereas the hybrid filling occurs by bursts of 1,36 mA at 352 MHz, such a difference might act upon the rate of conversion of a transient state with a lifetime in the nanoseconds range[53,152], meaning that in the hybrid mode, after a first bunch excites part of the sample there might be still some transient state presents in the sample when the next bunch illuminates the sample. Subsequent measurements beyond the scope of this work may clarify this point.

Fig. V.6 right panel reveals that the LIESST and SOXIESST effects may be combined to achieve a higher HS proportion. This means that it is possible to incrementally deploy the LIESST (SOXIESST) effect and then, starting from a steady state, to study the dynamics of the SOXIESST (LIESST) effect. Our investigation involves the XAS technique to measure the HS proportion, but one can imagine using the X-ray source exclusively to irradiate and deploying another technique, such as electric current measurement, to measure the HS proportion without altering it. With the superior penetration depth of X-ray techniques (including the similar technique HAXIESST) compared to LIESST, it can be a useful tool to affect the HS proportion in opaque devices. In our case, at T=4.8K and after renormalisation on the same quantity of matter, k_2 = 7.9×10-4 s^{-1} for the sample that was pre-illuminated with white light, while k_2 = 2.0×10-3 s^{-1} for the virgin sample. This suggests that the SCO dynamics are faster when part of the sample is already in the HS state at a given temperature, in agreement with the cooperativity processes that underscore how the SCO process is presently understood[57].

V.2.v Comparison with Fe-pyrz: same effect, different symptoms

In order to test of how cooperativity may impact the SCO dynamics, we compare our results on Fe-phen with those obtained on Fe-pyrz. As seen in chapter II and IV, and in contrast to Fe-phen, Fe-pyrz exhibits a thermal hysteresis in its thermal spin transition. Yet the HS → LS transition is thermally sharper than the LS → HS transition. Since the transition sharpness reflects the strength of the intermolecular cooperativity that takes part in the transition[38], this suggests that the HS → LS transition involves stronger intermolecular cooperativity than the LS → HS transition. As seen in

Fig. V.3, the XAS spectra for Fe-pyrz are quite similar to those found for Fe-phen. Since both molecules share the same octahedral arrangement (including the nitrogen « cage »), this was expected.

Intensity		Temperature (K)	k_1 (s^{-1})	k_2 (s^{-1})	Time constant (s)
I_o	Fe-pyrz	5	3.2×10^{-4}	3.2×10^{-4}	1560
	Fe-phen	5.2	5.9×10^{-4}	1.2×10^{-4}	1390
$20I_o$	Fe-pyrz	11	1.4×10^{-3}	1.1×10^{-3}	395
	Fe-phen	10	3.0×10^{-3}	2.3×10^{-4}	386

Table 1: Fit parameters for Fe-pyrz and Fe-phen for the two intensities.

The time constants $1/(k_1+k_2)$ for Fe-pyrz are very similar to those for Fe-phen. Yet, for the same intensity I_0 and at T=5K, the SOXIESST HS proportion achieved by Fe-pyrz (~0.4 at 3500s) is lower than that for Fe-phen (~0.8 at 3500s). This shows that Fe-pyrz requires greater X-ray photon intensity than Fe-phen in order to transit. Comparing both spectra, we notice that a peak at 711eV is absent from the Fe-pyrz spectrum. This peak is believed to be related to the hybridization between the Fe(II) 3d orbitals and the NCS ligands[119,164], meaning the increase of charge transfer from the metal to the ligands[116]. This is an indication that the SOXIESST effect, while non-resonant, relies mostly on MLCT bands, in a similar fashion as mentioned in chapter I with the LIESST effect. There seems to exist a series of desexcitations through a succession of excited states, in which MLCT states play a crucial role, probably in the final stages of the cascade. Taken together, these results suggest that, while the excitation process is the same for both molecules, compared to Fe-phen, the illumination of Fe-pyrz might less efficiently induce the LS → HS transition (k_1 lower) and, conversely, the HS → LS relaxation of Fe-pyrz might be more efficient (k_2 higher). This would be in agreement with the more strongly cooperative HS → LS, and more weakly cooperative LS → HS (possibly due to a crystallographic phase transition[178] or defects creation, or an intrinsically low-cooperative LS form), transitions observed for Fe-pyrz (see parts II.2.ii and IV.2). Further studies should be necessary to fully differentiate the contributions from MLCT states and cooperativity.

V.2.vi SOXIESST Dynamics in powder SCO molecules: conclusion

Through this part, we have reached a better understanding on the way the X-rays induce a

metastable HS state at low temperature, an effect that we confirmed unambiguously, and that should be taken into account in every study of SCO molecules at low temperatures with X-rays. The amplitude and the time constant of the SOXIESST effect depend not only on the intensity of the beam illuminating the sample, but also on the structure of the illuminating beam itself. We have adapted a basic exponential fit to the HS proportion evolution results, and find that it corresponds quite well to our data, allowing us to build a simple model for the physical parameters such as the rate of conversion to HS of the SOXIESST effect, the time constant, the saturation, and the rate of relaxation from HS to LS. The effect is similar in appearance to the more widely-known LIESST effect, as it seems to relies upon the MLCT states to initiate the deexcitation into the metastable HS state. The main difference is that the SOXIESST effect is non-resonant: the energy of the excitation does not impact the excitation process itself. This effect can be combined with LIESST, and they occur in the same time scales, therefore one can study the dynamics of LIESST by using previously SOXIESST, and vice-versa. Indeed, both dynamics are heavily dependent on cooperative behavior: one can imagine setting a precise HS proportion in the sample with one effect, and studying the dynamics of the other effect. Furthermore, we have observed that differences in cooperativity can influence the SOXIESST effect.

V.3 Thin films of Fe-Phen : the progress of cooperativity

After investigating in depth the influence of X-rays on powder samples, the next step is to use this technique to understand the behavior of SCO molecules in thin and ultra-thin films: as mentioned in chapter IV, SCO molecules in thin films behave very differently from bulk SCO molecules. The interaction between SCO molecules and the surface strongly impacts to the spin transition behavior.

V.3.i Thickness determination and similarities between surfaces

The depositions were carried out by *in-situ* thermal evaporation on Cu(100) or Co(100) surfaces. As presented in II.2.ii, the Cu(100) surfaces were obtained by cleaning a single crystal of Cu(100), and Co(100) is obtained by thermal deposition of a Co film (~12 to 24ML) on Cu(100). Since the thickness of Co has strictly no influence on the results (compare 1.1 and 1.4ML of Fe-phen on Co(100) surfaces in Fig. V.10), the Co surfaces are referred as Cu(100)//Co or simply Co in the rest of the study. Thicknesses of Fe-phen were determined using a combination of XAS signal integral intensity and STM measurements: several STM pictures were used to evaluate the coverage of a

calibration sample by observing the holes in the layers, until the Cu(100) substrate was recognized, as shown in Fig. V.10. Then the integral of the same sample XAS signal was determined, and this reference was used to deduce all thicknesses by comparing the XAS integral value for each signal. This is slightly different from the method used in the literature[148], that uses the edge jump for this purpose. As illustrated in Fig. V.10, we believe however that the integral value can be used as an identical or even more precise indicator of the coverage than the edge jump, especially at monolayer (ML) or sub-monolayer coverages. The bottom plot in Fig. V.10 confirms that the integral value of Fe L_3 is linearly proportional to the deposition time on Cu(100)//Co surface as a linear fit of the 4 thinner samples (black line) go through the origin, whereas the same fit for the edge jumps exhibits a higher offset. Furthermore, the deviation to the fit for the thickest sample is smaller in the integral case than for in the edge jump case. In contrary to STM checks that ascertained that Cu surfaces are clean after deposition, it was discovered that Co surfaces were polluted by what we believe to be phen groups on the surface, as illustrated in Fig. V.10. The more reactive Co surface compared to Cu might break molecules or adsorb phen groups that were not adsorbed by the Cu surface. Therefore, our estimations for Fe-phen coverage on Co might be inaccurate. The values of the coverages on Co presented correspond to “nominal” thicknesses, for example a 1.1ML on Co corresponds to the same quantity of Fe-phen deposited as a 1.1ML on Cu, but the *real* thickness of the Fe-phen+phen system on Co might be thicker. That said, the results described in the rest of this part suggest that this deviation is not too problematic.

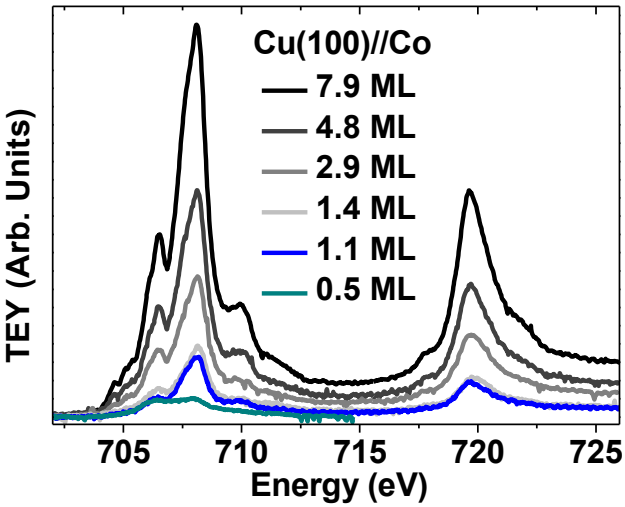

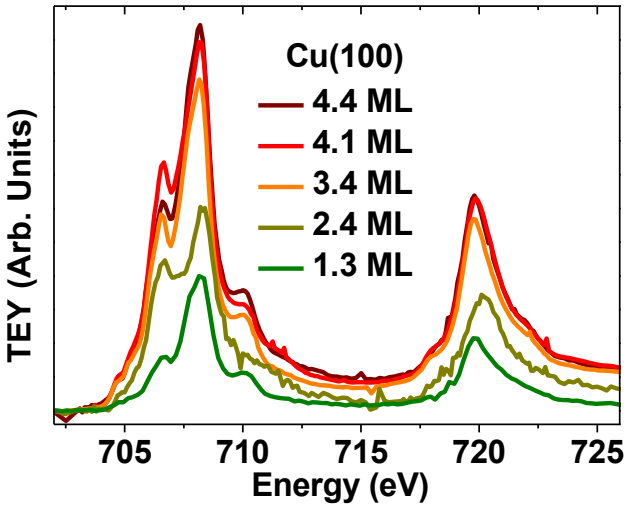

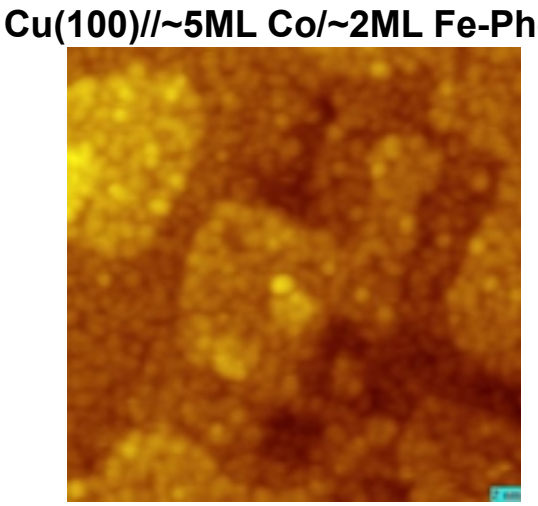

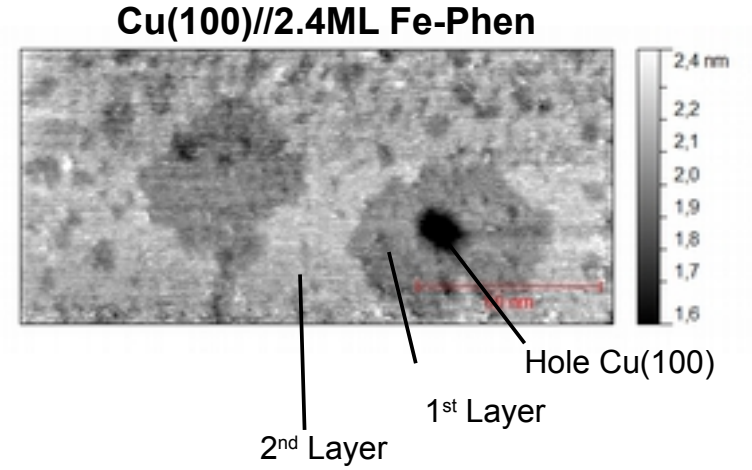

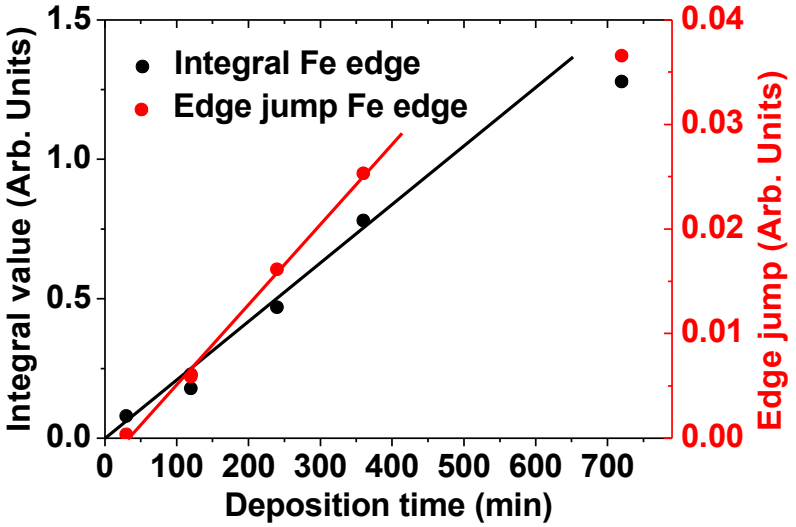

Fig. V.10: Top panels presents the raw XAS spectra of Fe-phen deposited on Cu(100)//Co (Top left) and Cu(100) (Top right) surfaces acquired at 200K and 10 I_0. The scales are different, and the normalized amplitude of Fe-phen 4.4 ML on Cu(100) surfaces corresponds roughly to Fe-phen 4.8 ML on Cu(100)//Co. Middle panels are STM picture acquired with the Karlsruhe STM (left, 30 × 30 nm, courtesy of M. Gruber) and the *in-situ* Deimos beamline STM (right, 161 × 75 nm) of Fe-phen deposited on the two surfaces. The bottom panel plots the integral of the spectra and a linear fit of

it (black, black line) and the edge jump and a linear fit of it (red, red line) as a function of the deposition time.

It is particularly obvious in the case of the sub-monolayer sample that the samples exhibit a coexistence of both spin states and a "pinned" spin state: we did not observe a change in the HS proportion across the temperature range tested (between 4 and 300K), as illustrated in Fig. V.11, which is consistent with our STM results for Cu(100). The near-monolayer samples only present a slight variability. Both states coexist on both surfaces, and all samples have a part that exhibits a "pinned" spin state as shown on Fig. V.11. This "pinned" spin state is defined as HS or LS molecules keep their spin state when submitted to the usual external stimuli (electric field in chapter IV and temperature/X-ray in this chapter). It is interesting to note that our sub-monolayer sample exhibits a comparable HS proportion than that of the literature[148], despite that Warner *et al.* made their deposition of a sub-monolayer of a *different* Fe(II)-based SCO molecule on an Au(111) surface and despite that our Co surface could be polluted by phen groups. Similarly, the HS proportion for 1.1 ML and 1.4 ML on Co and 1.3 ML on Cu are also nearly identical (~60%). However, Bernien *et al.*[153] did not observe a pinned spin state part of the sample with 0.8ML of a $Fe(II)(NCS)_2$-based SCO molecule on a graphite surface. We suggest that the HS/LS ratio of the pinned part on transition metal surfaces with similar lattice parameters is not a function of the surface or the molecule, but of the coverage exclusively, at least under 2 ML.

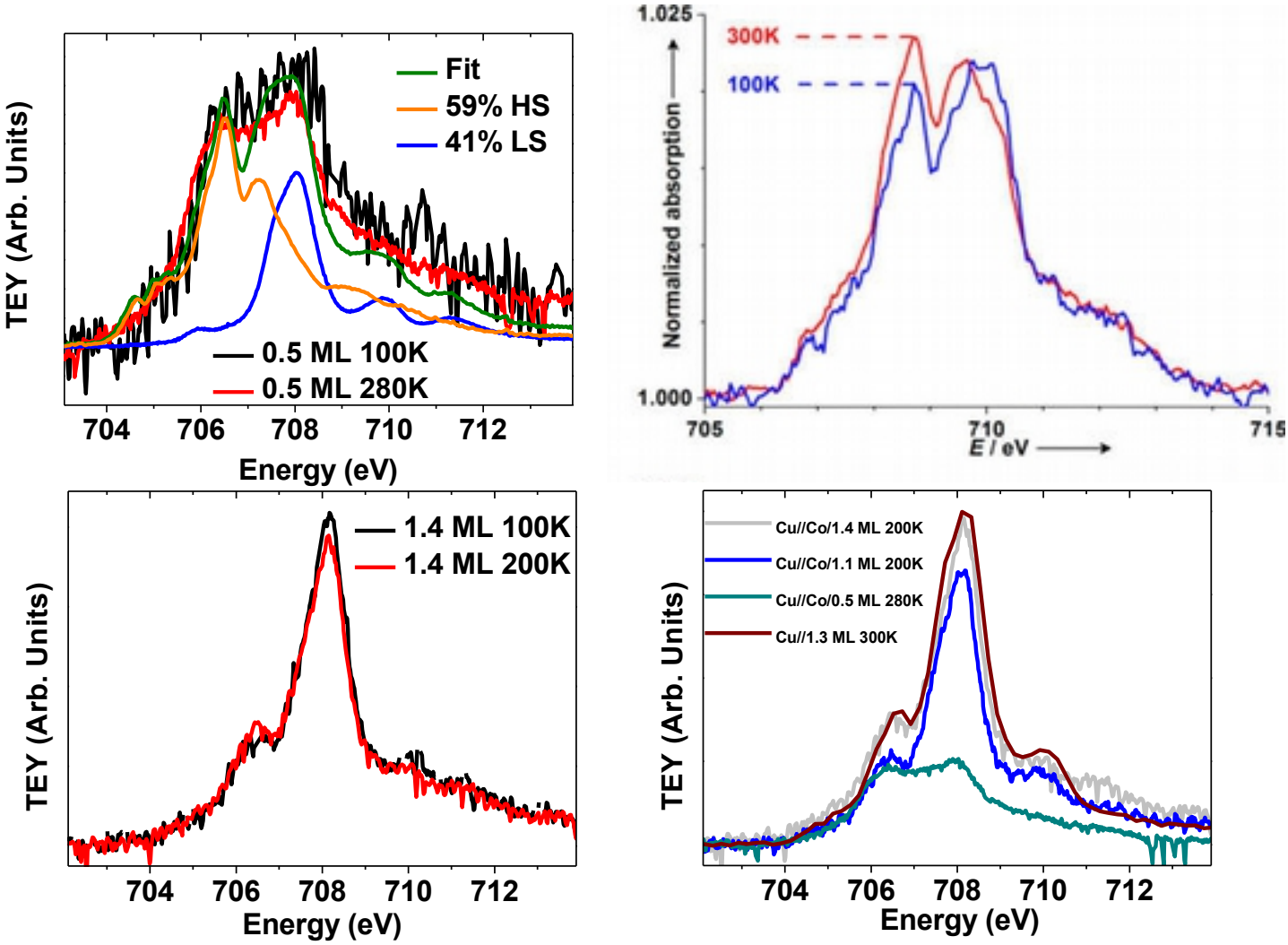

Fig. V.11: XAS spectra of the thinner samples of Fe-phen deposited on Co acquired at temperatures where the powder samples exhibit 100% LS (100K) and 100% HS (200K or 280K). The bottom right panel allows the comparison between the Co and the Cu surfaces: the XAS spectra are very similar. The top right panel is reproduced from [148], and correspond to a claimed 0.03-0.14ML of [Fe($H_2B(pz)_2)_2$(2,2'-bipy)] on a Au(111) surface.

V.3.ii Magnetic properties of Fe-phen on surfaces

The next question raised by SCO-molecule-on-surface systems are more fundamental: can we confirm that the HS state on the surface is identical to the HS state in the bulk? Is the HS Fe-phen coupled to magnetic surfaces like Co? Again, XMCD can provide answers to these question. Fig. V.12 presents the dichroic spectra obtained for the powder sample, and the two tested surfaces. At the temperature where these spectra were acquired, the XMCD signal comes entirely from the SOXIESST-induced HS for the powder and partially from the SOXIESST-induced HS for the thin film samples. Very few differences exist between those spectra. The features are present in all 3 spectra. Therefore the electronic states of the HS state of all 3 spectra must be nearly identical. An

exception might be the feature at LS main peak energy (708.1eV). The powder sample presents no contribution at this energy, as expected, but the thin films exhibit a small signal. This could be due to distortions in the nitrogen "cage" arrangement modifying the geometry of the LS state (and/or the HS state), or charge transfer to the molecule. In the particular case of Co, theoretical calculations hint that there might be some magnetism induced by the surface on the LS state, but these are preliminary results, and do not account for the similar behavior found on Cu surfaces. No coupling was found between the Co surface and the Fe-phen layers, surprisingly.

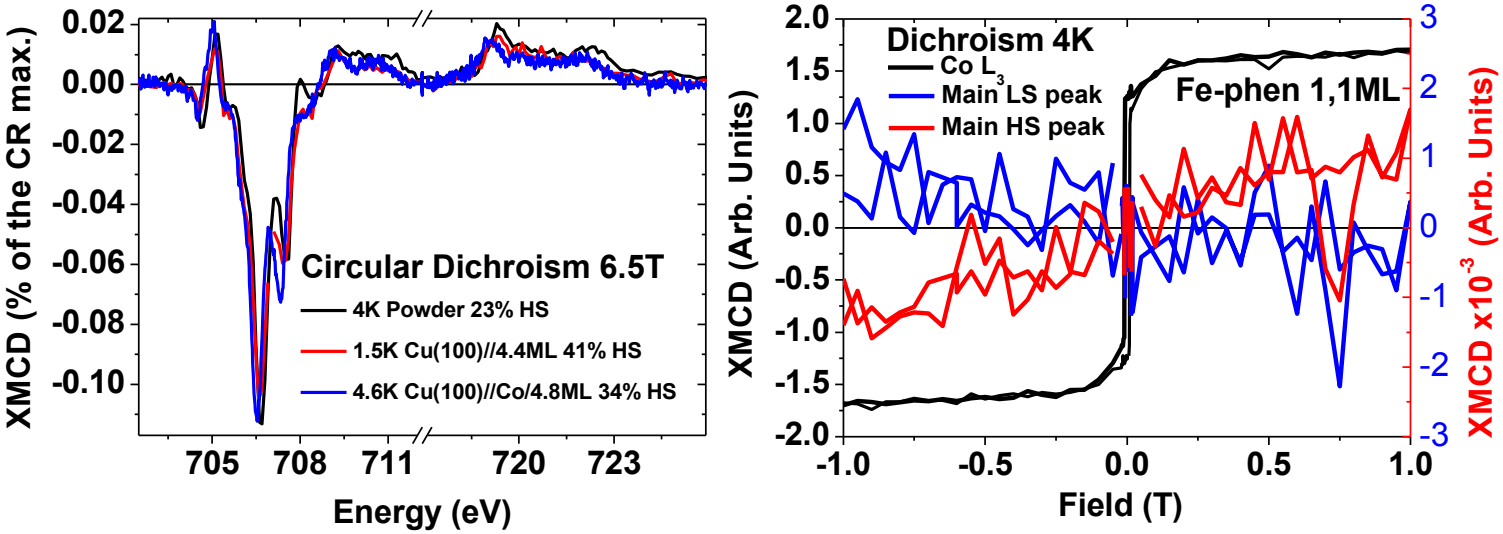

Fig. V.12: On the left, X-ray circular magnetic dichroism of powder, samples of Fe-phen deposited on Cu and Co. Slight deviations in energy of the peaks can be noticed, but as previously noted, they are due to differences in scan parameters. The XMCD signal intensities are adjusted for the HS proportion of each sample and are expressed in % of the maximum signal for the circular right XAS spectrum. The 712-717eV region exhibit no feature. The 3 XMCD are very similar, except maybe for the 708.1eV feature (the dotted line is a visual aid representing the position of this energy). On the right, the dependence on field of the main peaks of XMCD, increasing and decreasing the field: the Fe-phen dependence is clearly linear, and do not couple to the Co. The LS main peak seems very sligthly paramagnetic, but it could be due to a part of the XMCD signal for the HS molecule still present at this energy.

V.3.iii To switch or not to switch: pinned and variable parts of thin films of SCO

Between the STM results for ultra-thin films on Cu(100) and the SQUID results for thicker films on silicon, we wanted to know if it was possible to retrieve the thermal spin transition by increasing the thickness of the deposited layer, and if yes, what were the properties of the thermal spin transition in such low-dimensional systems. The thicker (>2 ML) samples exhibit a thermal spin transition, and the amplitude of the variation of the HS proportion is large enough to be unambiguously studied, results illustrated in Fig. V.13. The transition is, as previously stated,

incomplete: at 300K, a significant part of the sample is still in LS, whereas the powder is 100% HS. Thick films (300nm) of Fe-phen deposited on SiO_2 in a previous study[146] exhibit a rather abrupt full transition. Therefore, our opinion is that thin films of this molecule should adopt a behavior similar to the bulk when the thickness increases. Surprisingly, the medium value does not steadily increase to reach 50% of HS proportion, as expected, but rather seems to stabilize around 0.3 on Co and 0.4 on Cu, as evidenced in the bottom panel of Fig. V.13. This means that the latest-deposited layers are not 100% "switchable", and are still under the influence of the substrate, even if this influence is weakening. We do not notice a decrease of $T_{transition}$ with decreasing thickness, like for Fe-pyrz thick films on native Si reported in chapter IV, or $Fe(H_2B(pz)_2)_2(bipy)$ and $Fe(H_2B(pz)_2)_2(phen)$ thicks films on Kapton reported by Palamarciuc *et al.*[177]. On the opposite, we notice an increase of $T_{transition}$, which confirms Fe-phen thick films results. This behavior is further discussed in the next point.

The transitions are smoother in thin films than in the powder sample, the distribution of transition temperatures is wider: this is a sign of a reduced cooperativity[7] at low thicknesses. The thicker samples present a slightly more abrupt transition. This reduction of cooperativity was reported recently in the literature[148,153]: almost complete transition for $Fe(II)(NCS)_2L$ on graphite[153] and $Fe(H_2B\text{-}(pz)_2)_2(bipy)$ on silicon[177], incomplete transition for the latter molecule on Au(111)[148] and the present study. In details: Bernien *et al.* found a full transition with a slight loss of cooperativity for a sub-monolayer thin film of a $Fe(II)(NCS)_2L$ complex; Warner *et al.* reported a similar slight loss of cooperativity for a Fe(II) complex (with weak intermolecular interactions) with no sulfur binding groups (like NCS) deposited in a sub-monolayer on the surface, with a part of the sample similarly "pinned"; Palamarciuc *et al.* reported a full transition with a slight loss of cooperativity for thick films of the same Fe(II) complex with weak intermolecular interactions on silicon. Therefore, the significant loss in cooperativity we observe in Fig. V.13 can be with a high degree of certitude attributed to the influence of the surface through the affinity of first layer sulfur bonding to the surface, with a minor contribution from other possible factors, such as defects in the layer growth (coming from either an imperfectly crystalline growth or lattice mismatch) or the 2-dimensional nature of the layer (volume change of neighboring molecules being a determining factor in cooperative behavior[53]). A magnetic layer such as Co surprisingly does not seem to favor HS in 1-8 ML thickness range, despite high fields favoring HS in the bulk[98]. Instead, the mean HS proportion for the Co-deposited thin films seems significantly lower than for the non-magnetic Cu.

The spin-transiting part is also sensitive to the SOXIESST effect investigated in the previous point. Fig. V.13 therefore presents the static aspect of this effect. Dynamics were also obtained for Co-deposited substrates, and these results are present in the last point of this part. Unfortunately, the fast scan method was not implemented by that time during the experiments on Cu substrates, therefore the results exhibit only the resulting static SOXIESST effect, not its dynamics.

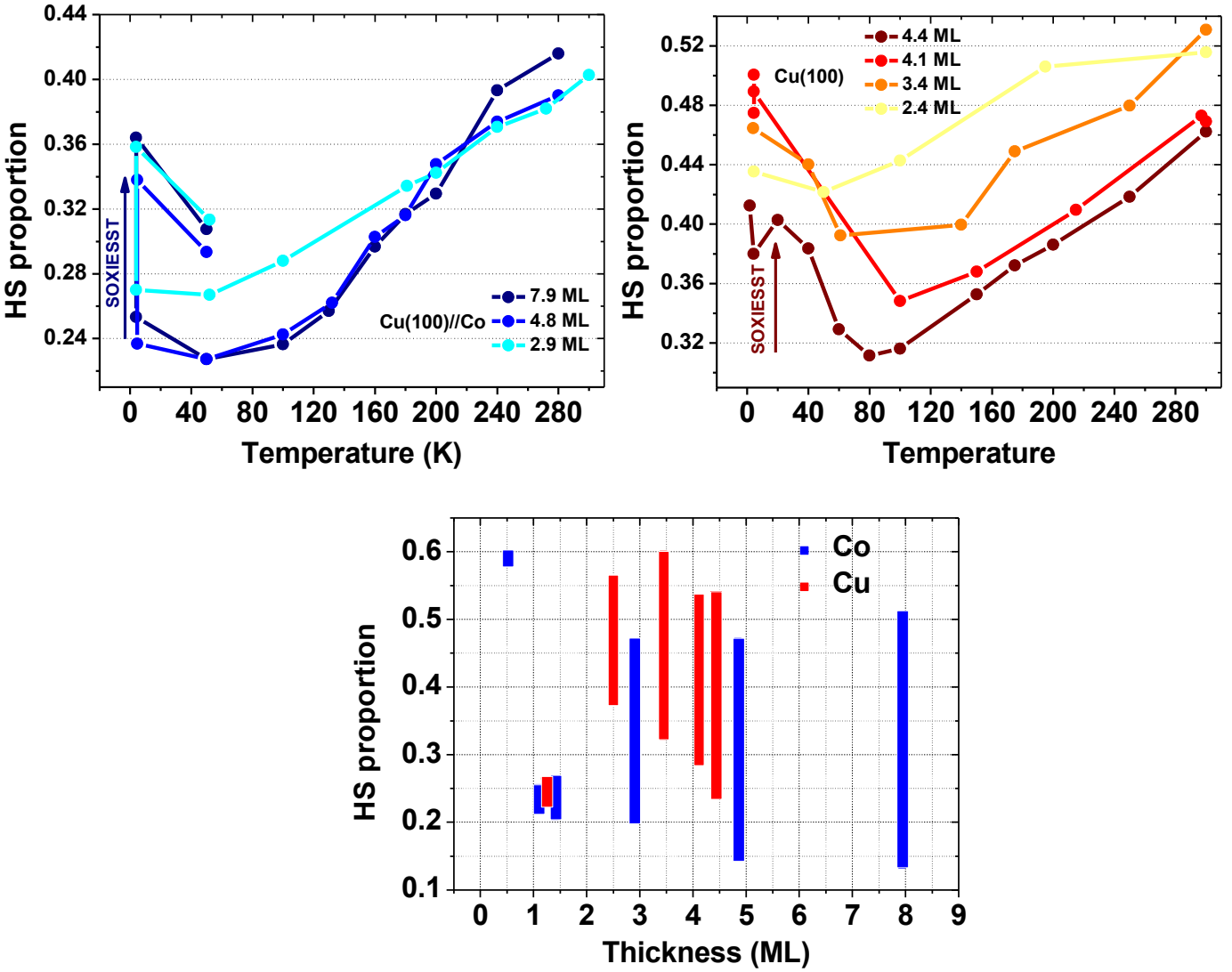

Fig. V.13: On the top are presented the temperature-dependent plot for all thicknesses that exhibit a sizable thermal transition. The full temperature range is presented in a similar fashion as Fig. V.5. The temperature is decreasing for all curves. Below $T_{SOXIESST}$, at approximately 60K, the SOXIESST effect is clearly observed: For the films deposited on Co, at T = 50K and T=4K, the HS proportion extracted from the first scan of a series is presented in the bottom, with a low HS proportion. The last of a series, corresponding to *SOXIESST with reset*, at $10I_0$, is presented above it, with a high HS proportion. The line between both types at 4K is given as a guide to the eye. The bottom panel presents the coverage-dependent plot for both surfaces for all thicknesses. The height of the rectangle corresponds to the amplitude of the transition (minimum HS proportion – maximum HS proportion).

V.3.iv Thermodynamic analysis of the thin films

It is possible to investigate more the details of the changes in the thermal transition compared to powder samples by fitting the thermally transiting part of the temperature-dependent plot with equation (I.6), with the HS proportion variable modified by an offset and a multiplier factor (named the amplitude) to account for the pinned part of the sample: $p_{HSfit} = p_{HS} \times \text{Amplitude} + \text{Offset}$, with p_{HS} defined by the implicit equation I.6. The results are presented in Fig. V.14, with the fitting equation V.3. It is important to note that the resulting equation has 5 independent variables (4 in practice because the offset is easily determined by observing the HS proportion at powder-100%-LS-temperature), when the number of data points fitted range from 4 to 8. Therefore, the incertitude on the fit parameters is high.

$$T\left(Amplitude \times p_{HS} + Offset\right) = \frac{\Delta H + \Gamma\left(1 - 2\left(A \times p_{HS} + O\right)\right)}{R \ln\left(\frac{1 - A \times p_{HS} - O}{A \times p_{HS} + O}\right) + \Delta S} \qquad \text{(V.3)}$$

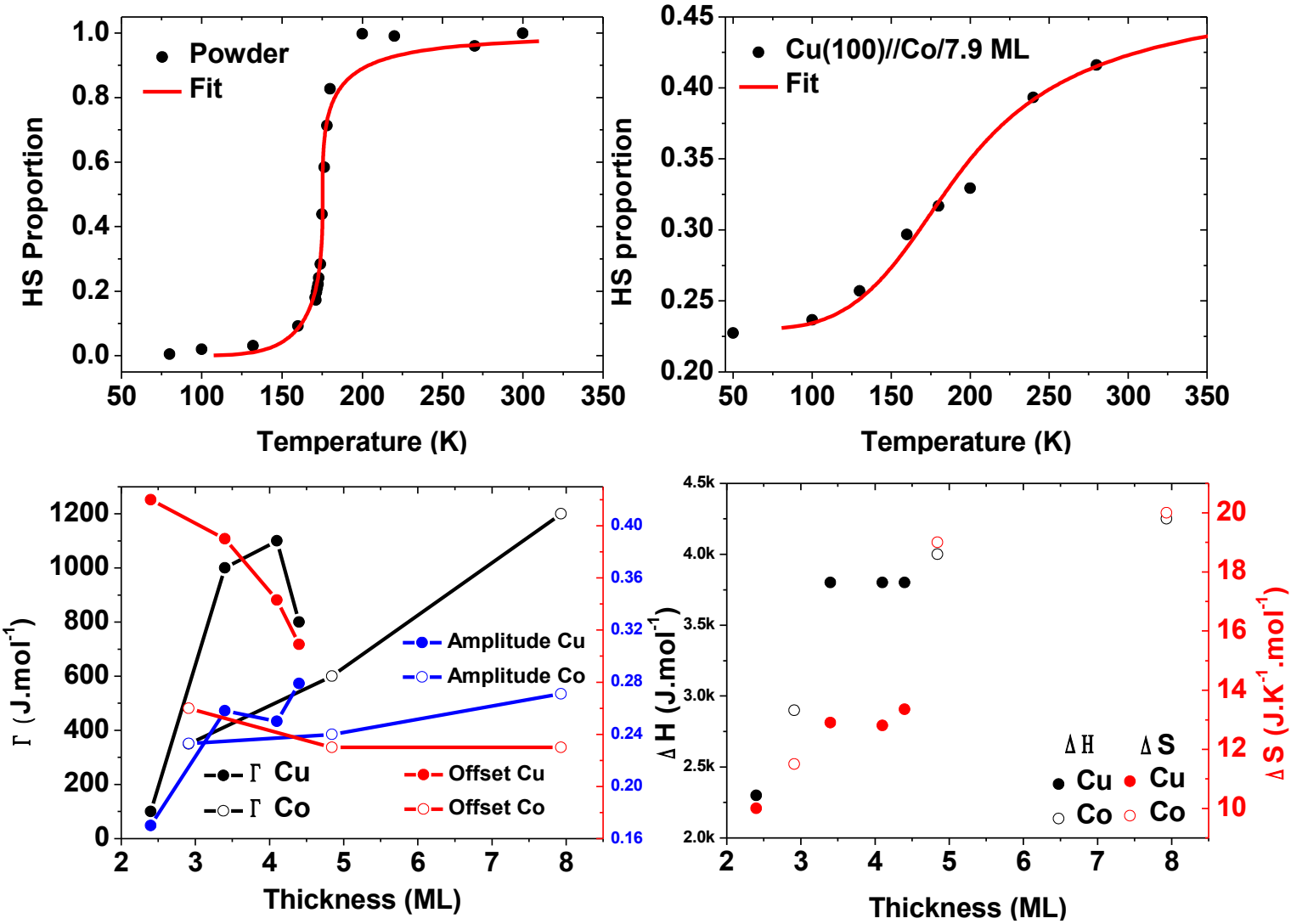

Fig. V.14: Plotted in top left and right panels are the fits of the thermal transition for the powder sample using equation I.6 and the Co-deposited 7.9ML sample the modified I.6 equation. The bottom panels presents the fit parameters: on the left the shape parameters (Γ, Amplitude, Offset), on the right the thermodynamic parameters (enthalpy, entropy) for both surfaces. Those results should be handled with care, as noted previously, because we fit the few points with 4 parameters.

The fit parameters for the powder sample obtained are $\Delta H = 8590$ J.mol^{-1}, $\Delta S = 49$ J.K^{-1}.mol^{-1}, very close to experimental values obtained by calorimetric measurements[45] and $\Gamma = 2900$ J.mol^{-1}. Thermodynamic parameters for the thicker thin films amount to 44% (Cu) 49% (Co) of bulk ΔH and 29% (Cu) 41% (Co) of bulk ΔS, a result comparable to those obtained for a sub-monolayer of weakly-interacting SCO molecules deposited on an also weakly-interacting HOPG surface[153] that exhibited 44% of bulk ΔH and 49% of bulk ΔS. The parameters deduced from the fit suggest that at low enough thickness, the entropy difference between the HS and the LS state is below Δs_{el} (13,38 J.K^{-1}.mol^{-1}), shown in the introduction to be the minimum ΔS of the system. This can be explained if

we consider the Kondo effect described in chapter IV: below the Kondo temperature determined to be 317K, the unpaired spin form a singlet with the substrate electron, the magnetic moment of the Fe vanishes and as a consequence, the magnetic entropy vanishes. Of course, we were not able to prove in chapter IV the existence of the Kondo effect on the molecules above the interface on Cu(100), but the presence of the Kondo effect on switchable molecules on CuN proves that the presence of the Kondo effect (strong coupling) is not a sign of the absence of spin transition.

Unfortunately, neither Warner *et al.*[148] or Palamarciuc *et al.*[177] who used SCO molecules with higher intermolecular interactions did this thermodynamic analysis on the thermal spin transition, but from the curves it seems that the loss of cooperativity is much stronger in our case. Therefore, this comparison suggests that for the thicker samples, the difference in thermodynamic parameters would come from the thin film nature itself of the sample, while the loss in cooperativity could come from the surface-molecule interaction. It is possible that it finds its origin in the "pinned" part of the sample: some molecules are "pinned" by influence of the surface into either LS or HS, but the molecules could be randomly "pinned" in a given layer, acting as "transition" defects and nucleation points, reducing the effect of intermolecular interaction. Interestingly, the reduction of Γ is also 38% (4.1 ML Cu) 41% (Co) of the bulk sample Γ, comparable to what is found for ΔH and ΔS.

Regarding coverage-dependence, ΔH and ΔS are noticeably smaller for thinner samples, indicating an enthalpically less preferred LS state, and an entropically less preferred HS state on the surface compared to the bulk sample. Thermodynamic parameters of "ultra-thin film" samples reach "thin film" values around 4 ML, while Γ, as expected from the intermolecular cooperativity parameter, increase from thinner to thicker samples, as the latest-deposited layers are less and less influenced by the substrate. Although it is unclear if there is a stable "thin film" value like for the thermodynamic parameters.

In chapter I, the thermal transition temperature was defined as $T_{transition} = \Delta H/\Delta S$. Using the fitting parameters, we can therefore plot the calculated $T_{transition}$ as a function of thickness in Fig. V.15. These results should be considered with caution, but, as a trend, it is apparent that the thermal transition temperature is significantly *higher* for thin film samples than for the bulk. A conclusion that matches the results for Fe-phen thick film on silicon described in chapter IV, but is surprisingly opposite to the conclusion reached for Fe-pyrz thick films in chapter IV and the results obtained on

a Fe-pyrz analogue by Palamarciuc *et al.*[177]. Indeed, both sets of results presented *lower* thermal transition temperatures for thin film samples. We propose the hypothesis that this behavior is linked to molecule-surface interaction: indeed, on one side Fe-phen is interacting strongly with the surface, which means that long-range constraints can "force" the film to transit at higher temperatures, even if the lack of short-range interactions do not favor the cooperativity of the transition. On the other side, Fe-pyrz is more weakly interacting with the surface, which means that the long-range constraints can be relaxed in the thin films compared to the bulk samples, leading to a lower spin transition temperature. Our thermodynamic model including cooperation is however not suited to fit the unusual spin transition of Fe-pyrz, therefore we cannot compare the thermodynamic parameters of Fe-phen and Fe-pyrz thick films. Further studies should clarify this behavior.

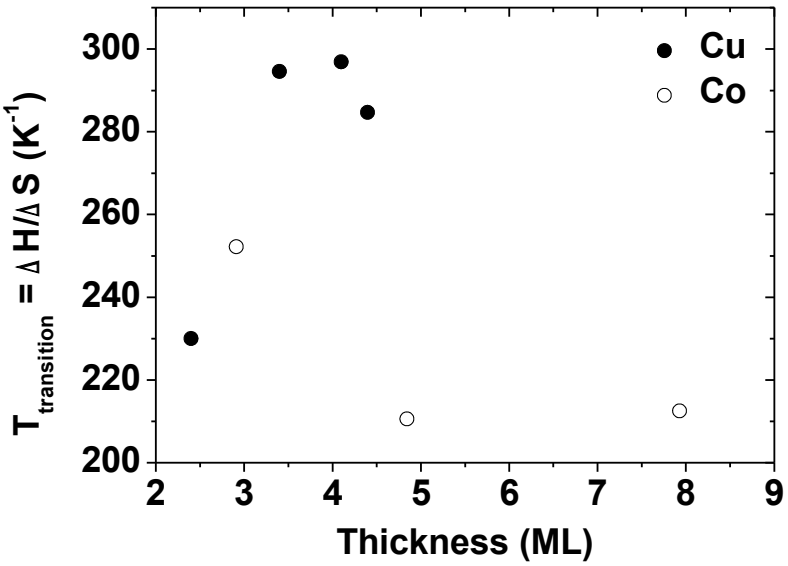

Fig. V.15: Plot of the thermal transition temperature extracted from the model as a function of the nominal thickness, for both surfaces.

V.3.v A simple model of Fe-phen spin transition in thin films

In order to provide a better theoretical understanding of the spin transition of SCO molecules influenced by the substrate, we have tried to fit the results obtained in the previous paragraph to a simple model of molecular layers. This model consists in assuming that the interface Fe-phen layer is 100% LS (at first), the topmost layer is 100% HS (as observed by STM) and the "volume" layers exhibit a bulk-like spin transition behavior. A schematic view of this model is presented in Fig. V.16. We have then compared the theoretical predictions of this model to the results acquired on Cu substrates, as the Cu substrates do not get contaminated by phen groups. The offset obtained by

the simple model is the proportion of the sample that is 100% LS, and the amplitude is the proportion of the sample that is "bulk". Fig. V.16 clearly suggest that this model is too simplistic to fit the experimental data. Changing the HS/LS proportion of the interface layer does not affect the shape of the evolution after 2ML, which is the main discrepancy. Fe-phen layers on transition metal surfaces present a non-trivial spin transition.

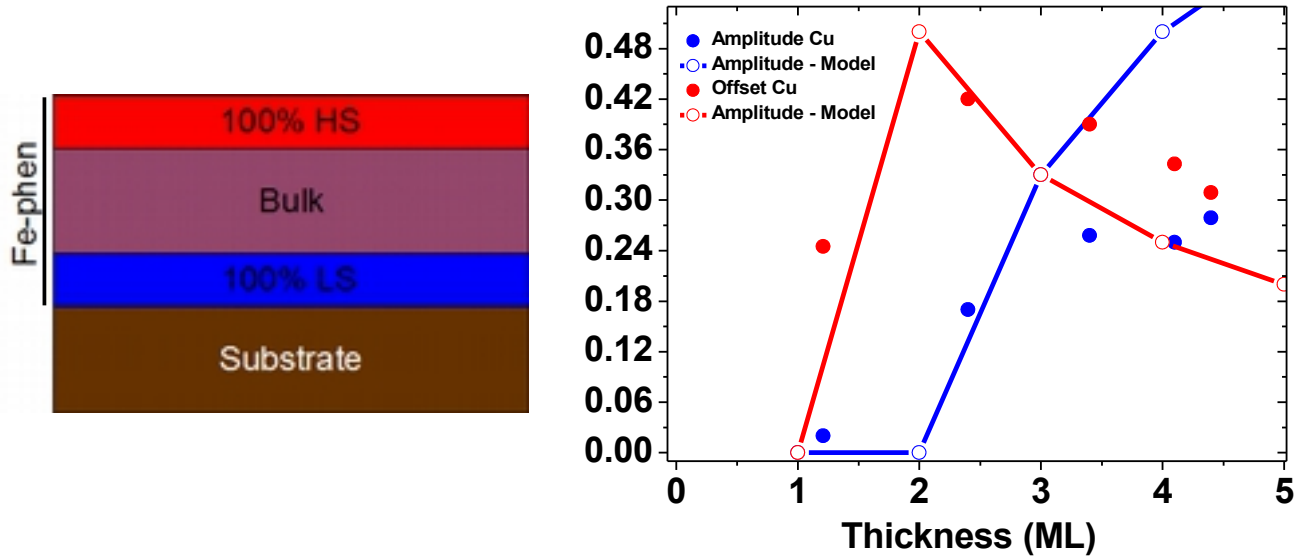

Fig. V.16: On the left, schematic view of the layer spin transition model used. On the right, theoretical predictions of this model compared to experimental results. Except the two first thicknesses, the experimental trend does not seem to follow the model chosen.

We suggest that the "bulk" part of the thin film is in fact influenced by the pinned-state interfaces: the "bulk" layers would still contain a pinned-state part. This pinned-state part could itself have various HS/LS ratios according to the distance with the interfaces. Fig. V.17 illustrates the idea. Of course, vacuum/sample and substrate/sample interface layers might have a different influence on the neighboring layers, namely each of the two intefaces could generate a pinned-state of a different size (the vacuum/sample interface should be less constrained than the substrate/sample interface) and of a different HS/LS ratio. Furthermore, when one includes the possible influence of the defects that could act as nucleation points for the pinned-state parts and the interplay between neighboring layers due to cooperativity, the final model can become very complex. Our set of data is however not extensive enough to provide an adequate view of the whole phenomenon, and further studies will be necessary to obtain a full picture of the structure of thin films of Fe-phen.

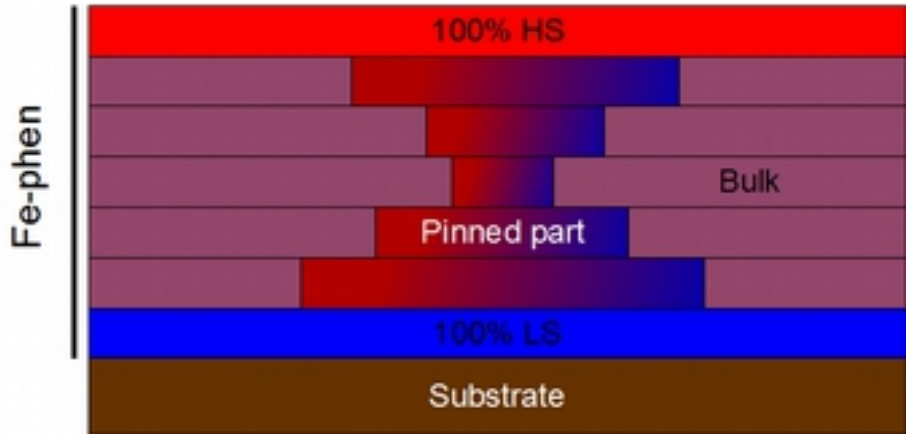

Fig. V.17: Schematic representation of a more complete model of a thin film sample.

V.3.vi SOXIESST effect in thin films

The last feature to yield information of thin films is the SOXIESST effect observed on the thin films deposited on surfaces. Recently, LIESST was observed for thin films[147] and Warner *et al.* [148] have observed a slight SOXIESST effect on a sub-monolayer of a molecule that seems only lightly sensitive to this effect (or the beam illumination was too weak). We confirm and expand this point: we have carried out a study similar to the study presented for the powder, and Fig. V.18 clearly exhibits that the thin films at 10 I_0present a similar SOXIESST effect as the powder sample. Unfortunately, we were not able to acquire SOXIESST dynamics for Cu ultra-thin samples. The dynamics curves were renormalised to the switchable part of the sample, which means that to each curve was subtracted the offset, then the curve was divided by the amplitude of the thermal spin transition, so the dynamics could be compared to each other and the powder sample by fitting the same equation (IV.1). As an equation, this gives us $P_{HS\text{-}SOXIESST\ Fit} = (P_{HS} — offset)/amplitude$.

The observation that the metastable HS → LS transition at $T_{SOXIESST}$ is still quite abrupt suggests that the SOXIESST effect affects random switchable molecules, like the LIESST[57].

For the thicker samples, the time constants are similar, but it seems that the SOXIESST loses efficiency, as the thin film effect amounts to 50% of the thermal transition amplitude determined by the model compared to 70% of the thermal transition observed in the bulk. This is shown in the top left panel of Fig. V.16 (the aberrant value for 4.1 ML on Cu is not presented). That said, the determination of the thermal transition amplitude by the model might not be perfect. An important point is that in “ultra-thin” films, below 4.5ML, the effect is even less effective. Results for 2.9 ML on Co suggest that the time constant is increasing at thicknesses below 4 ML, but one should treat these results with care: we have tested only 3 samples and 2 temperatures. K_1 are

slightly lower than that of bulk (1.1×10^{-3} and 1.4×10^{-3} s^{-1} for 4.8 and 7.9ML respectively, compared to $2,8\times10^{-3}$ s^{-1} for the bulk) and k_2 higher, not surprising considering the experimental results.

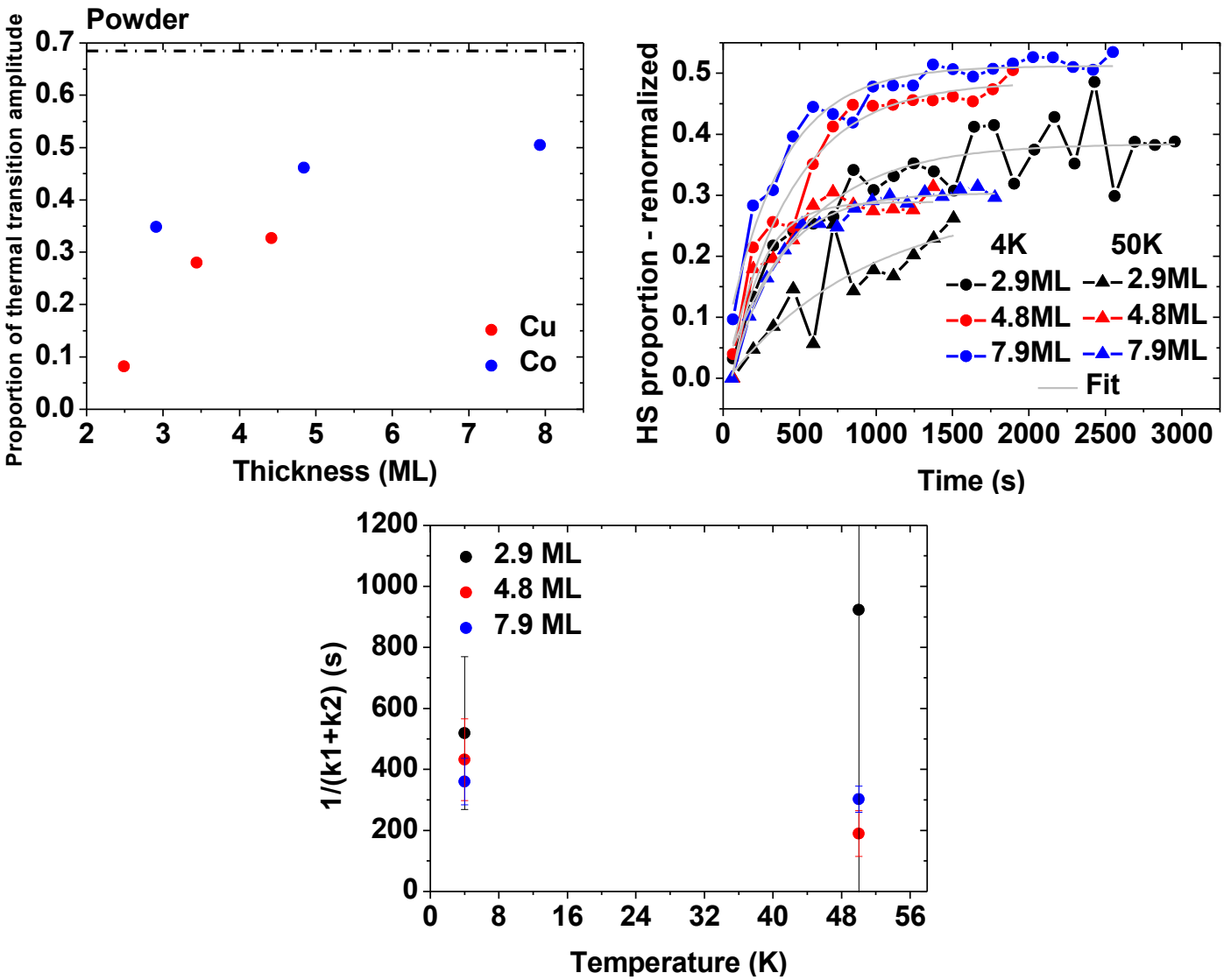

Fig. V.18: Plotted in top left panel is the proportion of SOXIESST/thermal transition amplitude, with the value for the powder noted as a dash-dotted line. Top right panel presents the SOXIESST dynamics obtained for the thin film on Co. Bottom middle show the results for the time constants of the different samples. Illumination intensity was $10I_0$.

V.3.vii Thin films of Fe-phen on Cu and Co surfaces: conclusion

We have shown that the spin state of the sample on the surface is entirely pinned below the monolayer, and nearly pinned just above the monolayer. The HS proportion of these samples is identical from one surface to one other, including a different Fe(II)-based SCO molecule on a Au(111) surface from the literature[148].

Our results and comparison with thick films samples, interacting and weakly-interacting molecules

on interacting and weakly-interacting substrates, seem to suggest as a whole, that SCO molecules on a surface yield different behaviors depending on the substrate-molecule interaction (the nature of the substrate compared to the nature of the molecule) and the molecule-molecule interaction (the behavior in the bulk is cooperative or not). In our case, highly cooperative molecules deposited on highly interacting substrate seems to generate several "zones": from the interface, until approximately 1 or 2 ML, a "pinned" zone where HS and LS coexist but are unable to switch. From 1 ML to approximately 4 ML, an "intermediate" zone where the direct influence of the substrate on the spin state of the molecules is still strong but fading. Starting from 4 ML, a "thin film" zone where the influence of the substrate is felt only through the layers underneath: an influence affecting especially the cooperative behavior of the sample. The transition from thick to thin films could not be observed in this study. We suspect that when this thin film reach a sufficient thickness, the behavior of the subsequent layers should get back to bulk behavior.[146]

V.4 XAS study of SCO molecules: conclusion

In the first part of this chapter, we have confirmed the existence of the SOXIESST effect, as a LS → HS transition excited by the X-ray beam, and investigated its properties: it is non-resonant, and the amplitude of the effect depends on the intensity and structure of the illuminating beam. It is possible to combine it with the LIESST. We have used a simple model to analyze the experimental data, and it follows from this analysis that the HS → LS relaxation rate exhibits a plateau between 10 and 40K, and a thermally activated part above 40K. The metal-ligand charge transfer states seems to be primordial in the efficiency of the effect; the cooperative behavior is suggested to also play a role in the effect. Besides, this first study ascertained that we do not detect a hypothetical excited state, and provided us with the reference spectra for the pure HS and LS states.

Based on these results, we have studied by XAS thin films of Fe-phen deposited on Cu and Co surfaces, in order to better understand the behavior of low-dimensional thin films of SCO molecules. We found that both spin states coexist on the two surfaces. Below 2ML, the layers exhibit exclusively a "pinned" part, which means that the HS proportion do not change according to the temperature, and is not sensitive to the SOXIESST effect or the LIESST effect. By comparing both surfaces and an example from the literature, we suggest that the HS proportion of the pinned part at the interface molecule/transition metal surface with similar lattice parameters does not depends on the nature of the surface or the molecule, but exclusively on the coverage. The

molecules do not exhibit a magnetic coupling with the Co surface. Above 2ML, some thermal spin transition occurs and the layers are sensitive to the SOXIESST effect, although the results hint that a significant part of the subsequent layers still present a pinned part. This transition is much smoother than in the bulk, which is a sign of reduced cooperativity. The cooperativity increases when the thickness of the sample increases, a propriety that can be quantified by fitting the thermal transition by a simple phenomenological model. We found that the calculated thermodynamic parameters reach a “thin film” value that is approximately 44% (Cu) 49% (Co) of bulk ΔH and 29% (Cu) 41% (Co) of bulk ΔS, which leads us to the conclusion that the thermal transition temperature of Fe-phen is much higher in thin films than in the bulk. The structure of the thin films seems however more complex than anticipated, and further studies will be necessary to fully elucidate this behavior.

VI Multilayer vertical device: preliminary results

a vertical multilayer device and its electrical measurements

The results discussed in chapter IV proved that the electrical properties of SCO molecules can be linked to their spin state. By combining memristive and spintronic capabilities in a single molecule, multifunctional devices can be foreseen. The final objective of our scientific process was to build a technological device that could be applied to industrial uses, and to study the electrical behavior of Fe-phen at the spin transition. The recent trend towards miniaturization of the SCO-based devices has led to various strategies to study the electrical properties of thin films[149], nanoparticles[41] and molecules, but some of them, like single-molecule junctions[96,188] or the STM switching mentioned in chapter IV, are very difficult to carry out in an industrial process. Since in chapter V it was proven that the thermal spin transition was retrieved when the films are thicker than 2ML, we present in this chapter the preliminary results for a vertical device based on the Electrode/Fe-phen thin film/Electrode.

VI.1 Structure of the device

VI.1.i General architecture

The previous horizontal devices used[146] do not allow very thin gap thicknesses. Therefore, we have designed three type of vertical junctions, with the various layers deposited by thermal evaporation.

- Type-1:
  - Au 25nm deposited by shadow mask on a thermal SiO_2 surface in the hybrid system (see chapter III).
  - Fe-phen thermally evaporated in the Plassys setup (see chapter III).
  - Top Au 20nm deposited by shadow mask on a sample cooled by liquid N_2 in the hybrid system.

    Important note: the sample was exposed to air during the transport from the hybrid system to the Plassys and back.
- Type-2:
  - Co 5nm/Au 30nm deposited by shadow mask on a thermal SiO_2 surface in the hybrid system.
  - Fe-phen thermally evaporated in the hybrid system.
  - Top Au 20nm deposited by shadow mask on a sample cooled by liquid N_2 in the hybrid system.

    This time, all the depositions were realized in the hybrid system, with only a transition through a N_2 glove box to fix the masks.
- Type-3:
  - Co 5nm/Au 30nm deposited by shadow mask on a thermal SiO_2 surface in the hybrid system.
  - Technical MgF_2 70nm deposited by shadow mask on the edges of the bottom electrode in the hybrid system, in order to avoid short-circuits.

- Fe-phen thermally evaporated in the hybrid system.
- Top Au 20nm deposited by shadow mask on a sample cooled by liquid N_2 in the hybrid system.

  This time, all the depositions were realized in situ, in the vacuum. We have used a mask manipulator to position the masks in the deposition chamber.

The basic architecture of such devices is illustrated in Fig. VI.1. The system consisting of the intersection of the top and bottom electrodes and the Fe-phen volume contained between them is called a junction. The volume tested is then 100 µm × 100 µm × Fe-phen thickness. In order to study the resistance of the Fe-phen layer exclusively, we have used 4 point measurements by setting a desired voltage between a top electrode pad and a bottom electrode pad, and measuring the current necessary to obtain this voltage between the second electrode pad and the second bottom electrode pad, a conventional method[189], presented in Fig. VI.1. When I is defined as *positive*, the current flow *from I+ to I-* and the voltage U is measured positive.

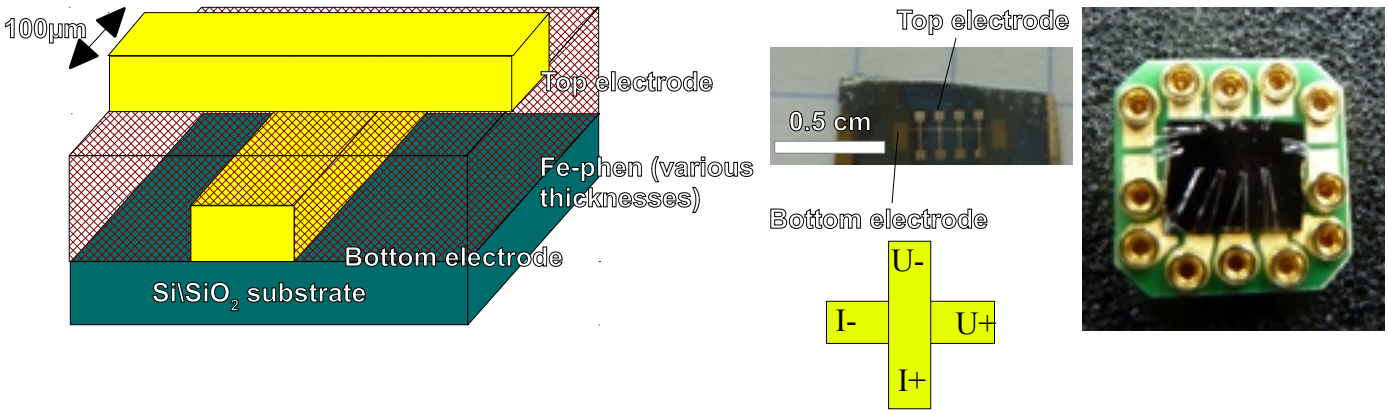

Fig. VI.1: Schematic view of the architecture of a type-1 device, and picture of a real device on the right, as well as the device mounted on a chip. There are 4 junctions per sample that can be tested.

VI.1.ii Bottom electrode

After the first electrical transport studies, we noticed that the bottom electrodes of type-1 devices present a peculiar morphology, as highlighted by SEM pictures presented in Fig. IV.2. To smooth the surface, we introduced a wetting layer of Co for type-2 and type-3 devices, leading to a homogeneous electrode surface. This also drastically improved the resistance: at room temperature, type-1 bottom electrodes have a resistance of typically 100kΩ, while type-2 and -3 bottom electrodes have a resistance of 140Ω, closer to the theoretical expected value of 50Ω.

Furthermore, the type-1 bottom electrodes are non-ohmic, while type -2 and -3 electrodes are ohmic.

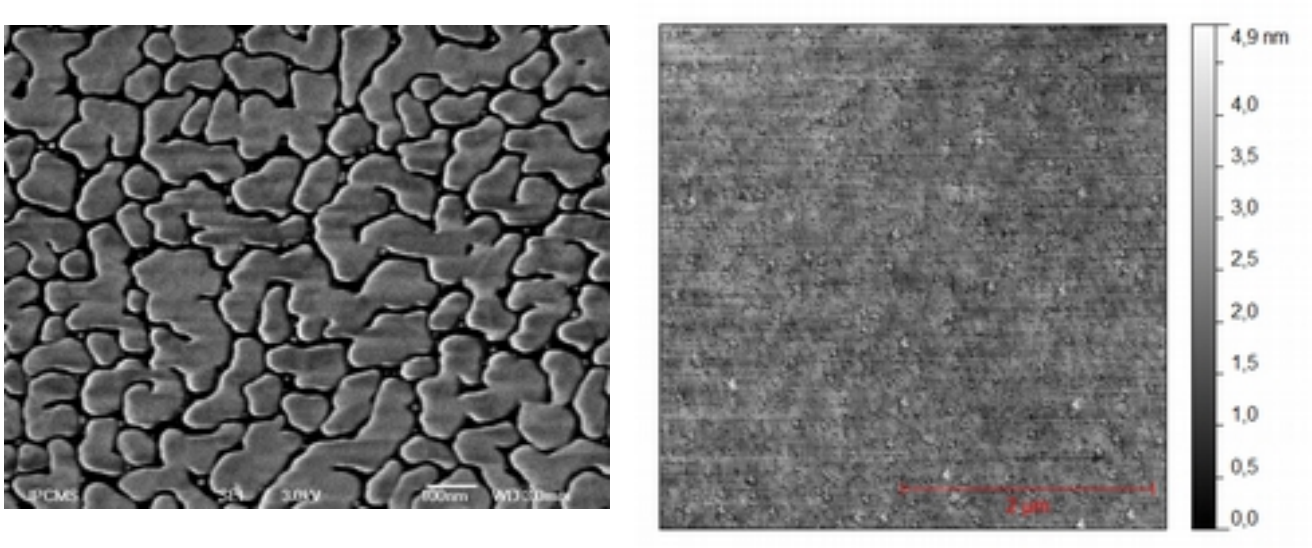

Fig. IV.2: The left picture is a SEM image of Au 40nm deposited on quartz. The right picture is an AFM image of Co 5nm/Au 26nm deposited on thermal Si. The RMS of 0.46nm of this picture indicate a far better roughness than the isolated crystallites of the quartz//Au sample.

VI.2 Electric transport measurements

VI.2.i Features

Using the Fert bench measurement setup, we then measured the evolution of U/I when several external parameters (temperature and applied field) are modified. We selected an applied voltage U to the sample and measured the current I necessary to maintain it. It is important to stress that these are preliminary results acquired exclusively on type-1 devices: we were unable to reproduce them with type-2 or type-3 devices. Furthermore, the devices tested have all a 15nm Fe-phen thickness: the resistance of the 25nm junctions was too high, and the 7nm junctions were instable, therefore we could not obtain results on these two thicknesses. The "operative" junctions represent 40 to 50% of the samples tested. The others were either short-circuited or the resistance was far too high, $>10^6\Omega$ at 300K. The electrical properties of the junctions present 3 main features, presented in Fig. VI.3: a low temperature (23K usually) feature, a 120K (but the temperature of this peak vary according to the voltage applied) feature, and a "diode" effect at a temperature compatible with the SCO.

The 120K feature was found to be due to the inhomogeneous bottom electrode, but this does not mean it does not originate in a Fe-phen behavior: it is possible that this feature is typical of

tunneling through Fe-phen across the gaps between the Au clusters. The telegraphic noise between 40 and 125K can also be linked to a probable effect of the bottom electrode, as illustrated in Fig. VI.3. However, we will consider in this work exclusively the features that can be attributed to the junction itself.

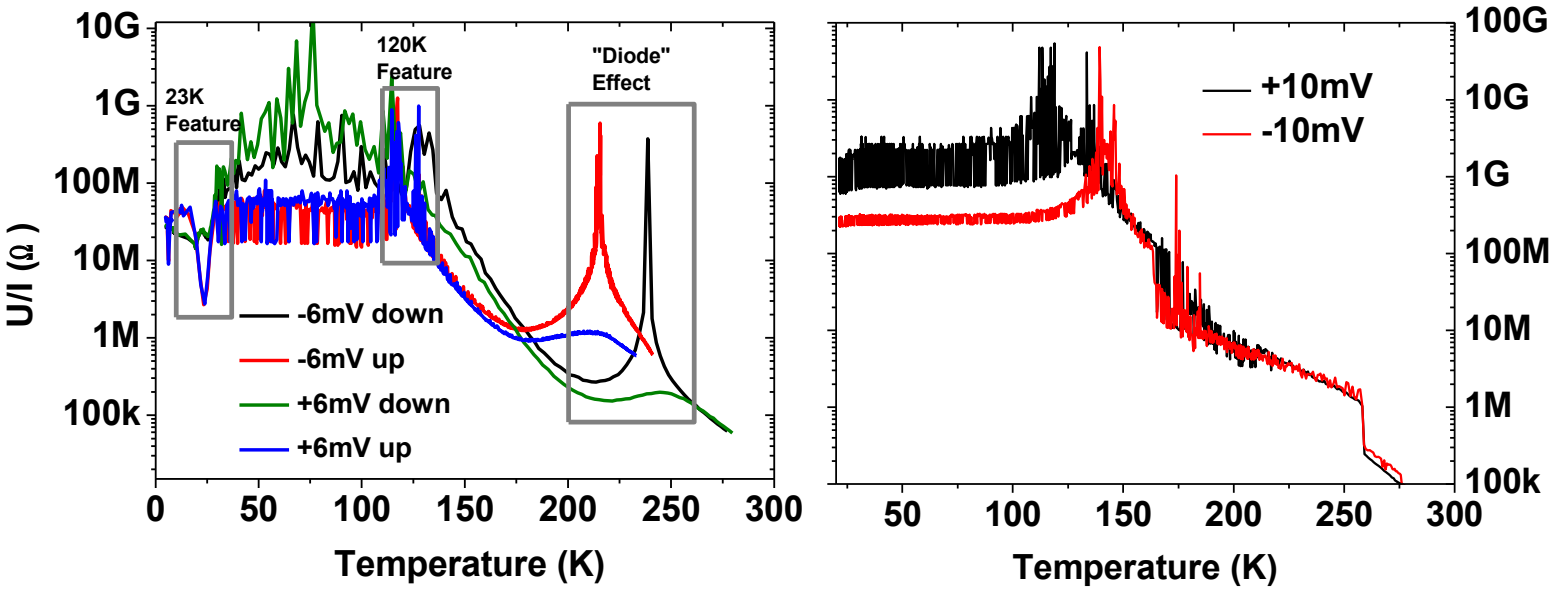

Fig. VI.3: Left panel is a plot of U/I as a function of the temperature, where the 3 features are clearly visible, for a 15nm-thick Fe-phen sample. The 120K Feature is an artefact from the bottom electrode, as evidenced by the right plot, a 2-points measurement of U/I for the bottom electrode, with the temperature decreasing. The "jumps" in the right plot are linked to caliber changes in the Keithley.

VI.2.ii 23K feature

This feature is the least reproducible, as some 50% of the junctions simply did not exhibit it. It consists in a dip in electrical resistivity when increasing the temperature, at low field and low temperature (the effect was observed between 17K and 40K usually). The shape, the magnitude and the temperature of this effect do not depend on the voltage. Fig. VI.4 presents cycles in temperature carried out at different positions in the feature. For example, let us describe the top right cycle: when we start to decrease the temperature at 60K, stop this decrease at 25K, then increase the temperature again, we observe that the intensity begins to go back to increasing temperature values. When decreasing the temperature again at 27K, we observe that the intensity go back sharply to decreasing-temperature values. These cycles can be reproduced, going up or down in temperature, but it seems that decreasing-temperature values are not reproducible (compare top right, middle right and bottom panels of Fig. VI.4).

This effect is highly field dependent, and disappears at 10 000 Oe.

The origin of this effect is unclear since no anomaly have been reported for the properties of Fe-phen bulk or thin films in this temperature range and this conditions (no illumination).

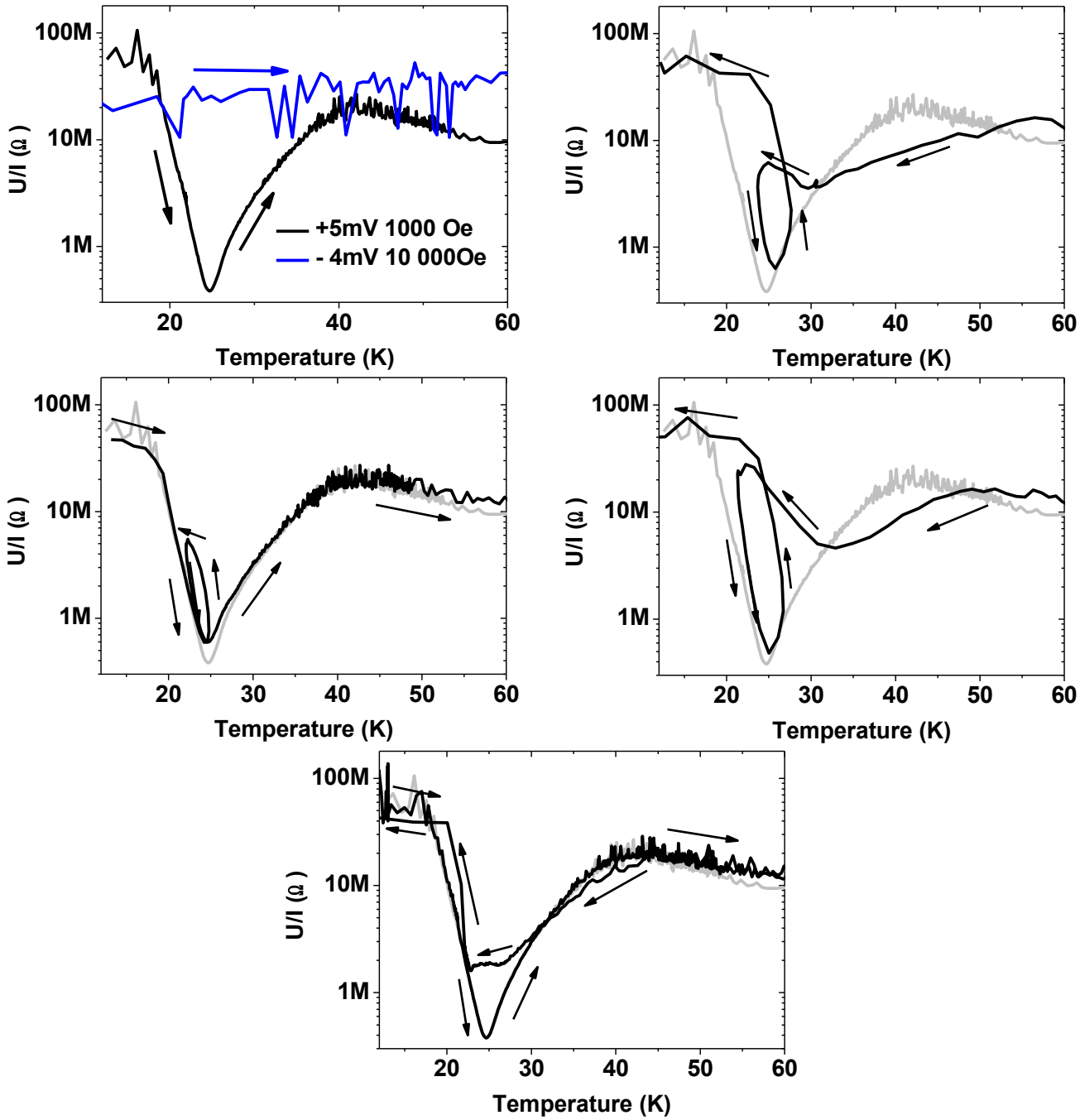

Fig. VI.4: U/I as a function of the temperature when the temperature is cycled, for a 15nm-thick Fe-phen sample and at a field of 1000 Oe. The plots present, from left to right and from top to bottom, successive temperature cycles, with the final bottom plot presenting a "full" cycle of the effect. The light gray curves on each plot correspond to the first plot (increase in temperature), represented as a mean of comparison between the cycles. The arrows represent the temperature sweep direction.

VI.2.iii "Diode" effect

This is the main effect observed on the junctions. It consists in a peak in electrical resistivity of 2 or 3 orders of magnitude when measuring negative voltage compared to a positive voltage of identical magnitude, at a temperature compatible with the spin transition as suggested by the higher spin transition temperatures obtained on Fe-phen thin films in chapter V. The exact temperature at which this peak occurs depends on the magnitude of the negative voltage. The dependencies are presented in Fig. VI.5: the temperature of occurrence depends on the sweeping direction, the applied field and the voltage. The exact values can vary from junction to junction, but the basics are conserved: the peak appears for temperatures higher than the spin transition; the peak temperature has an approximately linear dependence on the applied voltage as illustrated in the right plot of Fig. IV.5, and decreases when the magnitude of the negative voltage increases; the peak temperature is higher when the temperature is decreasing than when the temperature is increasing; and the peak temperature is reduced by an applied magnetic field. The effect is present until approx. -50mV (vary according to the junction), where the effect temperature reaches the spin transition temperature, which is another argument to link this effect with the spin transition. Indeed, if we link this peak to an electric-field driven spin transition, then at the usual thermal spin transition temperature, Fe-phen must switch thermally, and no further electrical switch will be possible.

We suggest that the mechanism is linked to the disorder at the spin transition. Indeed, at the spin transition the high number of nucleation sites increases dramatically the disorder during a relatively short range of temperature, which could increase the resistance of the junction. The anisotropy of this behavior would be explained by the anisotropy of the junction, as the Fe-phen molecules deposited on the bottom electrode would be "pinned", it is possible that the Fe-phen molecules of the topmost layer are only weakly bonded with the top electrode.

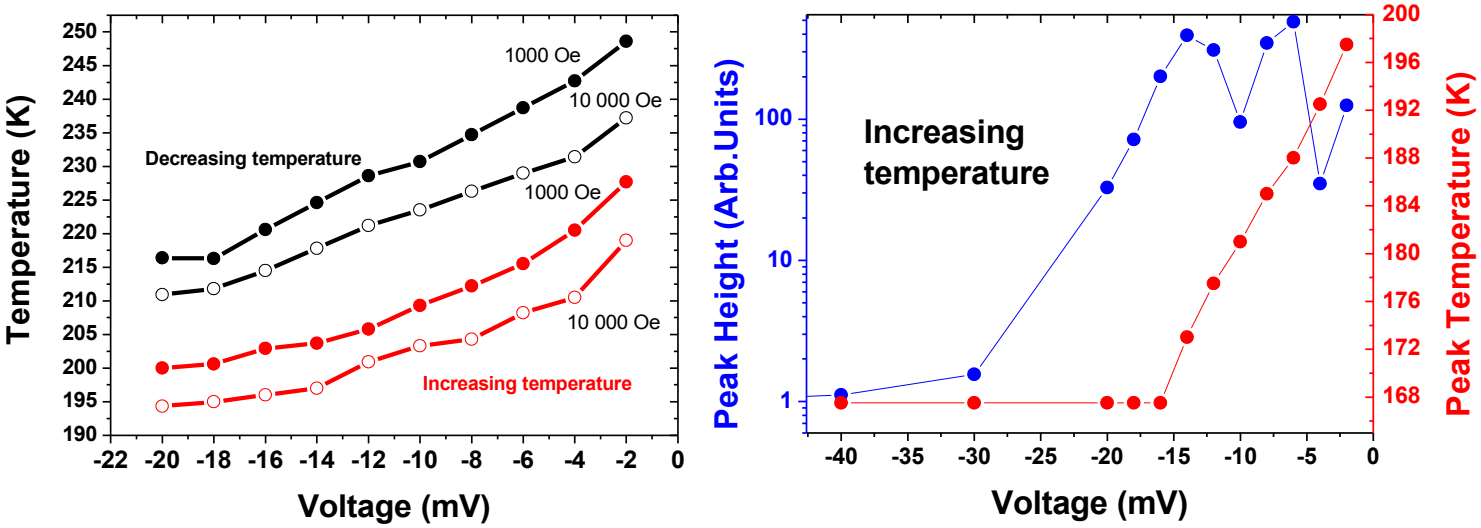

Fig. IV.5: On the left, plot of the temperature of the peak as a function of voltage for a 15nm-thick Fe-phen sample, presenting all the dependencies of the effect. The right plot presents the temperature dependence of the effect more in details, for a different 15nm-thick Fe-phen sample. The peak height is calculated as the ratio of the value of the peak for the negative voltage and the positive voltage of the same magnitude.

VI.2.iv On the irreproducibility

The results presented in this chapter were obtained exclusively with type-1 junctions. We have not been able to reproduce them with type-2 and type-3 junctions, despite the much cleaner deposition environment and proper bottom electrodes. Therefore, we suspect two possible origins of this behavior: the bottom electrode imperfections, which links to the tunneling between Au clusters through Fe-phen, and the possible contamination of the gold bottom electrode and the Fe-phen surface after the deposition, which can insert doping agents in the junction.

GENERAL CONCLUSION

In this work, we have provided what we believe to be essential steps in the understanding of SCO-molecule-on-substrate systems, and also insights on the too often neglected SOXIESST effect. We have investigated thick films of Fe-phen and Fe-pyrz on silicon substrates and isolated molecules and ultra-thin films of Fe-phen on two transition metal substrates (Cu(100) and Co(100)), while comparing with bulk behavior. Finally, we have presented preliminary results of electrical measurements of a technological device, a vertical multilayer Au/Fe-phen film/Au.

Regarding the SOXIESST effect on Fe-phen and Fe-pyrz powder, we confirm unambiguously its existence and observe its properties. It is non-resonant, such that we believe that SOXIESST and HAXIESST form two aspects of the same effect, the X-ray induced excited spin state trapping. The amplitude of the effect depends on the intensity and structure of the illuminating beam. It is possible to combine it with the LIESST. We have used a simple model to analyze the experimental data, and it follows from this analysis that the HS → LS relaxation rate exhibits a plateau between 10 and 40K, and a thermally activated part above 40K. The metal-ligand charge transfer states seem to be primordial in the efficiency of the effect; the cooperative behavior is suggested to also play a role in the effect.

The low-dimensional results, considered as a whole, suggest that when the thickness decreases a) the cooperativity of the thermal spin transition is reduced and b) the thermal spin transition temperature is modified, reduced for Fe-pyrz on silicon, but on the contrary increased for Fe-phen on silicon and transition metal surfaces. In the case of ultra-thin films of Fe-phen we quantify the first property using a phenomenological model of the spin transition with a cooperativity term. STM and XAS results confirm that both spin states coexist on transition metal surfaces. We can then divide the ultra-thin film sample in several domains. We observe at the interface a domain where the molecules are “pinned”, which means that their spin state (either HS or LS) cannot be switched by electrical field, current, SOXIESST effect or LIESST effect. In this domain, at least on transition metal surface with similar lattice parameters, the HS proportion seems to depend neither on the nature of the surface, neither on the nature of the molecule, but exclusively on the coverage. Above 2ML, the direct influence of the substrate decreases and we observe a transition domain where the cooperativity is reduced, a part of the sample is now sensitive to thermal and x-

ray induced spin transitions. Above 4ML, the sample exhibit a “thin film” domain, where the thermodynamic parameters deduced from the phenomenological model reach “thin film” values, at approximately 44% (Cu) 49% (Co) of bulk ΔH and 29% (Cu) 41% (Co) of bulk ΔS. The subsequent layers do not behave as the bulk: they still exhibit a significant pinned part, and the cooperativity of the transition is still reduced. The sharpness of the transition however increases when the thickness increases. When this thin film reaches a sufficient thickness, the behavior of the subsequent layers should get back to bulk behavior, but the transition from thin to thick films could not be observed in this study. A simple model of molecular layers was found to be unsuitable to explain the structure of the ultra-thin film samples: Fe-phen layers on transition metal surfaces present a non-trivial spin transition. Surprisingly, Fe-phen molecules do not seem coupled to the Co layer: this could reflect the contamination of the Co surface by what we believe to be phen groups.

Isolated Fe-phen molecules on Cu(100) are in a pinned state. We can however retrieve the spin transition by introducing an passivating CuN layer. Isolated Fe-phen molecules on Cu(100)//CuN can then be electrically switched reproducibly between the HS and LS states, leading to a single-molecule device whose state can be deterministically selected.

Electrical measurements of vertical devices should be considered with care, but nevertheless they exhibit two main features: a low-temperature (23K) feature and a “diode” peak feature. The 23K feature consists in a drop in resistance that is observed when increasing the temperature, but not when decreasing the temperature. This effect depends on the applied magnetic field, and disappears at 10 000 Oe. At the moment, no observed behavior of Fe-phen could explain this phenomenon. The “diode” peak consists in a peak in electrical resistivity of 2 or 3 orders of magnitude when applying negative voltage compared to a positive voltage of identical magnitude, at a temperature compatible with the spin transition. The temperature of this peak depends on the applied magnetic peak, the voltage, and the temperature sweeping direction. The peak height decreases when the temperature of the peak reaches the spin transition of the bulk. We consequently believe that this peak is due to the increased disorder at the spin transition induced by the current. The anisotropy of the Au/Fe-phen interfaces, the imperfections of the bottom electrodes and the introduction of doping agents in the junction by air contamination during the transport might explain the “diode” behavior of this effect.

This thesis provides practical insights on the study of SCO molecules by X-ray at low temperature, that should be relevant to the increasing number of groups interested in investigating SCO molecules by XAS or X-ray diffraction. The results presented also open perspectives on the technological applications of SCO-molecule-on-subtrate systems, by highlighting not only the rich physics and chemistry of low-dimensional SCO systems, but also the possibilities of these systems in the field of nanoscale devices. Further studies are necessary, but already memories and sensors are applications that can be imagined at room temperature. Furthermore, if the spin selectivity of the molecules can be thus reversibly switched by a wide range of external stimuli, including electric, this could provide a new avenue for molecular organic spintronics.

REFERENCES

[1] Cicoira, F. & Santato, C. *Organic Electronics: Emerging Concepts and Technologies*. (John Wiley & Sons, 2013).

[2] Wolf, S. A., Awschalom, D. D., Buhrman, R. A., Daughton, J. M., Von Molnar, S., Roukes, M. L., Chtchelkanova, A. Y. & Treger, D. M. Spintronics: A spin-based electronics vision for the future. *Science* **294,** 1488–1495 (2001).

[3] Editorial. Why going organic is good. *Nat. Mater.* **8,** 691-691 (2009).

[4] Szulczewski, G., Sanvito, S. & Coey, M. A spin of their own. *Nat. Mater.* **8,** 693-695 (2009).

[5] Pulizzi, F. A new face for organics. *Nat. Mater.* **8,** 696-697 (2009).

[6] Cambi, L. & Szegö, L. Über die magnetische Susceptibilität der komplexen Verbindungen. *Berichte Dtsch. Chem. Ges. B Ser.* **64,** 2591–2598 (1931).

[7] Gütlich, P., Garcia, Y. & Goodwin, H. A. Spin crossover phenomena in Fe(ii) complexes. *Chem. Soc. Rev.* **29,** 419-427 (2000).

[8] Baker Jr, W. A. & Bobonich, H. M. Magnetic properties of some high-spin complexes of iron (II). *Inorg. Chem.* **3,** 1184–1188 (1964).

[9] Jesson, J. P., Trofimenko, S. & Eaton, D. R. Spectra and structure of some transition metal poly(1-pyrazolyl) borates. *J. Am. Chem. Soc.* **89,** 3148-3158 (1967).

[10] Real, J. A., Gaspar, A. B., Muñoz, M. C., Gütlich, P., Ksenofontov, V. & Spiering, H. in *Spin Crossover Transit. Met. Compd. I* (Gütlich, P. & Goodwin, H. A.) **233,** 167-193 (Springer Berlin Heidelberg).

[11] Fedaoui, D., Bouhadja, Y., Kaiba, A., Guionneau, P., Létard, J.-F. & Rosa, P. Complexation of 2,6-Bis(3-pyrazolyl)pyridine–Bis(thiocyanato)iron(II) with a Bridging 4,4′-Bipyridine: A New Example of a Dinuclear Spin Crossover Complex. *Eur. J. Inorg. Chem.* **2008,** 1022–1026 (2008).

[12] Pelleteret, D., Clérac, R., Mathonière, C., Harté, E., Schmitt, W. & Kruger, P. E. Asymmetric spin crossover behaviour and evidence of light-induced excited spin state trapping in a dinuclear iron(II) helicate. *Chem. Commun. Camb. Engl.* **2,** 221-223 (2009).

[13] Vos, G., De Graaff, R. A. G., Haasnoot, J. G., Van der Kraan, A. M., De Vaal, P. & Reedijk, J. Crystal structure at 300 and 105 K, magnetic properties and Moessbauer spectra of bis(triaquatris(4-ethyltriazole-N1)iron(II)-N2,N2',N2")iron(II) hexakis(trifluoromethanesulfonate). A linear, trinuclear iron(II) compound, showing a unique high-spin-low-spin transition of the central iron atom. *Inorg. Chem.* **23,** 2905-2910 (1984).

[14] Garcia, Y., van Koningsbruggen, P. J., Lapouyade, R., Rabardel, L., Kahn, O., Wieczorek, M., Bronisz, R., Ciunik, Z. & Rudolf, M. F. Synthesis and spin-crossover characteristics of polynuclear 4-(2'-hydroxy-ethyl)-1,2,4-triazole Fe(II) molecular materials. *Comptes Rendus Académie Sci. - Ser. IIC - Chem.* **1,** 523-532 (1998).

[15] Murray, K. S. & Kepert, C. J. in *Spin Crossover Transit. Met. Compd. I* (Gütlich, P. & Goodwin, H. A.) **233,** 195-228 (Springer Berlin Heidelberg).

[16] Carmen Muñoz, M. & Antonio Real, J. in *Spin-Crossover Mater.* (Halcrow, L. a) 121–146 (John Wiley & Sons Ltd, 2013).

[17] Garcia, Y., Niel, V., Muñoz, M. C. & Real, J. A. in *Spin Crossover Transit. Met. Compd. I* (Gütlich, P. & Goodwin, H. A.) **233,** 229-257 (Springer Berlin Heidelberg).

[18] Kahn, O. & Martinez, C. J. Spin-Transition Polymers: From Molecular Materials Toward Memory Devices. *Science* **279,** 44-48 (1998).

[19] Holland, P. M. & Castleman, A. W. The thermochemical properties of gas-phase transition metal ion complexes. *J. Chem. Phys.* **76,** 4195-4205 (1982).

[20] Abis, L., Sen, A. & Halpern, J. Intramolecular reductive elimination of alkanes from cis-hydridoalkylbis(phosphine)platinum(II) complexes. *J. Am. Chem. Soc.* **100,** 2915-2916 (1978).

[21] Mond, L., Langer, C. & Quincke, F. L.—Action of carbon monoxide on nickel. *J. Chem. Soc. Trans.* **57,** 749-753 (1890).

[22] Demuynck, J. & Veillard, A. Electronic structure of the nickel tetracyanonickelate $Ni(CN)_4$ 2− and nickel carbonyl $Ni(CO)_4$. An ab-initio LCAO-MO-SCF calculation. *Theor. Chim. Acta* **28,** 241-265 (1973).

[23] Laskowski, E. J. & Hendrickson, D. N. Magnetic exchange interactions in transition-metal dimers. 13. Structural characterization of the two hydrogen bonded manganese(II) dimers $[Mn_2(tren)_2(NCS)_2](BPh_4)_2$ and $[Mn_2(tren)_2(NCO)_2](BPh_4)_2$. A series of outer-sphere manganese dimers formed from trigonal-bipyramidal manganese(II) complexes. *Inorg. Chem.* **17,** 457-470 (1978).

[24] Huisman, R., de Jonge, R., Haas, C. & Jellinek, F. Trigonal-prismatic coordination in solid compounds of transition metals. *J. Solid State Chem.* **3,** 56-66 (1971).

[25] Bersuker, I. B. *The Jahn-Teller Effect*. (Cambridge University Press, 2006).

[26] Miessler, G. L., Fischer, P. J. & Tarr, D. A. *Inorganic Chemistry*. (Prentice Hall, 2013).

[27] Jean, Y. *Les orbitales moléculaires dans les complexes: Cours et exercices corrigés*. (Editions Ecole Polytechnique, 2003).

[28] Crabtree, R. H. *The Organometallic Chemistry of the Transition Metals*. (John Wiley & Sons, 2009).

[29] Byrne, E. K., Richeson, D. S. & Theopold, K. H. Tetrakis(1-norbornyl)cobalt, a low spin tetrahedral complex of a first row transition metal. *J. Chem. Soc. Chem. Commun.* **19,** 1491-1492 (1986).

[30] Jorgensen, C. K. *Absorption spectra and chemical bonding in complexes*. (Pergamon Press, 1962).

[31] Bausk, N. V., Érenburg, S. B., Lavrenova, L. G. & Mazalov, L. N. EXAFS study of spin transition effect on the spatial and electronic structure of Fe(II) complexes with triazoles. *J. Struct. Chem.* **36,** 925-931 (1995).

[32] Gallois, B., Real, J. A., Hauw, C. & Zarembowitch, J. Structural changes associated with the spin transition in bis (isothiocyanato) bis (1, 10-phenanthroline) iron: a single-crystal x-ray investigation. *Inorg. Chem.* **29,** 1152–1158 (1990).

[33] MacLean, E. J., McGrath, C. M., O'Connor, C. J., Sangregorio, C., Seddon, J. M. W., Sinn, E., Sowrey, F. E., Teat, S. J., Terry, A. E., Vaughan, G. B. M. & Young, N. A. Structural Study of the Thermal and Photochemical Spin States in the Spin Crossover Complex$[Fe(phen)_2(NCSe)_2]$. *Chem. - Eur. J.* **9,** 5314-5322 (2003).

[34] Marchivie, M. Approche structurale du phénomène de transition de spin par diffraction des rayons X sous contraintes (T, P, hv). (2003).

[35] Legrand, V. Cristallographie et photo-cristallographie haute résolution de composés moléculaires à transition de spin: propriétés structurales, électroniques et mécanismes de conversion. (2005).

[36] Reiher, M. Theoretical Study of the $Fe(phen)_2(NCS)_2$ Spin-Crossover Complex with Reparametrized Density Functionals. *Inorg. Chem.* **41,** 6928-6935 (2002).

[37] Sorai, M. in *Spin Crossover Transit. Met. Compd. III* **235,** 153-170 (Springer-Verlag).

[38] Gütlich, P. & Goodwin, H. A. in *Spin Crossover Transit. Met. Compd. I* (Gütlich, P. & Goodwin, H. A.) **233,** 1-47 (Springer Berlin Heidelberg).

[39] Weber, B. in *Spin-Crossover Mater.* (Halcrow, L. a) 55–76 (John Wiley & Sons Ltd, 2013).

[40] Gütlich, P., Hauser, A. & Spiering, H. Thermal and Optical Switching of Iron(II) Complexes. *Angew. Chem. Int. Ed. Engl.* **33,** 2024–2054 (1994).

[41] Tissot, A. Commutation thermo-et photo-induite de solides moléculaires a transition de spin: du monocristal aux nano-objets. (2011).

[42] Hauser, A. in *Spin Crossover Transit. Met. Compd. I* (Gütlich, P. & Goodwin, H. A.) **233,** 49-58 (Springer Berlin Heidelberg).

[43] Tuchagues, J.-P., Bousseksou, A., Molnár, G., McGarvey, J. J. & Varret, F. in *Spin Crossover Transit. Met. Compd. III* **235,** 84-103 (Springer-Verlag).

[44] Nakamoto, T., Tan, Z.-C. & Sorai, M. Heat Capacity of the Spin Crossover Complex [Fe(2-pic) $_3$]Cl $_2$ ·MeOH: A Spin Crossover Phenomenon with Weak Cooperativity in the Solid State. *Inorg. Chem.* **40,** 3805-3809 (2001).

[45] Sorai, M. & Seki, S. Phonon coupled cooperative low-spin 1A1high-spin 5T2 transition in $[Fe(phen)_2(NCS)_2]$ and $[Fe(phen)_2(NCSe)_2]$ crystals. *J. Phys. Chem. Solids* **35,** 555-570 (1974).

[46] Létard, J.-F., Capes, L., Chastanet, G., Moliner, N., Létard, S., Real, J.-A. & Kahn, O. Critical temperature of the LIESST effect in iron(II) spin crossover compounds. *Chem. Phys. Lett.* **313,** 115-120 (1999).

[47] Guionneau, P., Létard, J.-F., Yufit, D. S., Chasseau, D., Bravic, G., Goeta, A. E., Howard, J. A. K. & Kahn, O. Structural approach of the features of the spin crossover transition in iron (II) compounds. *J. Mater. Chem.* **9,** 985-994 (1999).

[48] Pavlik, J. & Boča, R. Established Static Models of Spin Crossover. *Eur. J. Inorg. Chem.* **2013,** 697–709 (2013).

[49] Slichter, C. P. & Drickamer, H. G. Pressure-Induced Electronic Changes in Compounds of Iron. *J. Chem. Phys.* **56,** 2142-2160 (1972).

[50] Rao, P. S., Ganguli, P. & McGarvey, B. R. Proton NMR study of the high-spin-low-spin transition in $Fe(phen)_2(NCS)_2$ and $Fe(pic)_3Cl_2$.(EtOH or MeOH). *Inorg. Chem.* **20,** 3682-3688 (1981).

[51] Kepenekian, M., Le Guennic, B. & Robert, V. Magnetic bistability: From microscopic to macroscopic understandings of hysteretic behavior using ab initio calculations. *Phys. Rev. B* **79,** 094428 (2009).

[52] Kepenekian, M., Guennic, B. L. & Robert, V. Primary Role of the Electrostatic Contributions in a Rational Growth of Hysteresis Loop in Spin-Crossover Fe(II) Complexes. *J. Am. Chem. Soc.* **131,** 11498-11502 (2009).

[53] Real, J. A., Gaspar, A. B. & Muñoz, M. C. Thermal, pressure and light switchable spin-crossover materials. *Dalton Trans.* **12,** 2062 (2005).

[54] Ksenofontov, V., Gaspar, A. B. & Gütlich, P. in *Spin Crossover Transit. Met. Compd. III* **235,** 23-64 (Springer-Verlag).

[55] Boča, R. & Linert, W. Is There a Need for New Models of the Spin Crossover? *Monatshefte Für Chem. Chem. Mon.* **134,** 199-216 (2003).

[56] Varret, F., Nogues, M. & Goujon, A. in *Magn. Mol. Mater.* (Miller, J. S. & Rcillon) 257–295 (Wiley-VCH Verlag GmbH & Co. KGaA, 2003).

[57] Enachescu, C., Constant-Machado, H., Codjovi, E., Linares, J., Boukheddaden, K. & Varret, F. Direct access to the photo-excitation and relaxation terms in photo-switchable solids: non-linear aspects. *J. Phys. Chem. Solids* **62,** 1409–1422 (2001).

[58] Spiering, H. in *Spin Crossover Transit. Met. Compd. III* **235,** 171-195 (Springer-Verlag).

[59] Hauser, A. Cooperative effects on the HS→LS relaxation in the [Fe(ptz)6](BF4)2 spin-crossover system. *Chem. Phys. Lett.* **192,** 65-70 (1992).

[60] Enachescu, C., Nishino, M. & Miyashita, S. in *Spin-Crossover Mater.* (Halcrow, L. a) 455–474 (John Wiley & Sons Ltd, 2013).

[61] Naik, A. D., Tinant, B., Muffler, K., Wolny, J. A., Schünemann, V. & Garcia, Y. Relevance of supramolecular interactions, texture and lattice occupancy in the designer iron(II) spin crossover complexes. *J. Solid State Chem.* **182,** 1365-1376 (2009).

[62] Gütlich, P., Köppen, H. & Steinhäuser, H. G. Deuterium isotope effect on the high-spin α low-spin

transition in deuterated solvates of tris(2-picolylamine) iron(II) chloride. *Chem. Phys. Lett.* **74,** 475-480 (1980).

[63] Cavallini, M., Bergenti, I., Milita, S., Kengne, J. C., Gentili, D., Ruani, G., Salitros, I., Meded, V. & Ruben, M. Thin Deposits and Patterning of Room-Temperature-Switchable One-Dimensional Spin-Crossover Compounds. *Langmuir* **27,** 4076-4081 (2011).

[64] Pillet, S., Legrand, V., Weber, H.-P., Souhassou, M., Létard, J.-F., Guionneau, P. & Lecomte, C. Out-of-equilibrium charge density distribution of spin crossover complexes from steady-state photocrystallographic measurements: experimental methodology and results. *Z. Für Krist.* **223,** 235-249 (2008).

[65] Zhong, Z. J., Tao, J.-Q., Yu, Z., Dun, C.-Y., Liu, Y.-J. & You, X.-Z. A stacking spin-crossover iron(II) compound with a large hysteresis. *J. Chem. Soc. Dalton Trans.* **3,** 327-328 (1998).

[66] Bučko, T., Hafner, J., Lebègue, S. & Ángyán, J. G. Spin crossover transition of Fe(phen)2(NCS)2: periodic dispersion-corrected density-functional study. *Phys. Chem. Chem. Phys.* **14,** 5389-5396 (2012).

[67] Böttger, L. H., Chumakov, A. I., Matthias Grunert, C., Gütlich, P., Kusz, J., Paulsen, H., Ponkratz, U., Rusanov, V., Trautwein, A. X. & Wolny, J. A. Spin- and phase transition in the spin crossover complex [Fe(ptz)6](BF4)2 studied by nuclear inelastic scattering of synchrotron radiation and by DFT calculations. *Chem. Phys. Lett.* **429,** 189-193 (2006).

[68] Gueddida, S. & Alouani, M. Spin crossover in a single $Fe(phen)_2(NCS)_2$molecule adsorbed onto metallic substrates: An ab initio calculation. *Phys. Rev. B* **87,** 144413 (2013).

[69] Paulsen, H. & Trautwein, A. X. in *Spin Crossover Transit. Met. Compd. III* **235,** 197-219 (Springer-Verlag).

[70] Jensen, K. P. & Cirera, J. Accurate Computed Enthalpies of Spin Crossover in Iron and Cobalt Complexes. *J. Phys. Chem. A* **113,** 10033-10039 (2009).

[71] Brehm, G., Reiher, M. & Schneider, S. Estimation of the Vibrational Contribution to the Entropy Change Associated with the Low- to High-Spin Transition in $Fe(phen)_2(NCS)_2$ Complexes: Results Obtained by IR and Raman Spectroscopy and DFT Calculations. *J. Phys. Chem. A* **106,** 12024-12034 (2002).

[72] Baranović, G. & Babić, D. Vibrational study of the $Fe(phen)_2(NCS)_2$ spin-crossover complex by density-functional calculations. *Spectrochim. Acta. A. Mol. Biomol. Spectrosc.* **60,** 1013-1025 (2004).

[73] Bousseksou, A., McGarvey, J. J., Varret, F., Real, J. A., Tuchagues, J.-P., Dennis, A. C. & Boillot, M. L. Raman spectroscopy of the high- and low-spin states of the spin crossover complex Fe(phen)2(NCS)2: an initial approach to estimation of vibrational contributions to the associated entropy change. *Chem. Phys. Lett.* **318,** 409-416 (2000).

[74] Zimmermann, R. & König, E. A model for high-spin/low-spin transitions in solids including the effect of lattice vibrations. *J. Phys. Chem. Solids* **38,** 779-788 (1977).

[75] Paradis, N., Chastanet, G. & Létard, J.-F. When Stable and Metastable HS States Meet in Spin-Crossover Compounds. *Eur. J. Inorg. Chem.* **2012,** 3618–3624 (2012).

[76] Shores, M. P., Klug, C. M. & Fiedler, S. R. in *Spin-Crossover Mater.* (Halcrow, L. a) 281–301 (John Wiley & Sons Ltd, 2013).

[77] Toyazaki, S., Nakanishi, M., Komatsu, T., Kojima, N., Matsumura, D. & Yokoyama, T. Control of Tc by isomerization of counter anion in Fe(II) spin crossover complexes, $[Fe(4\text{-}NH_2trz)_3](R\text{-}SO_3)_2$. in *Synth. Met.* **121,** 1794-1795 (Elsevier).

[78] Renz, F., Hasegaw, M., Hoshi, T., El-ayaan, U., Linert, W. & Fukuda, Y. Anisotropic Effect after Stretching of the Spin-Crossover Compound [Fe(II)(2,6-bis-(benzimidazol-2'-yl)pyridine) $_2$] (C1O $_4$) $_2$ in Polyvinylalcohol Polymer Matrix. *Mol. Cryst. Liq. Cryst. Sci. Technol. Sect. Mol. Cryst. Liq. Cryst.* **335,** 531-540 (1999).

[79] Renz, F., Souza, P. A. D., Klingelhöfer, G. & Goodwin, H. A. in *Ind. Appl. Mössbauer Eff.* (Cook, D. C. & Hoy, G. R.) 699-704 (Springer Netherlands, 2002).

[80] Ganguli, P., Gütlich, P., Müller, E. W. & Irler, W. Further studies on the spin cross-over phenomenon in di-isothiocyanatobis(1,10-phenanthroline)iron(II). *J. Chem. Soc. Dalton Trans.* **2,** 441-446 (1981).

[81] Long, G. J. & Hutchinson, B. B. Spin equilibrium in iron (II) poly (1-pyrazolyl) borate complexes: low-temperature and high-pressure Moessbauer spectral studies. *Inorg. Chem.* **26,** 608–613 (1987).

[82] Varret, F., Chong, C., Slimani, A., Garrot, D., Garcia, Y. & Naik, A. D. in *Spin-Crossover Mater.* (Halcrow, L. a) 425–441 (John Wiley & Sons Ltd, 2013).

[83] Hauser, A. in *Spin Crossover Transit. Met. Compd. II* **234,** 155-198 (Springer Berlin Heidelberg).

[84] Guionneau, P., Marchivie, M., Bravic, G., Létard, J.-F. & Chasseau, D. in *Spin Crossover Transit. Met. Compd. II* **234,** 97-128 (Springer Berlin Heidelberg).

[85] Cartier dit Moulin, C., Rudolf, P., Flank, A. M. & Chen, C. T. Spin transition evidenced by soft X-ray absorption spectroscopy. *J. Phys. Chem.* **96,** 6196–6198 (1992).

[86] Kojima, N., Murakami, Y., Komatsu, T. & Yokoyama, T. EXAFS study on the spin-crossover system, [Fe(4-NH2trz)3](R-SO3). in *Synth. Met.* **103,** (Elsevier).

[87] Bressler, C., Milne, C., Pham, V.-T., ElNahhas, A., Veen, R. M. van der, Gawelda, W., Johnson, S., Beaud, P., Grolimund, D., Kaiser, M., Borca, C. N., Ingold, G., Abela, R. & Chergui, M. Femtosecond XANES Study of the Light-Induced Spin Crossover Dynamics in an Iron(II) Complex. *Science* **323,** 489-492 (2009).

[88] Boillot, M.-L., Zarembowitch, J., Itié, J.-P., Polian, A., Bourdet, E. & Haasnoot, J. G. Pressure-induced spin-state crossovers at room temperature in iron(II) complexes: comparative analysis; a XANES investigation of some new transitions. *New J. Chem.* **26,** 313-322 (2002).

[89] Vankó, G., Bordage, A., Glatzel, P., Gallo, E., Rovezzi, M., Gawelda, W., Galler, A., Bressler, C., Doumy, G., March, A. M., Kanter, E. P., Young, L., Southworth, S. H., Canton, S. E., Uhlig, J., Smolentsev, G., Sundström, V., Haldrup, K., van Driel, T. B., Nielsen, M. M., Kjaer, K. S. & Lemke, H. T. Spin-state studies with XES and RIXS: From static to ultrafast. *J. Electron Spectrosc. Relat. Phenom.* **188,** 166-171 (2013).

[90] Granier, T., Gallois, B., Gaultier, J., Real, J. A. & Zarembowitch, J. High-pressure single-crystal x-ray diffraction study of two spin-crossover iron(II) complexes: $Fe(Phen)_2(NCS)_2$ and $Fe(Btz)_2(NCS)_2$. *Inorg. Chem.* **32,** 5305-5312 (1993).

[91] Jeftić, J., Hinek, R., Capelli, S. C. & Hauser, A. Cooperativity in the Iron(II) Spin-Crossover Compound $[Fe(ptz)_6](PF_6)_2$ under the Influence of External Pressure (ptz = 1-n-Propyltetrazole). *Inorg. Chem.* **36,** 3080-3087 (1997).

[92] Bousseksou, A., Molnár, G., Tuchagues, J.-P., Menéndez, N., Codjovi, É. & Varret, F. Triggering the spin-crossover of $Fe(phen)_2(NCS)_2$ by a pressure pulse. Pressure and magnetic field induce 'mirror effects'. *Comptes Rendus Chim.* **6,** 329-335 (2003).

[93] Ksenofontov, V., Levchenko, G., Spiering, H., Gütlich, P., Létard, J.-F., Bouhedja, Y. & Kahn, O. Spin crossover behavior under pressure of $Fe(PM\text{-}L)_2(NCS)_2$ compounds with substituted 2'-pyridylmethylene 4-anilino ligands. *Chem. Phys. Lett.* **294,** 545-553 (1998).

[94] Halcrow, M. A. in *Spin-Crossover Mater.* (Halcrow, L. a) 147–169 (John Wiley & Sons Ltd, 2013).

[95] Renz, F. Physical and chemical induced spin crossover. *J. Phys. Conf. Ser.* **217,** 012022 (2010).

[96] Meded, V., Bagrets, A., Fink, K., Chandrasekar, R., Ruben, M., Evers, F., Bernand-Mantel, A., Seldenthuis, J. S., Beukman, A. & van der Zant, H. S. J. Electrical control over the Fe(II) spin crossover in a single molecule: Theory and experiment. *Phys. Rev. B* **83,** 245415 (2011).

[97] Mahfoud, T., Molnár, G., Bonhommeau, S., Cobo, S., Salmon, L., Demont, P., Tokoro, H., Ohkoshi, S.-I., Boukheddaden, K. & Bousseksou, A. Electric-Field-Induced Charge-Transfer Phase Transition: A Promising Approach Toward Electrically Switchable Devices. *J. Am. Chem. Soc.* **131,** 15049-15054

(2009).

[98] Bousseksou, A., Negre, N., Goiran, M., Salmon, L., Tuchagues, J.-P., Boillot, M.-L., Boukheddaden, K. & Varret, F. Dynamic triggering of a spin-transition by a pulsed magnetic field. *Eur. Phys. J. B - Condens. Matter Complex Syst.* **13,** 451-456 (2000).

[99] Qi, Y., Müller, E. W., Spiering, H. & Gütlich, P. The effect of a magnetic field on the high-spin=low-spin transition in [Fe(phen)2(NCS)2]. *Chem. Phys. Lett.* **101,** 503-505

[100] Bousseksou, A., Varret, F., Goiran, M., Boukheddaden, K. & Tuchagues, J. P. in *Spin Crossover Transit. Met. Compd. III* **235,** 65-84 (Springer-Verlag).

[101] Decurtins, S., Gutlich, P., Hasselbach, K. M., Hauser, A. & Spiering, H. Light-induced excited-spin-state trapping in iron(II) spin-crossover systems. Optical spectroscopic and magnetic susceptibility study. *Inorg. Chem.* **24,** 2174-2178 (1985).

[102] Hayami, S., Gu, Z., Einaga, Y., Kobayasi, Y., Ishikawa, Y., Yamada, Y., Fujishima, A. & Sato, O. A Novel LIESST Iron(II) Complex Exhibiting a High Relaxation Temperature. *Inorg. Chem.* **40,** 3240-3242 (2001).

[103] Gallé, G., Etrillard, C., Degert, J., Guillaume, F., Létard, J.-F. & Freysz, E. Study of the fast photoswitching of spin crossover nanoparticles outside and inside their thermal hysteresis loop. *Appl. Phys. Lett.* **102,** 063302 (2013).

[104] Létard, J.-F., Chastanet, G., Guionneau, P. & Desplanches, C. in *Spin-Crossover Mater.* (Halcrow, L. a) 475–506 (John Wiley & Sons Ltd, 2013).

[105] Desaix, A., Roubeau, O., Jeftic, J., Haasnoot, J. G., Boukheddaden, K., Codjovi, E., Linares, J., Nogues, M. & Varret, F. o. Light-induced bistability in spin transition solids leading to thermal and optical hysteresis. *Eur. Phys. J. B-Condens. Matter Complex Syst.* **6,** 183–193 (1998).

[106] Herber, R. & Casson, L. M. Light-induced excited-spin-state trapping: evidence from VTFTIR measurements. *Inorg. Chem.* **25,** 847-852

[107] Cannizzo, A., Milne, C. J., Consani, C., Gawelda, W., Bressler, C., van Mourik, F. & Chergui, M. Light-induced spin crossover in Fe(II)-based complexes: The full photocycle unraveled by ultrafast optical and X-ray spectroscopies. *Coord. Chem. Rev.* **254,** 2677-2686 (2010).

[108] Hauser, A., Adler, P., Deisenroth, S., Gütlich, P., Hennen, C., Spiering, H. & Vef, A. Intersystem crossing in Fe (II) coordination compounds. *Hyperfine Interact.* **90,** 77–87 (1994).

[109] Chergui, M. in *Spin-Crossover Mater.* (Halcrow, L. a) 405–424 (John Wiley & Sons Ltd, 2013).

[110] Marchivie, M., Guionneau, P., Howard, J. A. K., Chastanet, G., Létard, J.-F., Goeta, A. E. & Chasseau, D. Structural Characterization of a Photoinduced Molecular Switch. *J. Am. Chem. Soc.* **124,** 194-195 (2002).

[111] Poganiuch, P., Decurtins, S. & Guetlich, P. Thermal- and light-induced spin transition in [Fe(mtz)6](BF4)2: first successful formation of a metastable low-spin state by irradiation with light at low temperatures. *J. Am. Chem. Soc.* **112,** 3270-3278 (1990).

[112] Chastanet, G., Tovee, C. A., Hyett, G., Halcrow, M. A. & Létard, J.-F. Photomagnetic studies on spin-crossover solid solutions containing two different metal complexes, [Fe(1-bpp)(2)](x)[M(terpy)$_2$](1-x)[BF_4]$_2$ (M = Ru or Co). *Dalton Trans. Camb. Engl. 2003* **41,** 4896-4902 (2012).

[113] Kato, K., Takata, M., Moritomo, Y., Nakamoto, A. & Kojima, N. On-off optical switching of the magnetic and structural properties in a spin-crossover complex. *Appl. Phys. Lett.* **90,** 201902 (2007).

[114] Gütlich, P. in *Spin Crossover Transit. Met. Compd. II* **234,** 231-260 (Springer Berlin Heidelberg).

[115] Collison, D., Garner, C. D., McGrath, C. M., Mosselmans, J. F. W., Roper, M. D., Seddon, J. M. W., Sinn, E. & Young, N. A. Soft X-ray induced excited spin state trapping and soft X-ray photochemistry at the iron L2,3 edge in [Fe(phen)$_2$(NCS)$_2$] and [Fe(phen)$_2$(NCSe)$_2$] (phen = 1,10-phenanthroline). *J. Chem. Soc. Dalton Trans.* **22,** 4371-4376 (1997).

[116] Lee, J.-J., Sheu, H., Lee, C.-R., Chen, J.-M., Lee, J.-F., Wang, C.-C., Huang, C.-H. & Wang, Y. X-ray Absorption Spectroscopic Studies on Light-Induced Excited Spin State Trapping of an Fe(II) Complex. *J. Am. Chem. Soc.* **122,** 5742-5747 (2000).

[117] Bernien, M. X-Ray Absorption Spectroscopy of Fe Complexes on Surfaces: Electronic Interactions and Tailoring of the Magnetic Coupling. (2009).

[118] Vankó, G., Renz, F., Molnár, G., Neisius, T. & Kárpáti, S. Hard-X-ray-Induced Excited-Spin-State Trapping. *Angew. Chem. Int. Ed.* **46,** 5306–5309 (2007).

[119] Briois, V., dit Moulin, C. C., Sainctavit, P., Brouder, C. & Flank, A.-M. Full multiple scattering and crystal field multiplet calculations performed on the spin transition FeII (phen) $_2$ (NCS) $_2$ complex at the iron K and $L_{2,3}$ X-ray absorption edges. *J. Am. Chem. Soc.* **117,** 1019–1026 (1995).

[120] Murray, K. S. in *Spin-Crossover Mater.* (Halcrow, L. a) 1–54 (John Wiley & Sons Ltd, 2013).

[121] Lindner, A., Menzel, M., Renz, F., Kurth, D. G. & Thünemann, A. F. in *ICAME 2005* (Lippens, P.-E., Jumas, J.-C. & Génin, J.-M. R.) 465-468 (Springer Berlin Heidelberg, 2007).

[122] Boillot, M.-L., Zarembowitch, J. & Sour, A. in *Spin Crossover Transit. Met. Compd. II* **234,** 261-276 (Springer Berlin Heidelberg).

[123] Martinho, P. N., Rajnak, C. & Ruben, M. in *Spin-Crossover Mater.* (Halcrow, L. a) 375–404 (John Wiley & Sons Ltd, 2013).

[124] Volatron, F., Catala, L., Rivière, E., Gloter, A., Stéphan, O. & Mallah, T. Spin-Crossover Coordination Nanoparticles. *Inorg. Chem.* **47,** 6584-6586 (2008).

[125] Hung, T. Q., Terki, F., Kamara, S., Dehbaoui, M., Charar, S., Sinha, B., Kim, C., Gandit, P., Gural'skiy, I. A., Molnar, G., Salmon, L., Shepherd, H. J. & Bousseksou, A. Room Temperature Magnetic Detection of Spin Switching in Nanosized Spin-Crossover Materials. *Angew. Chem. Int. Ed.* **52,** 1185–1188 (2013).

[126] Coronado, E., Galán-Mascarós, J. R., Monrabal-Capilla, M., García-Martínez, J. & Pardo-Ibáñez, P. Bistable Spin-Crossover Nanoparticles Showing Magnetic Thermal Hysteresis near Room Temperature. *Adv. Mater.* **19,** 1359–1361 (2007).

[127] Galán-Mascarós, J. R., Coronado, E., Forment-Aliaga, A., Monrabal-Capilla, M., Pinilla-Cienfuegos, E. & Ceolin, M. Tuning Size and Thermal Hysteresis in Bistable Spin Crossover Nanoparticles. *Inorg. Chem.* **49,** 5706-5714 (2010).

[128] Neville, S. M., Etrillard, C., Asthana, S. & Létard, J.-F. Light-Induced Stored Information in Nanoparticles. *Eur. J. Inorg. Chem.* **2010,** 282–288 (2010).

[129] Prins, F., Monrabal-Capilla, M., Osorio, E. A., Coronado, E. & van der Zant, H. S. J. Room-Temperature Electrical Addressing of a Bistable Spin-Crossover Molecular System. *Adv. Mater.* **23,** 1545-1549 (2011).

[130] Etrillard, C., Faramarzi, V., Dayen, J.-F., Letard, J.-F. & Doudin, B. Photoconduction in $[Fe(Htrz)_2(trz)](BF_4)\cdot H_2O$ nanocrystals. *Chem. Commun.* **47,** 9663-9665 (2011).

[131] Duriska, M. B., Neville, S. M., Moubaraki, B., Cashion, J. D., Halder, G. J., Chapman, K. W., Balde, C., Létard, J.-F., Murray, K. S., Kepert, C. J. & Batten, S. R. A Nanoscale Molecular Switch Triggered by Thermal, Light, and Guest Perturbation. *Angew. Chem. Int. Ed.* **48,** 2549–2552 (2009).

[132] Bousseksou, A., Molnár, G., Salmon, L. & Nicolazzi, W. Molecular spin crossover phenomenon: recent achievements and prospects. *Chem. Soc. Rev.* **40,** 3313-3335 (2011).

[133] Mader, D., Pillet, S., Carteret, C., Stébé, M.-J. & Blin, J.-L. Confined Growth of Spin Crossover Nanoparticles in Surfactant-Based Matrices: Enhancing Shape Anisotropy. *J. Dispers. Sci. Technol.* **32,** 1771-1779 (2011).

[134] Cavallini, M., Bergenti, I., Milita, S., Ruani, G., Salitros, I., Qu, Z.-R., Chandrasekar, R. & Ruben, M. Micro- and Nanopatterning of Spin-Transition Compounds into Logical Structures. *Angew. Chem. Int. Ed.* **47,** 8596–8600 (2008).

[135] Martinho, P. N., Lemma, T., Gildea, B., Picardi, G., Müller-Bunz, H., Forster, R. J., Keyes, T. E., Redmond, G. & Morgan, G. G. Template Assembly of Spin Crossover One-Dimensional Nanowires. *Angew. Chem. Int. Ed.* **51,** 11995–11999 (2012).

[136] Soyer, H., Mingotaud, C., Boillot, M.-L. & Delhaes, P. Spin Crossover of a Langmuir−Blodgett Film Based on an Amphiphilic Iron(II) Complex. *Langmuir* **14,** 5890-5895 (1998).

[137] Gandolfi, C., Miyashita, N., Kurth, D. G., Martinho, P. N., Morgan, G. G. & Albrecht, M. Organization of spin- and redox-labile metal centers into Langmuir and Langmuir–Blodgett films. *Dalton Trans.* **39,** 4508-4516 (2010).

[138] Cobo, S., Molnár, G., Real, J. A. & Bousseksou, A. Multilayer Sequential Assembly of Thin Films That Display Room-Temperature Spin Crossover with Hysteresis. *Angew. Chem. Int. Ed.* **45,** 5786–5789 (2006).

[139] Ruben, M., Rojo, J., Romero-Salguero, F. J., Uppadine, L. H. & Lehn, J.-M. Grid-Type Metal Ion Architectures: Functional Metallosupramolecular Arrays. *Angew. Chem. Int. Ed.* **43,** 3644–3662 (2004).

[140] Molnár, G., Cobo, S., Real, J. A., Carcenac, F., Daran, E., Vieu, C. & Bousseksou, A. A Combined Top-Down/Bottom-Up Approach for the Nanoscale Patterning of Spin-Crossover Coordination Polymers. *Adv. Mater.* **19,** 2163–2167 (2007).

[141] Kuroiwa, K., Shibata, T., Sasaki, S., Ohba, M., Takahara, A., Kunitake, T. & Kimizuka, N. Supramolecular control of spin-crossover phenomena in lipophilic Fe(II)-1,2,4-triazole complexes. *J. Polym. Sci. Part Polym. Chem.* **44,** 5192–5202 (2006).

[142] Alam, M. S., Stocker, M., Gieb, K., Müller, P., Haryono, M., Student, K. & Grohmann, A. Spin-State Patterns in Surface-Grafted Beads of Iron(II) Complexes. *Angew. Chem. Int. Ed.* **49,** 1159-1163 (2010).

[143] Matsuda, M. & Tajima, H. Thin Film of a Spin Crossover Complex $[Fe(dpp)_2](BF_4)_2$. *Chem. Lett.* **36,** 700-701 (2007).

[144] Wang, Y. & Zhou, W. A Review on Inorganic Nanostructure Self-Assembly. *J. Nanosci. Nanotechnol.* **10,** 1563-1583 (2010).

[145] Shepherd, H. J., Molnár, G., Nicolazzi, W., Salmon, L. & Bousseksou, A. Spin Crossover at the Nanometre Scale. *Eur. J. Inorg. Chem.* **2013,** 653–661 (2013).

[146] Shi, S., Schmerber, G., Arabski, J., Beaufrand, J.-B., Kim, D. J., Boukari, S., Bowen, M., Kemp, N. T., Viart, N., Rogez, G., Beaurepaire, E., Aubriet, H., Petersen, J., Becker, C. & Ruch, D. Study of molecular spin-crossover complex $Fe(phen)_2(NCS)_2$ thin films. *Appl. Phys. Lett.* **95,** 043303-043303-3 (2009).

[147] Naggert, H., Bannwarth, A., Chemnitz, S., Hofe, T. von, Quandt, E. & Tuczek, F. First observation of light-induced spin change in vacuum deposited thin films of iron spin crossover complexes. *Dalton Trans.* **40,** 6364-6366 (2011).

[148] Warner, B., Oberg, J. C., Gill, T. G., El Hallak, F., Hirjibehedin, C. F., Serri, M., Heutz, S., Arrio, M.-A., Sainctavit, P., Mannini, M., Poneti, G., Sessoli, R. & Rosa, P. Temperature- and Light-Induced Spin Crossover Observed by X-ray Spectroscopy on Isolated Fe(II) Complexes on Gold. *J. Phys. Chem. Lett.* **4,** 1546-1552 (2013).

[149] Mahfoud, T., Molnár, G., Cobo, S., Salmon, L., Thibault, C., Vieu, C., Demont, P. & Bousseksou, A. Electrical properties and non-volatile memory effect of the [Fe (HB (pz) $_3$) $_2$] spin crossover complex integrated in a microelectrode device. *Appl. Phys. Lett.* **99,** 053307 (2011).

[150] Zhang, X., Palamarciuc, T., Rosa, P., Létard, J.-F., Doudin, B., Zhang, Z., Wang, J. & Dowben, P. A. Electronic Structure of a Spin Crossover Molecular Adsorbate. *J. Phys. Chem. C* **116,** 23291-23296 (2012).

[151] Gopakumar, T. G., Matino, F., Naggert, H., Bannwarth, A., Tuczek, F. & Berndt, R. Electron-Induced Spin Crossover of Single Molecules in a Bilayer on Gold. *Angew. Chem. Int. Ed.* **51,** 6262–6266 (2012).

[152] Miyamachi, T., Gruber, M., Davesne, V., Bowen, M., Boukari, S., Joly, L., Scheurer, F., Rogez, G.,

Yamada, T. K., Ohresser, P., Beaurepaire, E. & Wulfhekel, W. Robust spin crossover and memristance across a single molecule. *Nat. Commun.* **3,** 938 (2012).

[153] Bernien, M., Wiedemann, D., Hermanns, C. F., Krüger, A., Rolf, D., Kroener, W., Müller, P., Grohmann, A. & Kuch, W. Spin Crossover in a Vacuum-Deposited Submonolayer of a Molecular Iron(II) Complex. *J. Phys. Chem. Lett.* **3,** 3431-3434 (2012).

[154] Pronschinske, A., Chen, Y., Lewis, G. F., Shultz, D. A., Calzolari, A., Buongiorno Nardelli, M. & Dougherty, D. B. Modification of Molecular Spin Crossover in Ultrathin Films. *Nano Lett.* **13,** 1429-1434 (2013).

[155] Wende, H. Revelation of the crucial interactions in spin-hybrid systems by means of X-ray absorption spectroscopy. *J. Electron Spectrosc. Relat. Phenom.* doi:10.1016/j.elspec.2013.04.010

[156] Bhandary, S., Ghosh, S., Herper, H., Wende, H., Eriksson, O. & Sanyal, B. Graphene as a Reversible Spin Manipulator of Molecular Magnets. *Phys. Rev. Lett.* **107,** 257202 (2011).

[157] Naik, A. D., Stappers, L., Snauwaert, J., Fransaer, J. & Garcia, Y. A Biomembrane Stencil for Crystal Growth and Soft Lithography of a Thermochromic Molecular Sensor. *Small* **6,** 2842–2846 (2010).

[158] Létard, J.-F., Guionneau, P. & Goux-Capes, L. in *Spin Crossover Transit. Met. Compd. III* **235,** 221-249 (Springer-Verlag).

[159] Halder, G. J., Kepert, C. J., Moubaraki, B., Murray, K. S. & Cashion, J. D. Guest-Dependent Spin Crossover in a Nanoporous Molecular Framework Material. *Science* **298,** 1762-1765 (2002).

[160] Vasudevan, S., Vasan, H. N. & Rao, C. N. R. Pes study of spin-state transitions in d6 transition metal complexes and oxides. *Chem. Phys. Lett.* **65,** 444-451 (1979).

[161] Jain, P. C., Singru, R. M. & Gopinathan, K. P. Positron Annihilation. (1985).

[162] Shioyasu, N., Kagetsu, K., Mishima, K., Kubo, M. K., Tominaga, T., Nishiyama, K. & Nagamine, K. Positive muons in spin-crossover complex $[Fe(NCS)_2(phen)_2]$. *Hyperfine Interact.* **84,** 477-481 (1994).

[163] Akabori, K., Matsuo, H. & Yamamoto, Y. Thermal properties of tris(1,10-phenanthroline) complexes of iron(II) and nickel(II) salts. *J. Inorg. Nucl. Chem.* **35,** 2679-2690 (1973).

[164] Jesson, J. P. Mössbauer and Magnetic Susceptibility Investigation of the 5T2−1A1 Crossover in Some Octahedral Ferrous Complexes in the Solid State. *J. Chem. Phys.* **48,** 2058 (1968).

[165] Long, G. J., Grandjean, F. & Reger, D. L. in *Spin Crossover Transit. Met. Compd. I* (Gütlich, P. & Goodwin, H. A.) **233,** 91-122 (Springer Berlin Heidelberg).

[166] Oliver, J. D., Mullica, D. F., Hutchinson, B. B. & Milligan, W. O. Iron-nitrogen bond lengths in low-spin and high-spin iron(II) complexes with poly(pyrazolyl)borate ligands. *Inorg. Chem.* **19,** 165-169 (1980).

[167] Daillant, J. & Gibaud, A. *X-ray and Neutron Reflectivity: Principles and Applications*. (Springer, 2009).

[168] Zhang, L., Miyamachi, T., Tomanić, T., Dehm, R. & Wulfhekel, W. A compact sub-Kelvin ultrahigh vacuum scanning tunneling microscope with high energy resolution and high stability. *Rev. Sci. Instrum.* **82,** 103702 (2011).

[169] Yano, J. & Yachandra, V. K. X-ray absorption spectroscopy. *Photosynth. Res.* **102,** 241-254 (2009).

[170] Ohresser, P., Otero, E., Choueikani, F., Stanescu, S., Deschamps, F., Ibis, L., Moreno, T., Polack, F., Lagarde, B., Marteau, F., Scheurer, F., Joly, L., Kappler, J.-P., Muller, B. & Sainctavit, P. Polarization characterization on the DEIMOS beamline using dichroism measurements. *J. Phys. Conf. Ser.* **425,** 212007 (2013).

[171] Beaurepaire, E. *Magnetism and synchrotron radiation: new trends ; [fifth School on Magnetism and Synchrotron Radiation held at Mittelwihr in October 2008]*. (Springer, 2010).

[172] Stavitski, E. & de Groot, F. M. F. The CTM4XAS program for EELS and XAS spectral shape analysis of transition metal L edges. *Micron Oxf. Engl. 1993* **41,** 687-694 (2010).

[173] Ternes, M., Heinrich, A. J. & Schneider, W.-D. Spectroscopic manifestations of the Kondo effect on single adatoms. *J. Phys. Condens. Matter* **21,** 053001 (2009).

[174] Komeda, T., Isshiki, H., Liu, J., Zhang, Y.-F., Lorente, N., Katoh, K., Breedlove, B. K. & Yamashita, M. Observation and electric current control of a local spin in a single-molecule magnet. *Nat. Commun.* **2,** 217 (2011).

[175] Sandler, N., Dias da Silva, L. & Ulloa, S. Conductance Fano lineshapes for Kondo impurities on surfaces: A numerical renormalization group description. in *APS Meet. Abstr.* **-1,** 37012 (2006).

[176] Hirjibehedin, C. F., Lutz, C. P. & Heinrich, A. J. Spin Coupling in Engineered Atomic Structures. *Science* **312,** 1021-1024 (2006).

[177] Palamarciuc, T., Oberg, J. C., Hallak, F. E., Hirjibehedin, C. F., Serri, M., Heutz, S., Létard, J.-F. & Rosa, P. Spin crossover materials evaporated under clean high vacuum and ultra-high vacuum conditions: from thin films to single molecules. *J. Mater. Chem.* **22,** 9690-9695 (2012).

[178] Capes, L., Létard, J.-F. & Kahn, O. Photomagnetic Properties in a Series of Spin Crossover Compounds $[Fe(PM\text{-}L)_2(NCX)_2]$ (X=S, Se) with Substituted 2'-Pyridylmethylene- 4-amino Ligands. *Chem. – Eur. J.* **6,** 2246–2255 (2000).

[179] Langford, J. I. & Wilson, A. J. C. Scherrer after sixty years: A survey and some new results in the determination of crystallite size. *J. Appl. Crystallogr.* **11,** 102–113 (1978).

[180] Tauc, J., Grigorovici, R. & Vancu, A. Optical Properties and Electronic Structure of Amorphous Germanium. *Phys. Status Solidi B* **15,** 627-637 (1966).

[181] Tauc, J. *Amorphous and liquid semiconductors*. (Plenum, 1974).

[182] Moubah, R., Colis, S., Gallart, M., Schmerber, G., Gilliot, P. & Dinia, A. Thickness-dependent optical band gap in one-dimensional Ca3Co2O6 nanometric films. *J. Lumin.* **132,** 457-460 (2012).

[183] Moubah, R. *Structure et magnétisme des couches minces de cobaltite de types $Ca_3Co_2O_6$ et $Ca_3Co_4O_9$ déposées par ablation laser pulsée*. (Strasbourg, 2010).

[184] Yakuphanoglu, F., Sekerci, M. & Balaban, A. The effect of film thickness on the optical absorption edge and optical constants of the Cr(III) organic thin films. *Opt. Mater.* **27,** 1369-1372 (2005).

[185] Yakuphanoglu, F. & Sekerci, M. Optical characterization of an amorphous organic thin film. *Opt. Appl.* **35,** (2005).

[186] Félix, G., Abdul-Kader, K., Mahfoud, T., Gural'skiy, I. A., Nicolazzi, W., Salmon, L., Molnár, G. & Bousseksou, A. Surface Plasmons Reveal Spin Crossover in Nanometric Layers. *J. Am. Chem. Soc.* **133,** 15342-15345 (2011).

[187] Varret, F., Boukheddaden, K., Codjovi, E., Enachescu, C. & Linarès, J. in *Spin Crossover Transit. Met. Compd. II* **234,** 199-229 (Springer Berlin Heidelberg).

[188] Wagner, S., Kisslinger, F., Ballmann, S., Schramm, F., Chandrasekar, R., Bodenstein, T., Fuhr, O., Secker, D., Fink, K., Ruben, M. & Weber, H. B. Switching of a coupled spin pair in a single-molecule junction. *Nat. Nanotechnol.* **8,** 575-579 (2013).

[189] Pedersen, R. J. & Vernon, F. L. Effect of film resistance on low-impedance tunneling measurements. *Appl. Phys. Lett.* **10,** 29-31 (1967).

Publications during the thesis

Miyamachi, T., Gruber, M., **Davesne, V.**, Bowen, M., Boukari, S., Joly, L., Scheurer, F., Rogez, G., Yamada, T. K., Ohresser, P., Beaurepaire, E. & Wulfhekel, W. Robust spin crossover and memristance across a single molecule. *Nat. Commun.* **3**, 938 (2012).

Davesne, V., Gruber, M., Miyamachi, T., V. Da Costa, Boukari, S., Scheurer, F., Joly, L., Ohresser, P., Otero, E., Choueikani, F., Gaspar, A.B., Real, J.A., Wulfhekel, W., Bowen, M., & Beaurepaire, E. First glimpse of the soft x-ray induced excited spin-state trapping effect dynamics on spin cross-over molecules. *J. of Chem. Phys.* **139** (2013)

Gruber, M., **Davesne, V.**, Bowen, M., Boukari, S., Beaurepaire, E., Wulfhekel, W., & Miyamachi, T. Spin state of spin-crossover complexes: from single molecules to ultra-thin films, *submitted*

Arabksi, J., Jabbar, H., Beaurepaire, E., Bowen, M., Boukari, S., **Davesne, V.**, Gruber, M., Wulfhekel, W., Weber, W., Joly, L., Scheurer, F., Martins, M., Exchange bias between antiferromagnetic phthalocyanines and cobalt, *to be published*

Vincent DAVESNE

ORGANIC SPINTRONICS : AN INVESTIGATION ON SPIN-CROSSOVER COMPLEXES FROM ISOLATED MOLECULES TO THE DEVICE

Résumé

Nous avons étudié par STM, SQUID, Réflectivité X, Diffraction des rayons X, absorption optique et XAS des échantillons de $Fe(phen)_2(NCS)_2$ et $Fe\{[3,5\text{-dimethylpyrazolyl}]_3BH\}_2$ déposé par évaporation thermique sur des substrats de Cu(100), Co(100) et SiO_2, et comparé avec des échantillons en poudre. Nous avons confirmé l'existence de l'effet de piégeage d'état de spin induit par les rayons X (SOXIESST), et étudié ses propriétés, en particulier dynamiques. Celui-ci dépend de l'intensité et de la structure du faisceau X appliqué, et est non-résonant. Nous suggérons que son efficacité est influencée également par les états de transfert de charge métal-ligand (MLCT). L'étude des molécules isolées a montré que l'on pouvait les faire transiter par une impulsion électrique, et construire ainsi des dispositifs memrésistifs, mais seulement si l'influence du substrat est suffisamment réduite. À l'aide d'un modèle thermodynamique simple, nous avons alors étudié les couches minces et montré que la coopérativité est réduite et que la température de transition est modifiée (plus grande pour la Fe-phen, plus faible pour la Fe-pyrz). Enfin, nous utilisons ces résultats pour construire des dispositifs multicouche verticaux Au/Fe-phen/Au dont les propriétés électriques, d'après nos résultats préliminaires, sont dépendantes des stimuli extérieurs (température, champ magnétique). Notamment, ils présentent un effet « diode » à la transition de spin.

Mots-clés : Spintronique organique, transition de spin, $Fe(phen)_2(NCS)_2$, absorption par rayons X

Summary

We have studied by STM, SQUID, X-ray reflectivity, X-ray diffraction, optical absorption and XAS $Fe(phen)_2(NCS)_2$ and $Fe\{[3,5\text{-dimethylpyrazolyl}]_3BH\}_2$ samples deposited by thermal evaporation on Cu(100), Co(100) and SiO_2 substrates, and compared with results on powder samples. We have confirmed the existence of the soft X-ray induced excited spin state trapping (SOXIESST), and investigated its properties, in particular dynamic aspects. The effect is sensitive to the intensity and the structure of the applied X-ray beam, and is non-resonant. We suggest that its efficiency is also governed by metal-ligand charge transfer states (MLCT). The study of single molecules has revealed that they could be switched by voltage pulses, and by this way building memristive devices, but only if the influence of the substrate is sufficiently reduced. We have then investigated thin films with the help from a simple thermodynamic model, and evidenced that the cooperativity was reduced and the transition temperature is modified (higher for Fe-phen, and lower for Fe-pyrz). Finally, we use these results to build multilayer vertical devices Au/Fe-phen/Au, and its electrical properties depends, according to our preliminary results, on the external stimuli (temperature, magnetic field). Notably, they present a “diode” effect at the spin transition.

Keywords : Organic spintronics, spin-crossover, $Fe(phen)_2(NCS)_2$, X-ray absorption, SOXIESST